UNIVERSITÀ DEGLI STUDI DI PARMA

DIPARTIMENTO DI FARMACIA

Dottorato di Ricerca in Biofarmaceutica-Farmacocinetica

Ciclo XXVII (2012-2014)

IONTOPHORESIS AS A NON-INVASIVE ENHANCEMENT TECHNIQUE FOR THE ADMINISTRATION OF DRUGS ACROSS BIOLOGICAL MEMBRANES

Coordinatore: Chiar.mo Prof. Paolo Colombo

Relatore: Chiar.ma Prof.ssa Patrizia Santi

Tutor: Chiar.ma Prof.ssa Cristina Padula

Dottoranda:

Elena Tratta

Index

1 Abstract

Iontophoresis, a technique that consists in applying low density current to a membrane, has been widely investigated in order to enhance the permeation of drugs through different biological barriers such as the skin, the buccal mucosa and the sclera in order to obtain a systemic or local (in case of trans-scleral administration) effect without the need of an injection.

The aim of this thesis was to investigate the effect of iontophoresis on these three barriers, considering the different state of the art for each of them.

Concerning trans-scleral iontophoresis, there are many studies with small molecules, and some on neutral and negatively charged macromolecules, while there's a lack of data on positively charged macromolecules, which can be useful for the treatment of different posterior segment eye diseases. Cytochrome c (12.4 kDa, charge +7.9 at pH 8.2) was chosen as a model molecule. Passive transport of cytochrome c was evaluated across the sclera and the bilayer choroid-Bruch's membrane. The affinity of cytochrome c for melanin was measured by means of in vitro binding experiments. Iontophoretic permeation was studied as a function of donor concentration (5 to 70 mg/ml) and current density (1.51 to 5.83 mA/cm²), and the contribution of electroosmosis on cytochrome c transport was determined using a high molecular weight fluorescent dextran (FD-150) as neutral marker. Moreover, also the possibility of a fine tuning of the release was assessed. The results showed that cytochrome c permeated across isolated sclera with a permeability coefficient of about $2.5*10^{-6}$ cm/s, comparable to molecules with a similar radius. Choroid-Bruch's membrane bilayer was an important barrier to permeation, also because of the presence of melanin in this tissue. Iontophoresis (2.92 mA/cm²) enhanced cytochrome c permeation across the sclera at all the concentrations tested, increasing about 10 times the amount permeated after 2 hours. The effect was proportional to current density. Iontophoretic experiments performed with FD-150, an electroosmotic flow marker, demonstrated that the presence of cytochrome c dramatically reduced the EO flow and that, despite the high molecular weight, the main mechanism for cytochrome c iontophoretic permeation is electromigration. Finally,

experiments performed with an alternation of current-assisted and passive permeation showed that a modulation of the release was possible.

Buccal mucosa is an interesting alternative site to administer drugs, since it can avoid first pass effect. However, permeation is limited by the barrier properties of the buccal epithelium. Thus, iontophoresis may be useful to promote the permeation of drugs. Recently, pig esophageal epithelium has been proposed as a model for buccal epithelium, since it is easier to obtain and separate, and it has shown to be similar in structure and lipid composition compared to buccal tissue. There are limited data about buccal iontophoresis, so the aim of this part of the project was to characterize the properties of esophageal epithelium under the application of electrical current. Sumatriptan succinate was chosen as a model, because of its well characterized behavior during transdermal iontophoresis. The effect of raise in current density (0-5.83 mA/cm^2) and of concentration in the donor solution were assessed. The increase in the amount permeated was proportional both to the increase in current and in donor concentration.

On the other side, data in literature on transdermal iontophoresis are abundant, on both small molecules and macromolecules. In this case, we studied the effect of iontophoresis compared to laser microporation, another physical enhancement technique, on the permeation and deposition of Thymosin α1. This is a 28 amino acids peptide used to treat different pathological conditions and as an adjuvant for vaccination. Even though the amounts permeated were probably not enough to elicit a systemic response from the immune system, iontophoresis allowed higher permeation in a shorter period of time compared to laser microporation.

2 Introduction

Iontophoresis is a physical enhancement technique, which consists in the application of low density current to a membrane in order to promote the penetration of a substance, either charged or neutral, across this membrane.

The first documented experiment regarding iontophoresis dates back to 1908, when Leduc demonstrated that rabbits suffered fatal seizures shortly after transcutaneous iontophoretic application of strychnine [1]. Fifty years later, Gibson and Cooke proved an induction of the sweating after iontophoretic application of pilocarpine. From then on, iontophoresis was studied for transporting steroids for the treatment of musculoskeletal diseases, osteoarthritis and some urological conditions.

Nowadays, iontophoresis is a widely studied enhancement technique. It is particularly appealing, since it offers the possibility of systemic delivery in a controlled fashion, and can broaden the spectrum of molecules that can be administered transdermally [2]. Moreover, its application now has been extended also to the eye and to the buccal mucosa.

Data available for transdermal, trans-scleral and buccal iontophoresis are different for each membrane. Transdermal iontophoresis has been widely investigated over many years for the systemic delivery of many drugs, such as opioids, antiemetics, antihypertensives and steroids. More recently, research has focused on transdermal iontophoretic administration of peptides and proteins and on targeted cutaneous delivery. Buccal iontophoresis, on the contrary, is still in its early stages: studies are still focusing on the characterization of the epithelium properties during and after current application [3]. Trans-scleral iontophoresis has been studied for the last 20 years, and is particularly appealing for the local therapy of posterior segment eye diseases, since it could be possible to avoid more invasive procedures and systemic exposure to the drug [4].

An iontophoretic device consists of a power supply connected to a positively charged electrode, the anode, and a negatively charged one, the cathode (Figure 1).

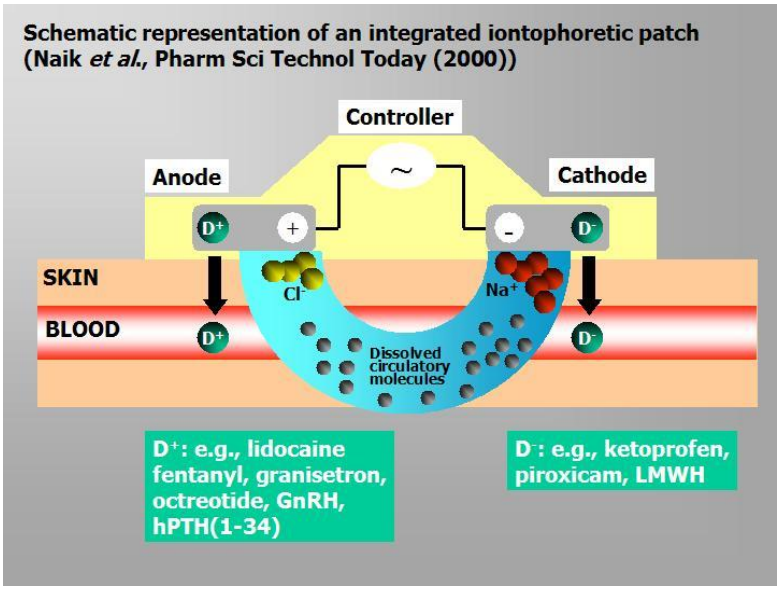

Figure 1 Representation of an iontophoretic device [5]

The charged drug in solution is placed under the electrode that carries the same charge. When current is applied, the drug is transported in the subjacent tissue, and can reach the systemic circulation. When the drug is positively charged, it is placed under the anode, and the process is called anodal iontophoresis. On the contrary, when it is negatively charged, it is placed under the cathode, and the process is called cathodal iontophoresis.

Usually the electrodes of choice are silver/silver chloride, since they do not cause water electrolysis. In this way, there is no production of protons that could compete with the drug to carry the charge, and there is no sharp decrease in the pH, which could lead to acid-induced burns and may have an adverse effect on drug stability [6].

The anode, made of silver, oxidizes and forms insoluble silver chloride.

$$Ag^0(s) + Cl^-(aq) \rightarrow AgCl(s) + e^-$$

Equation 1

In the cathodal compartment, silver chloride reduces to metallic silver:

$$AgCl\,(s) + e^- \rightarrow Ag^0(s) + Cl^-(aq)$$

Equation 2

2.1 Iontophoretic transport mechanisms [6, 7]

The flux of a drug across a membrane can be defined by the following equation:

$$J_{tot} = J_{PASS} + J_{ER} + J_{EO}$$

Equation 3

J_{PASS} represents the passive flux, J_{ER} is the electromigratory flux and J_{EO} refers to the electroosmotic flow contribution.

The term electromigration indicates the ordered movement of charged species upon the application of an electric field.

$$J_{EM} = \frac{z_x \mu_x c_x}{\sum_0^i z_i \mu_i c_i} \left(\frac{1}{z_x F}\right) I_d$$

Equation 4

I_d is the applied current density, while F is the Faraday constant.

z_x, μ_x and c_x refer respectively to the charge, mobility and concentration of the drug in the membrane, while the denominator takes into account these parameters for all the ions present in solution.

This way of expressing electromigratory contribution shows very clearly how the presence of competitor ions in the donor solution reduces the extent of electromigration.

Electroosmotic flow, on the other hand, can be expressed by:

$$J_{EO} = C_x v$$

Equation 5

Where C_x is drug concentration, and v the electroosmotic solvent velocity.

Electroosmotic flow is a convective solvent flow that depends on the permselectivity properties of the membrane. The skin, the sclera and buccal mucosa carry fixed negative charges at physiological pH. Since all these membrane are electroneutral, the negative charges are neutralized by small cations with high electrophoretic mobilities, such as Na^+, thus forming a thin, positively charged layer. When an externally applied electric field interacts with the net surplus of charged ions in the diffuse part of an electrical double layer, a bulk solvent flow originates. In the case on negatively charged membranes, the flux is directed from anode to cathode and is the only responsible for the movement of neutral molecules.

2.2 Factors affecting iontophoretic transport

Different factors, linked either to properties of the drug itself or to the properties of the iontophoretic system, can influence iontophoretic transport. The factors directly related to the drug are its concentration in the donor solution, its physicochemical properties and the presence in the formulation of competing ions [8].

Drug concentration is one of the most investigated experimental parameters. Although the equation describing iontophoretic transport (Equation 5 and Equation 6) would suggest a direct proportionality between drug concentration in the donor solution and iontophoretic permeation, this is not always confirmed by permeation experiments. This happens for mainly three reasons: first, an increase of concentration in the formulation does not correspond always to an increase also in the membrane, second, the presence of competing ions and their concentration plays a major role in the transport, and third, the drug can interact with different structures along the iontophoretic pathway [6].

Physicochemical properties of the drug, such as molecular size, also influence iontophoretic transport. A bigger size of the molecule usually results in a lower permeation. With the extension of the use of iontophoresis on macromolecules, charge/mass ratio has become a more appreciated descriptor than just the mass, since it takes into account the effect of multiple charges on the molecule.

The presence of competing ions, either co-ions or counterions, results in a reduction of the transport of the drug, especially if the competing ions are more mobile, like those present in commonly used biological buffers [8].

The pH of the formulation in contact with the membrane can influence iontophoretic permeation to different extents. As a first remark, it determines the degree of ionization of the drug, that needs to be the highest possible for an optimization of the electromigratory contribution. In addition, the solution pH can affect the membrane with which it is in contact. The skin has an isoelectric point of 4-4.5, the sclera about 3 [9]. This means that above these pH values they behave as permselective membranes which, upon the application of current, give rise to electroosmotic flow, introducing another iontophoretic transport mechanism [6].

Finally, current density is one of the most important factors affecting iontophoretic delivery. It can be seen from Equation 4 that electromigratory flux should increase proportionally with

the raise in current density. This is valid for small molecules and peptides. However at higher current densities, in some cases, the response reached a plateau, thus suggesting the presence of a saturation phenomenon [10].

3 General purpose

The general aim of this thesis was the evaluation of iontophoresis as a non-invasive enhancement technique for the permeation of drugs across the sclera, buccal mucosa and skin, considering the different features and state of art for each membrane.

For trans-scleral delivery, the focus is on the non-invasive delivery of macromolecular drugs, thus cytochrome c, a positively charged macromolecule, was chosen as model compound and the possibility of enhancing its ocular permeation with iontophoresis was evaluated.

On the other hand, the investigation on buccal iontophoresis is still in its early stages, and characterization steps are still needed. Sumatriptan succinate was selected as model drug to give a further insight into the behavior of porcine esophageal epithelium, which can be a useful model for buccal epithelium, when iontophoresis is applied.

Data on transdermal iontophoresis, on the contrary, are abundant. In this case, the aim was to study the effect of iontophoresis on transdermal permeation of Thymosin α1, a negatively charged polypeptide, in comparison with laser microporation, another widely used physical enhancement technique.

4 Trans-scleral delivery

4.1 State of the art

Posterior segment eye diseases assume a major importance in ophthalmology, since they account for many cases of blindness worldwide. Innovative therapies for the treatment of these diseases involve the use of macromolecular drugs, either charged or neutral, such as proteins, oligonucleotides and monoclonal antibodies. Due to their physicochemical properties, like high molecular weight, presence of charges and poor permeability across the ocular tissue, they are usually administered via intravitreal injection, a very invasive procedure that can cause complications such as endophtalmitis, cataract and retinal detachment. Thus, alternative non-invasive routes of administration are needed. Trans-scleral delivery consists in the application of drugs on the scleral surface, which can then diffuse across the underlying tissues to reach their target in the posterior segment of the eye and it could be an alternative to intravitreal injection, because of the large surface area, accessibility and convenience [11].

4.1.1 Anatomy of the eye [12]

The eye is the principal organ of the sight. It is placed in the orbitary cavity in the cranium, and it is fixed to the adipose body, the fat tissue that occupies most of the cavity, by a fibrous septum, known as Tenon's capsule. The eye globe has an average mass of 7.5 g and an average volume of 6 cm^3. It is shaped like a slightly asymmetric sphere with a smaller frontal unit, called cornea, and a bigger posterior part, the sclera. The corneal segment, which represents 1/6 of the eye, has a 8 mm radius, while the sclerotic chamber has a typical radius of 12 mm. A ring called limbus connects the cornea to the sclera.

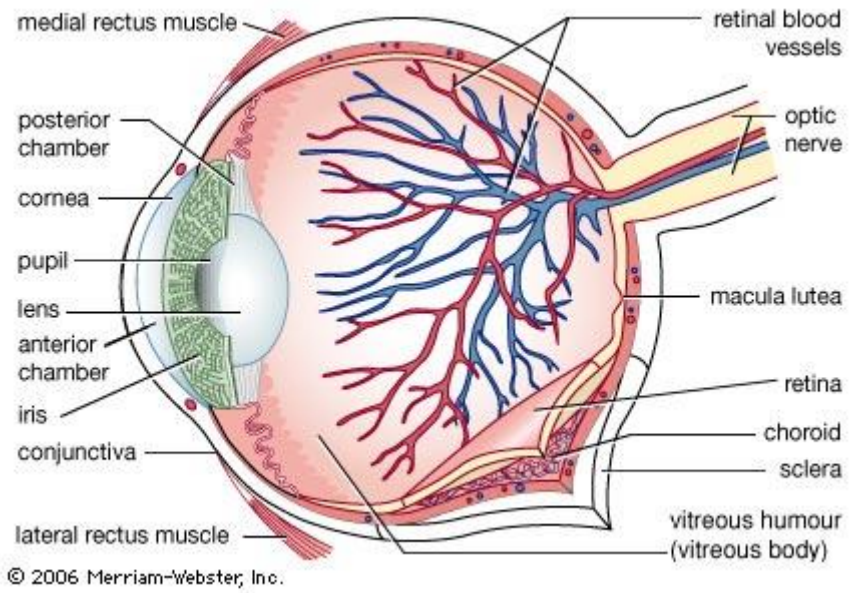

Figure 2 Anatomy of the human eye

The eye globe is composed of an anterior chamber, delimitated by cornea, iris and lens, a small posterior chamber and the vitreous chamber. Anterior and posterior chambers contain the aqueous humor, a liquid consisting of glucose, electrolytes and proteins. Vitreous humor, a clear jelly made up of water (98%), collagen and hyaluronic acid, fills the vitreous chamber, the larger cavity enclosed by the sclera, the ciliary body and the lens. It has dioptric functions.

Three layers, which enclose the optically clear aqueous humor, lens and vitreous body, compose the eye. From the external side inwards, a fibrous, a vascular and neural tunic can be identified. The cornea and the sclera compose the outermost fibrous tunic. Cornea is a transparent window made up of five layers: epithelium, Bowman's membrane, stroma, Descemet's membrane and endothelium. The stroma represent 90% of corneal volume, and is composed of collagen. The sclera is essentially the continuation backward of the cornea, the collagen fibres of the cornea being, in effect, continuous with those of the sclera. It is pierced by many vessels and nerves. Its histological structure will be further elucidated in section 4.1.4. Choroid, ciliary body and iris are the vascular layer or uvea. The choroid is essentially a layer of blood vessels and connective tissue, while the ciliary body is a muscular ring whose function is mainly to provide accommodation to the lens to adjust vision. It is covered by the ciliary epithelium, a double layer of cells that secretes the aqueous humor.

The innermost tunic is the retina, or neural tunic. It is 0.25 mm thick and is composed by two superimposed layers: the pigmented epithelium, a single layer of cuboidal cells that separates

it from the choroid, and acts as a restraining barrier to the diffusion of substances to the retina. The second layer is called neuroretina and is made up of three layers of nerve cells bodies separated by two layers containing synapses made by the axons and dendrites of these cells. The tier of cells at the back of the retina contains rods and cones, the light-sensitive cells responsible for the transmission of the visual stimulus to the nervous system. Neuroretina has its own vascularization: retinal vessels, which are branches of the ophthalmic arteries, supply the innermost part of the neural tunica, on the other hand, light sensitive elements nourishment depends on the interstitial fluid that filters from the choroid.

Anatomically the eye can be divided in anterior segment [13], the front third of the eye that includes the structures in front of the vitreous humor: the cornea, iris, ciliary body and lens, and a posterior segment. The posterior segment includes the anterior hyaloid membrane and all the structures behind it: the vitreous humor, retina, choroid and optic nerve. This division is particularly useful in eye pathology, where the diseases are classified as anterior or posterior segment eye diseases.

4.1.2 Posterior segment eye diseases

As previously stated, ophthalmic diseases are generally classified in anterior and posterior segment eye diseases. Posterior segment eye diseases comprise all the disorders referring to the retina, the choroid and the vitreous. Among them, diabetic retinopathy, age related macular degeneration (ARMD) and glaucoma are of particular interest, since, along with cataract, they are leading causes for visual impairment in the industrialized world.

Diabetic retinopathy [14, 15] is a condition affecting people with diabetes, which causes progressive damage to the retina. It is the result of microvascular damage induced by hyperglycaemia. Hyperglycaemia-induced intramural pericyte death and thickening of the basement membrane lead to incompetence of the vascular wall. This can cause different problems, such as microaneurisms, exudates-small leaks of fluid from damaged blood vessels, hemorrhages and blockages. This last condition can starve the retina of blood and oxygen, with subsequent formation of weak new blood vessels on the surface of the retina. Scar tissue can also form, that can pull the retina and eventually cause its detachment. Diabetic retinopathy is classified in three stages on the basis of its severity. The first stage is called pre-clinical. The second stage is named non-proliferative and can be further divided into mild, medium and severe or pre-proliferative. In this phase, the patient experiences no symptoms.

In the third stage, or proliferative, abnormal blood vessels (neovascularization) form at the back of the eye, and they can burst and bleed. Nowadays, the treatment for diabetic retinopathy involves laser photocoagulation, but also intravitreal injection of anti-VEGF (anti-vascular endothelial growth factors) such as bevacizumab, ranibizumab and pegaptanib.

Age related macular degeneration (ARMD) is the leading cause of visual impairment among the elderly in the developed world [16]. It accounts for 8.7% of new blindness cases worldwide. Its advanced stage can be classified in dry and wet (or exudative) ARMD. The dry form begins with yellow deposits, called drusen, in the macula, between the retinal pigmented epithelium and the choroid. Central geographic atrophy results from atrophy of the retinal pigmented epithelium, which causes vision loss because of the loss of photoreceptors in the central part of the eye [16]. Up to now, there is no treatment for dry ARMD, even if ciliary neurotrophic factor is giving promising results as possible therapeutic agent [17]. Wet ARMD is characterized by a rapid vision loss, which depends on choroidal neovascularization, caused by a complex pathophysiological process. This form is treated with laser photocoagulation or, similarly to diabetic retinopathy, with anti-angiogenic drugs, such as pegaptanib, ranibizumab, aflibercept and bevacizumab [18].

Glaucoma [19] is a multifactorial optical neuropathy that presents a characteristic loss in retinal ganglion cells at a superior extent than normal age related loss, which can lead to atrophy of the optic nerve [20]. It is the second cause of blindness, accounting for 12.3 % of all the cases worldwide. It is characterized usually by a raise in intraocular pressure above 21 mm Hg, and it can be classified as primary, where the cause of this raise can be found in the eye itself, and secondary, in which another disease, such as hypertension, causes indirectly the increase of intraocular pressure. Regardless of the typology, the progression of the disease determines atrophy of the nervous fibers at the blind spot in the retina. This can be due either to the direct effect of the mechanical pressure on the cones and rods, or to the insufficient blood supply, with subsequent necrosis of the photoreceptors. Glaucoma is treated with topically applied drugs that reduce the production of aqueous humor or that facilitate the efflux in Schlemm's canal, a venous vessel that merges with the episcleral blood flow.

4.1.3 Drug delivery to the eye

Drugs can be delivered to the eye by four principal routes: topical, systemic, intravitreal and trans-scleral (Figure 3).

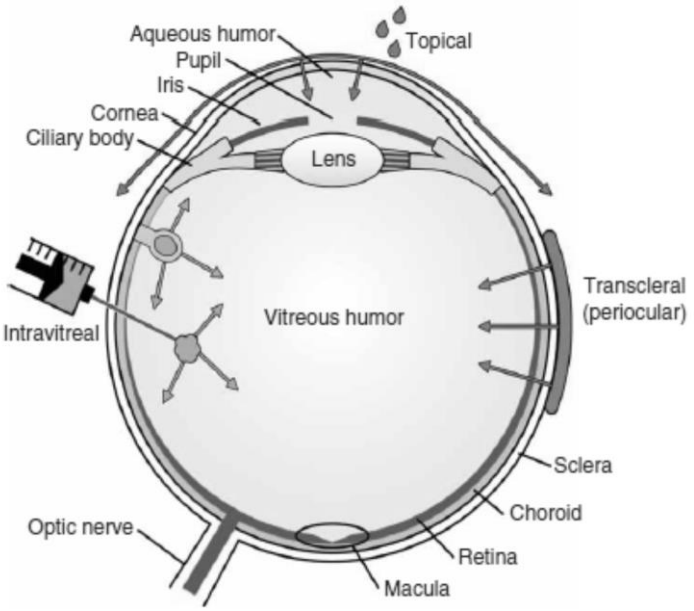

Figure 3 Drug delivery modalities for the treatment of ocular diseases (adapted from [21])

Topical delivery, in the form of eye drops, is generally preferred for the treatment of anterior segment diseases, while it is usually ineffective for the treatment of posterior segment eye diseases. This is due to the fact that most part of the formulation is cleared before entering the eye, and typically less than 5% of the applied dose reaches the aqueous humor, owing to lacrimation, tear turnover and nasolacrimal drainage [21].

Systemic administration can be used to treat posterior segment eye diseases. This route of administration is not targeted and the drug is available in the systemic blood circulation. Penetration of drugs into the posterior segment is limited by the presence of the blood-retinal barrier, that is composed by an outer barrier and an inner barrier. RPE, which is a tight ion transporting barrier, represents the outer part, while the blood vessels of the retina serve as the inner part of this barrier. The endothelial cells of the retinal vessels are in fact lined by tight junctions that prevent paracellular transport of most compounds. Only extremely lipophilic compounds penetrate the blood-retinal barrier and achieve therapeutically significant concentrations in the posterior segment following systemic administration. Therefore, large doses of drug need to be administered, which can lead to the onset of unwanted side effects [22].

Intravitreal delivery is achieved with an injection at the level of the limbus. It provides immediate access to the vitreous chamber and it has been used for decades to deliver many

different drugs, such as corticosteroids and anti-VEGF factors, for the treatment of AMD, pseudophakic cystoid macular edema and macular edema following retinal vascular occlusion. It is a quite invasive route of administration, and can cause rare but serious complications, such as retinitis, endophtalmitis, retinal detachment and cataract [21]. Moreover it requires frequent administrations, for example the current protocol for the treatment of AMD recommends up to 24 injections in 24 months [23].

Trans-scleral delivery, on the other hand, is an attractive alternative to intravitreal injection, since it offers targeted delivery with a less invasive procedure. The relatively high permeability of the sclera to macromolecules supports the study of their trans-scleral administration. However, up to now, trans-scleral delivery has not yet been proven as clinically effective as intravitreal injection in the treatment of posterior segment eye diseases. This is ascribable to the fact that drugs have to cross several different tissues, which hinder their permeation, before reaching their target [24].

4.1.4 Transport barriers in trans-scleral delivery

Trans-scleral delivery can be achieved by suconjunctival, sub-Tenon, peribulbar, posterior juxtascleral and retrobulbar injection. Drugs can reach the posterior segment from the periocular space mainly through a direct penetration pathway across the sclera.

The permeation of the drug is then limited by the presence of many barriers in the eye, both static and dynamic. Conjunctiva and sclera offer diffusive resistance, while retinal pigmented epithelium is selectively permeable. In addition, conjunctival and choroidal blood circulation and lymphatic flow contribute to the clearance of drugs. Moreover, melanin contained in the ocular tissue (e.g. retinal pigmented epithelium, choroid) can bind to the drug and thus impede its diffusion.

The conjunctiva is made up of a stratified columnar epithelium and a lamina propria. The rate limiting barrier to the permeation is the outermost cell layer of the epithelium, which contains tight junctions. The conjunctival tissue is also metabolically active.

The sclera is composed by a scaffold of protein fibrils, collagen and elastin, together with intercellular proteoglycans and glycoproteins surrounding a sparse population of cells. Collagen is the main component of the sclera (75% scleral dry weight). The sclera consists of three layers, that are episclera, stroma and lamina fusca. Episclera is the outermost layer and

is made of collagen clusters interlaced with fibroblasts, proteoglycans and rare melanocytes. In the stroma, the bundles of collagen become larger and form bands of lamellae. The stroma contains also elastic tissue and fibroblasts. The innermost layer, lamina fusca, is a component of both sclera and uvea. It is composed of loosely ordered collagen clusters that are interwoven with melanocytic and mesodermal cellular elements [11]. Scleral permeability properties are determined by the matrix characteristics, such as proteoglycans concentration, orientation of collagen fibers and amount of free space that can be occupied by molecules of solute. Moreover, it also depends on the thickness: it is relatively thick near the limbus (0.53±0.14 mm), while it becomes thinner at the equator (0.25 mm or less) and significantly thickens near the optic nerve. Therefore, trans-scleral delivery directed near the equator could maximize trans-scleral flux [11]. Permeability through the sclera depends more on the molecular radius than on the molecular weight [23]. It has been demonstrated that passive permeation across the sclera is feasible for molecules with molecular weights up to 150 kDa [24].

The choroid, that lines the inner part of the sclera, is, as stated before, a network of capillaries supported by the Bruch's membrane, which is a 2-4 μm thick connective membrane with function of support that also represents the basement membrane of the RPE. Probably Bruch's membrane is the main static barrier to transport across the choroid-Bruch's membrane bilayer [23]. Its permeability decreases as the size of the drug increases. In addition to the barrier properties of the Bruch's membrane, the presence of melanin in the choroid can represent an obstacle toward drug permeation, since many drugs have affinity for ocular melanin. This has been shown for small molecules [25, 26], while limited data are available for macromolecules[27-29].

Retinal pigmented epithelium (RPE) consists of a single layer of hexagonal cells which contains melanin granules and are bound by *zonula adherens* and by *zonula occludens* respectively in the basal and apical region. The presence of these tight junctions, as well as the active transport mechanisms and metabolism present in this membrane, can heavily influence its permeability. Literature data, however, show that cultured RPE monolayers are permeable to macromolecules such as inulin (5 kDa) and horseradish peroxidase (35 kDa) [30], and that bovine RPE-choroid is permeable towards FITC labelled dextrans with molecular weights up to 80 kDa [31].

Dynamic barriers are represented by the conjunctival, episcleral and choroidal blood flow, and by conjunctival lymphatic drainage. They used to be considered as the main limiting factor to trans-scleral drug delivery. However, it has been demonstrated that these clearance mechanisms have a more limited effect on the elimination of macromolecules than on small molecules [23]. For the choroid this can be attributed to the presence in the fenestration of the capillaries of a diaphragm, made up of radially oriented fibers, which restricts the diameter from 80-100 nm to only 30 nm. The presence of transporter proteins in the retinal pigmented epithelium has also to be underlined: they are mainly represented by drug efflux pumps, such as P-glycoproteins and multidrug resistance associated proteins, which have a broad substrate specificity, and organic ion transporters [24]. Their role in the elimination of trans-sclerally administered drugs, however, remains to be clarified [23].

Drug metabolizing enzymes, which represent the metabolic barriers, are mainly found in the ciliary body and RPE. Higher levels of metabolizing enzymes are necessary in these tissues, because they are responsible for the detoxification of substances carried by systemic blood flow. These enzymes are mainly members of the cytochrome P-450 family and lysosomal enzymes. There are few reports on their effect on ocular pharmacokinetics [32], thus, the significance of metabolic barriers in trans-scleral delivery has to be further elucidated [24].

Because of the presence of these barriers, achievement of relevant drug concentrations at the target site can be challenging. Thus, the use of physical enhancement techniques, such as iontophoresis, can be helpful to overcome the trans-scleral tissue boundaries.

4.1.5 Trans-scleral iontophoresis

Trans-scleral iontophoresis has been widely investigated for the delivery of small molecules such as acetyl salicylic acid, methylprednisolone, gentamicin, amikacin and carboplatin [33].

It is a well tolerated technique: studies conducted on healthy volunteers [34] showed that a current density of 6 mA/cm² is well tolerated for 20 minutes, while 3 mA/cm² are tolerated up to 40 minutes. Possible unwanted side effects are itching and burning at the site of application of the electrode.

A device for trans-scleral iontophoresis has been recently made available, the EyeGate II Delivery System (EGDS; Eyegate Pharmaceuticals, Inc., Waltham, MA, USA). The system is composed by two parts: a reusable battery-powered generator and a disposable, annular

shaped applicator that contains the drug. It has been tested with a dexamethasone phosphate ophthalmic formulation (EPG-437) tailored for iontophoretic delivery for the treatment of dry eye or anterior uveitis. The promising results obtained on anterior uveitis led to preclinical studies on RNAi molecules for the treatment of neovascular AMD, a disease that affect the posterior segment [35]. A very similar device, called Visulex® (Aciont Inc., Salt Lake City, Utah,USA), is currently being tested for trans-scleral iontophoretic administration of different corticosteroids (https://clinicaltrials.gov/ct2/show/NCT02309385).

Up to now, in addition to the studies on small molecules, trans-scleral iontophporesis has been investigated also on neutral or negatively charged macromolecules.

Davies et al. used iontophoresis to enhance trans-scleral delivery of DNA and DNA hybrids (up to 8000 kDa) [36] obtaining promising results even if the current intensity applied was far too high for clinical purposes (34-56 mA).

Chopra et al. investigated in vitro iontophoretic transport of bovine serum albumin (BSA, M.W. 60 kDa), polystyrene sulfonic acid and bevacizumab (150 kDa) [37]. They demonstrated that iontophoresis was feasible for the permeation enhancement of charged macromolecules across the sclera. Moreover, the investigation on the mechanisms involved showed that for BSA the main transport mechanism was electroosmosis.

Nicoli et al., on the other hand, studied trans-scleral iontophoresis of high molecular weight labelled dextrans (M.W. 4.4-120 kDa), neutral compounds used as model molecules, and of bevacizumab[9, 38] . For all the molecules tested, anodal iontophoresis originated significantly higher fluxes and permeability coefficients. The enhancement was ascribable only to the electroosmotic flow generated by iontophoresis.

Cathodal iontophoresis was used to promote the permeation of negatively charged oligonucleotides: in this case, an increase in current density did not reflect in increased flux, probably because of hindering effect of electroosmotic flow, directed from anode to cathode.

Although a certain number of studies could be found on neutral and negatively charged macromolecules, there’s a lack of data regarding positively charged macromolecules, which could also be useful for therapeutic application. In the case of a positively charged molecule, anodal iontophoresis would be applied, and both electrorepulsion and electroosmosis would contribute to electrophoretic transport.

4.1.6 Cytochrome c

Cytochrome c (Figure 4) is a highly conserved protein across the spectrum of the species, and can be found in plants, animals and many unicellular organisms. It consists of a single 104 amino acids residues chain, with one heme group covalently attached to Cys^{14} and Cys^{17}. It has a molecular weight of 12400 Da and an isoelectric point of 10, thus it is positively charged at physiological pH. Because of its ubiquitous nature and well-characterized structure it is widely used as a model molecule.

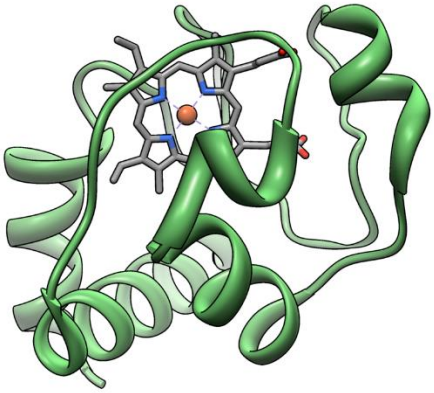

Figure 4 Three-dimensional structure of cytochrome c (green) with a heme molecule coordinating a central Iron atom (orange). PDB id, 1HRC, Bushnell et al., "High-resolution three-dimensional structure of horse heart cytochrome c." J Mol Biol. 1990 Jul 20;214(2):585-95. PubMed PMID: 2166170.

The primary function of cytochrome c is of electron carrying mitochondrial protein. It changes its oxidative status from ferrous to ferric within the cell, thus it is an effective biological electron transporter and plays a vital role in cellular oxidation [39]. Its main function in cellular respiration is to transport electrons from cytochrome c reductase (complex III) to cytochrome c oxidase (Complex IV). More recently, it has been identified as a mediator in the apoptotic pathway. In fact, its release in the cytoplasm stimulates apoptosis and is commonly used as an indicator of the apoptotic process [40].

Its structure [41] is roughly spherical, with a diameter of 30 Å. It has 19 positively charged lysine residues, plus 2 arginines, while having 12 acidic residues (aspartic or glutamic acid).

Cytochrome c does not have specific therapeutic application, but it was chosen here as a model molecule because of its well defined structure and thermodynamic stability. In addition, it is highly soluble in water, and it absorbs in the UV at 214 nm [42].

4.2 Aim of the study

The aim of this part of the work was to study the penetration of cytochrome c, a positively charged macromolecule (M.W. 12.4 kDa, pI 10.0), across different ocular tissues, and to evaluate the potential of anodal iontophoresis to enhance and modulate the trans-scleral transport. The role of choroid-Bruch's membrane and melanin in cytochrome c passive diffusion was investigated performing passive permeation experiments across isolated sclera, trilayer (sclera-choroid-Bruch's membrane) and choroid-Bruch's membrane bilayer at different donor concentrations. In addition, cytochrome c binding to melanin was assessed.

Different factors known to affect iontophoretic permeation, such as donor solution concentration, current density, vehicle pH and ionic strength, were evaluated in current assisted experiments, in order to determine their effect on cytochrome c penetration across the isolated sclera. The possibility of a fine tuning of cytochrome c release across the sclera was also assessed.

Finally, current assisted experiments were performed with FD-150, a fluorescent neutral marker (M.W. 120 kDa), in order to determine whether the principal mechanism of transport was electromigration or electroosmosis, and to investigate the effect of cytochrome c itself on electroosmotic flow.

4.3 Materials and methods

4.3.1 Materials

Cytochrome c, FD-150 (fluorescein isothiocyanate dextran, M.W. ~120 kDa), HEPES (2-[4-(2-hydroxyethyl)piperazin-1-yl]ethanesulfonic acid) and melanin from *Sepia Officinalis* were all from Sigma-Aldrich (Saint-Louis, MO, USA).

Eudragit ® FS 30 D was from Röhm Pharma (Weiterstadt, Germany), Kollidon® K90 and Lutrol® F127 were from BASF (Ludwigshafen, Germany), Alginic acid was from Sigma Aldrich (Saint-Louis, MO, USA), Acritamer ®940 was from ACEF (Fiorenzuola d'Arda, PC, IT).

All other chemicals were of analytical grade.

4.3.2 Buffers

PBS (phosphate buffered saline) had a concentration of 150 mM NaCl, 17 mM Na_2HPO_4 and 1.4 mM KH_2PO_4. pH was adjusted to 7.4. Overall ionic strength: 194 mM.

HEPES buffered saline contained NaCl 150 mM and HEPES 25 mM. pH was adjusted to 7.4. Overall ionic strength: 150 mM.

Citrate buffers (pH= 4, 6.1 and 8.1) were prepared mixing appropriate volumes of stock solutions of 25 mM citric acid and sodium citrate.

Borate buffer was a 25 mM solution of sodium tetraborate ($B_4Na_2O_7$) in distilled water. pH was adjusted to 6.4.

4.3.3 Tissue preparation

Porcine eye globes were obtained from a local slaughterhouse (Annoni S.p.A., Madonna dei Prati, Busseto, Parma, Italy). The pigs used were of mixed breed Landrace-Large White, 10-11 months old, weighing 145-90 kg, raised for human consumption. The eyes, kept in ice bath after the excision, were brought to the lab within 2 hours. The muscular tissue surrounding the globe was immediately removed with the help of rounded scissors.

After that, a circular incision was practiced around the limbus (about 5 mm below the cornea), in order to separate the anterior and posterior segment of the eye (Figure 5, panel A). The anterior segment was removed together with the vitreous humor (Figure 5, panels B and C). Retina and RPE (retinal pigmented epithelium) were then removed from the posterior chamber by repeated application of filter paper soaked in physiological solution (Figure 5,

panel D). Then, the chamber was cut along the ciliary arteries, obtaining two fragments. Each fragment was composed by a three-layered structure: sclera,choroid and Bruch's membrane (Figure 5, panel E). When the trilayer membrane was needed, the fragments were used like that. For experiments with isolated sclera or with choroid- Bruch's membrane, the choroid-Bruch's membrane was detached using forceps, cutting with a scalpel the vessels engaged in the sclera (Figure 5, panel F). The isolated sclera fragments were wrapped in parafilm, frozen at -80 °C for at least 24 hour, and then kept at -20 °C up to the moment of use, while the bilayer choroid-Bruch's membrane was used fresh.

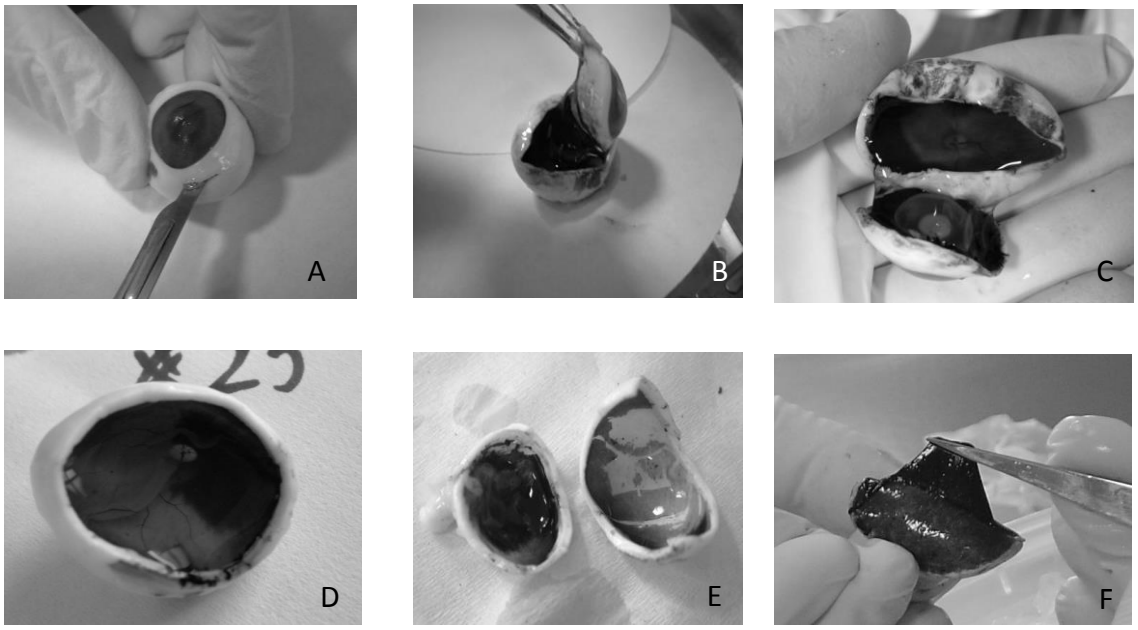

Figure 5 Tissue separation from fresh excised porcine globes.

Prior to use the fragments were thawed for 1 hour at room temperature still wrapped in parafilm.

4.3.4 Cytochrome c stability

Cytochrome c stability to current application and magnetic stirring were evaluated.

Stability to current was evaluated by applying 3.5 mA, using salt bridges, to a 100 µg/ml solution of cytochrome c in HEPES buffer pH 7.4. Samples were taken after 1 and 2 hours and then analyzed by HPLC.

In order to assess cyt c stability to magnetic stirring, three ml of a solution of cytochrome c in HEPES buffer pH 7.4 (25 and 100 µg/ml) were put under constant magnetic stirring on a stirrer plate at 350 rpm. The conditions chosen were similar to what happened in the permeation

experiments. Samples were taken at times 0, 5, 24 and 48 h and analyzed by HPLC-UV. Non-stirred solution were used as controls. Each experiment was performed in triplicate.

4.3.5 Partition coefficient determination

Partitioning experiments were performed in order to determine the partition coefficient of cytochrome c between HEPES buffer and sclera [43].

Scleral fragments were cut in small pieces and 100 mg were exactly weighed. Each sample was put in contact with 1 ml of cytochrome c solution in HEPES buffer (concentrations tested 50, 500, 1000, 5000 µg/ml). The samples were agitated manually every 30 minutes. After 4 hours they were centrifuged and the supernatant was analyzed by HPLC-UV to determine cyt c residual content.

Partition coefficient was then calculated according to Equation 6:

$$K_{par} = \frac{[C_{sclera}]}{[C_{HEPES}]} = \frac{(Q_{i\,HEPES} - Q_{f\,HEPES})}{(Q_{f\,HEPES})} \times \left(\frac{V_{HEPES}}{V_{sclera}}\right)$$

Equation 6

C_{sclera} and C_{HEPES} indicate respectively cyt c concentration in the sclera and in HEPES buffer (after partitioning). $Q_{i\,HEPES}$ and $Q_{f\,HEPES}$ represent respectively the amount of free cytochrome c in the buffer at the beginning and at the end of the experiment. V_{sclera} was calculated from the weight, assuming a density= 1 g/ml.

Each experiment was performed in triplicate.

4.3.6 Binding experiments

Binding experiments were performed in vitro using melanin from *Sepia Officinalis*. 1.5 mg of melanin were exactly weighted in a glass vial, then 0.75 ml of HEPES buffered saline or distilled water was added. The so-obtained suspension was sonicated for 20 minutes, then 0.75 ml cytochrome c solution, with concentration ranging from 0.8 to 40 µM (10-500 µg/ml), was added. The suspensions were incubated at 25 °c for 1 hour under magnetic stirring, after that they were centrifuged at 12000 rpm at room temperature for 10 min. The supernatant was aspirated and analyzed by HPLC-UV.

The interaction between a drug and granules of melanin can be considered similar to the adsorption of a drug on a solid, thus data were processed with Langmuir type I binding isotherm:

$$B = \frac{B_{max} \times [L]}{K_d + [L]}$$

Equation 7

Where B is the observed amount of ligand bound per mg of melanin (nmol/mg), $[L]$ is the free concentration of the ligand (µM), B_{max} is the maximum binding of the ligand to melanin (nmol/mg) and K_d is the equilibrium dissociation constant for the binding complex ligand-melanin (µM).

4.3.7 Experimental set-up

Permeation experiments were performed in Franz-type vertical diffusion cells with an area of 0.6 cm² when sclera or trilayer (sclera-choroid-Bruch's membrane) were employed, or 0.2 cm² when isolated choroid-Bruch's membrane was used. The tissue was mounted with the scleral side facing the donor chamber. The receptor compartment contained 4 ml of degassed HEPES buffered saline (pH 7.4). It was thermostatted at 37 °C and kept under constant magnetic stirring to avoid any boundary layer effect. The donor compartment contained 0.3 ml of a cytochrome c solution. Samples of 0.3 ml were taken from the receptor compartment at predetermined time intervals (0, 30, 60, 80, 100, 120, 180, 240, 300 min) and analyzed by HPLC-UV.

Passive permeation was evaluated across isolated sclera and across the trilayer at different donor solution concentrations: 5, 10, 40 (only isolated sclera) and 70 mg/ml. Passive permeation across the bilayer choroid-Bruch's membrane, coming from both pigmented and not pigmented eyes [44], was assessed at 0.5 mg/ml. Donor solutions were prepared in HEPES buffered saline.

In current assisted experiments anodal iontophoresis was applied with a constant current generator (Iono 1, Cosmic, Pesaro, Italy) connected with a multimeter (MK 7701 Mitek, NL Industries, Milano, Italy) to silver/silver chloride electrodes. The electrodes were connected to the cell via salt bridges, made of agar 2% in KCl 1 M, in order to avoid direct contact of the electrode with cyt c. Current was applied for 2 hours and permeation was followed up to 5

hours. An example of experimental set-up for a current assisted experiment is shown in Figure 6.

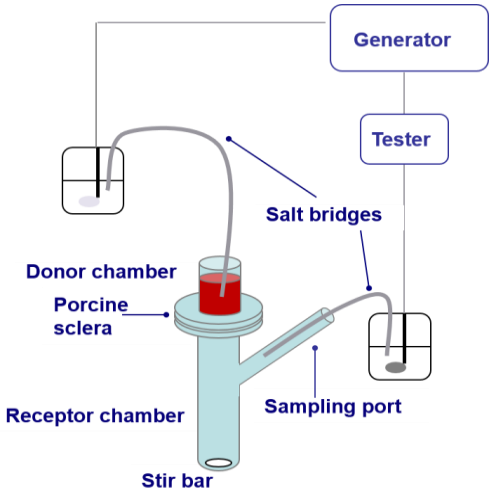

Figure 6 Experimental set-up for current assisted permeation experiments

The effect of different parameters, known to influence iontophoretic transport, was evaluated. The effect of vehicle composition, current density and donor solution concentration were tested. The effect of pH on cytochrome c iontophoretic permeation was determined by varying the pH of a donor solution of cytochrome c (40 mg/ml) in citrate buffer 25 mM.

Current assisted experiments were also performed adding a hydrogel-forming polymer to the donor solution, in order to evaluate the effect on cyt c permeation. Different polymers were tested, both charged and neutral: Eudragit® FS 30D, Acritamer® 940, Alginic acid, Kollidon® K90, Lutrol® F127 and alginate. As a first step, compatibility between the polymer and cytochrome c was determined by mixing a polymer solution with cytochrome c. Two neutral polymers (Lutrol® F127 and Kollidon® K90) and a negatively charged one (Alginate) were selected as donors for iontophoretic permeation. The different experimental conditions tested are shown in Table 1.

Table 1 Experimental conditions for current assisted experiments

Vehicle	Donor concentration (mg/ml)	Current density (mA/cm^2)	Aim
HEPES	10	2.92	Evaluation of the effect of buffer composition
PBS			
Water			
Borate buffer (pH 6.4)	40		
Citrate buffer (pH 4)	40	2.92	Evaluation of the effect of buffer pH and composition
Citrate buffer (pH 6.1)			
Citrate buffer (pH 8.1)			
HEPES	10	1.51	Evaluation of current density effect
		2.92	
		5.83	
HEPES	5	2.92	Evaluation of donor solution concentration
	10		
	40		
	70		
Lutrol® F127 8.35% in H_2O (pH=7.25)	10	2.92	Evaluation of the effect of polymers
Kollidon® K90 5% in H_2O (pH=6.93)			
Alginate 0.75% in H_2O (pH=8.2)			

In order to evaluate the contribution of electroosmotic flow to cytochrome c permeation, and to determine the effect of cytochrome c itself on electroosmotic flow, passive and current

assisted experiments were carried out following the permeation of a neutral marker, fluorescein isothyocyanate dextran (FD-150, M.W.~ 120 kDa, 1 mg/ml), in presence or in absence of cytochrome c. In these experiments, cytochrome c concentration was 1, 5 or 70 mg/ml, and 2.92 mA/cm^2 were applied for 2 hours, then current was discontinued and passive permeation was followed for 3 more hours.

4.3.8 Modulation of the release

The possibility of tuning cytochrome c permeation rate was evaluated alternating current at different densities and passive permeation in the same experiment (Table 2). A cyt c solution 70 mg/ml in HEPES buffered saline was placed in the donor compartment.

Table 2 Iontophoresis application schedule for modulation of the release assessment

Time (min)	Current density (mA/cm^2)
0-80	2.92
81-120	0
121-180	5.83
181-240	0
241-300	2.92

Samples were taken at time points 0, 30, 60, 80, 100, 120, 180, 240, 300 min.

4.3.9 Cytochrome c analysis

Cytochrome c was analyzed by HPLC-UV (Flexar, Perkin Elmer, Norwalk, CT, USA). The column was a Jupiter C18, 5 µm silica reversed particles, 150*4.6 mm produced by Phenomenex, LePecq, France, equipped with a security guard pre-column (Security Widepore).

The mobile phase was composed by:

A (aqueous): 0.1% TFA in H_2O:CH_3CN 95:5 (V/V)

B (organic): 0.1% TFA in CH_3CN

Flux was set at 1.6 ml/min and gradient elution was performed with the following scheme:

STEP	TIME (min)	%A	%B
1	0	75	25
2	6	45	55
3	3	45	55
4	3	75	25

Run time was set to 12 min, retention time of cytochrome c was about 4.5 min.

The obtained peaks were integrated using Chromera software.

Linearity was obtained in the range 5-500 µg/ml. LLOQ (Lower Limit Of Quantification) and LOD (Limit Of Detection) were respectively 5 and 2.5 µg/ml.

4.3.10 FD-150 analysis

FD-150 containing samples were analyzed without further separation using a fluorescence microplate reader (Viktor^3 1420 (Wallac), Perkin Elmer, Walthman, CT, USA).

λ_{ex} was set at 485 nm, while λ_{em} at 535 nm.

LOD was 12 ng/ml, while LLOQ 25 ng/ml.

4.3.11 Data analysis

Trans-scleral flux (J, µg/cm^{2}h) was calculated as the slope of the regression line at steady state. Instantaneous fluxes, on the contrary, were obtained from the slopes (ΔQ/Δt) for all the time points. ΔQ represents the variation of the cumulative amount permeated, while Δt is the time interval expressed in minutes. Permeability coefficient (P, cm/s) was determined at steady state with the following equation:

$$P = \frac{J}{C_d}$$

Equation 8

Where J is the flux, and C_d is the donor solution concentration.

Time lag (min) was represented by the intercept of the regression line at steady state.

Since steady state was not reached in every condition tested, in order to determine the effect of the application of current, enhancement factors were calculated as follows:

$$EF = \frac{Q_{ionto}}{Q_{passive}}$$

Equation 9

Where Q is the amount permeated after 2 hours respectively in current assisted and passive permeation experiments.

Inhibition Factors (IF) were determined to quantify the hindering effect of cytochrome c on electroosmotic flow:

$$IF = \frac{Q_{FD150\ control}}{Q_{FD150\ Cyt}}$$

Equation 10

$Q_{FD150\ control}$ and $Q_{FD150\ Cyt}$ are respectively the cumulative amounts of FD-150 permeated in absence and presence of cytochrome c in the donor solution.

Statistically significant differences were assessed using one-way ANOVA followed by Bonferroni correction ($p<0.05$).

Data are reported ±SEM (standard error of the mean).

4.4 Results and discussion

4.4.1 Cytochrome c stability

Cytochrome c was chosen as model compound because of its well defined structure and the presence, at physiological pH, of positive charges that could drive electromigration, as well as for its stability in a wide range of experimental conditions [45]. However, preliminary data suggested that this molecule may have a limited stability in presence of magnetic stirring, used to avoid the boundary layer in the receptor solution. Cytochrome c stability to magnetic stirring and to current application was then evaluated. Constant magnetic stirring compromised cytochrome c stability. As shown in Figure 7, after 48 hours the amount of cytochrome c in the solution was significantly reduced to about 40 % for both the concentrations tested. After 5 hours, cytochrome c concentration was respectively 93.52±3.76 % and 98.20±0.46 % of the initial values for 25 and 100 µg/ml, then this was chosen as maximum duration for the permeation experiments performed.

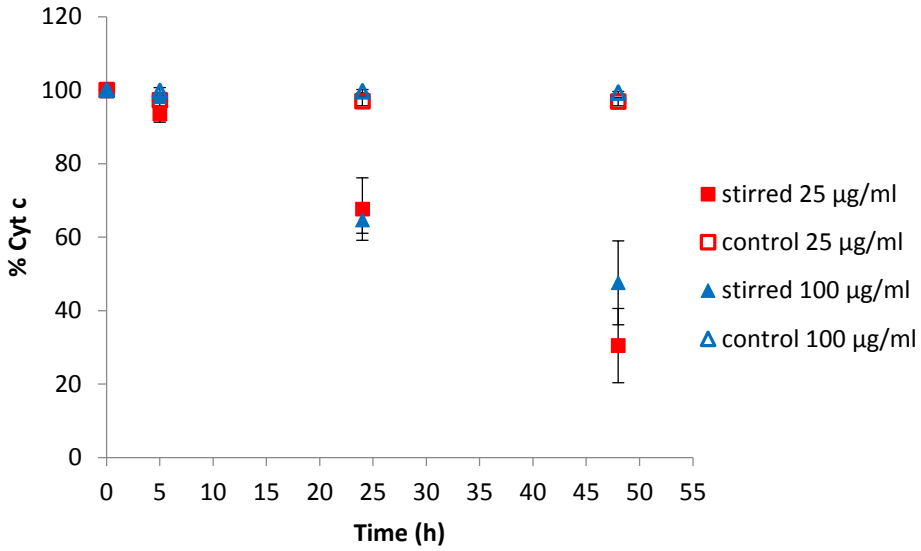

Figure 7 Effect of constant magnetic stirring on cytochrome c stability.

Cytochrome c was stable upon current application: after 2 hours at 3.5 mA, the highest current intensity tested, the loss in cyt c concentration was less than 10% (data not shown). Moreover, no variations in peak shape or symmetry were noticed by HPLC analysis.

4.4.2 Determination of the partition coefficient

The partition coefficients (K_{par}) between HEPES buffer and sclera were determined for 4 concentrations of cytochrome c. The aim was to evaluate the affinity between cytochrome c and the scleral tissue.

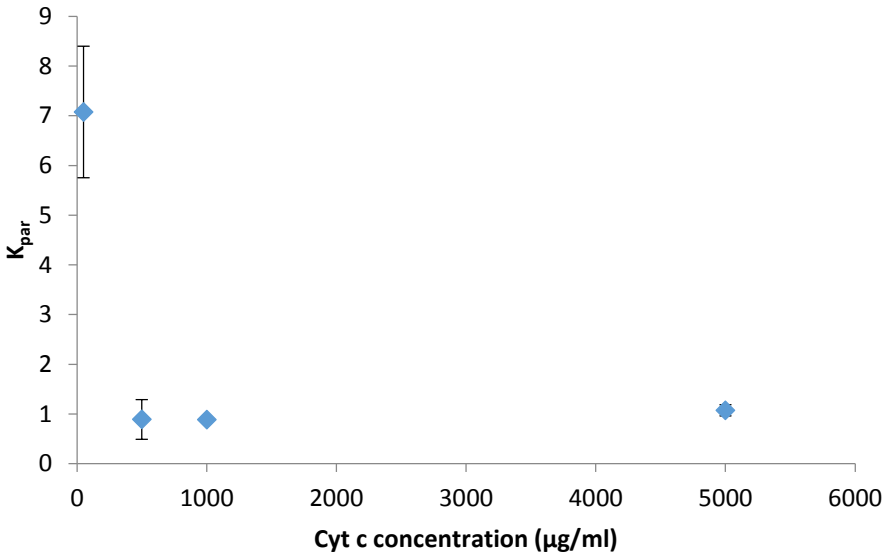

Figure 8 Partition coefficients as a function of cytochrome c concentration

The results obtained (Figure 8) show a low affinity of cytochrome c for the tissue.

Table 3 show the K_{par} values and the amount bound per mg of tissue for each concentration.

Table 3 Partition coefficient (K_{par}) and Amount bound to the sclera for different cytochrome c concentrations.

Cyt c concentration (µg/ml)	K_{par}	Q_{bound} (µg/mg)
50	6.86±1.27	0.21± 0.03
500	0.66± 0.27	0.21 ±0.12
1000	0.88± 0.02	0.81± 0.01
5000	1.07±0.11	4.63±0.39

The highest partition value was obtained for the lowest concentration, while the other three are significantly lower and similar among them. This result suggests that there is not a real partition, but a superficial adsorption phenomenon, ascribable to the binding of the positive charged cytochrome c to the negative charges carried by surface glycosaminoglycan groups on the sclera.

The amount of cyt c bound per mg of tissue (Q_{bound}) increases as a function of its concentration, and, although there is no difference between 50 and 500 µg/ml, raising the concentration to 5000 µg/ml led to a significant increase in the amount bound. This result contributes to explain the effect of cytochrome c on electroosmotic flow, and will be further discussed in section 4.4.5.4.

4.4.3 Passive permeation

Cytochrome c passive permeation across isolated sclera was evaluated at different concentrations (Figure 9).

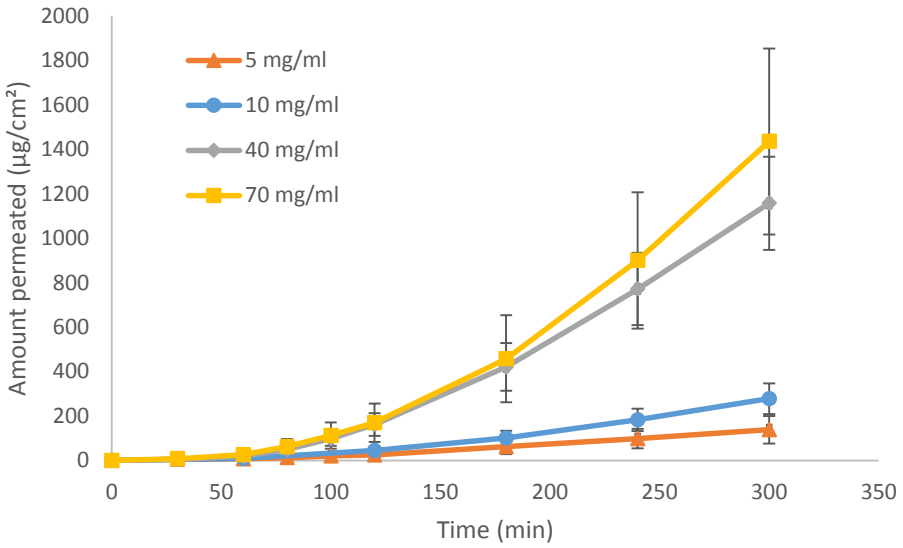

Figure 9 Passive permeation of cytochrome c across isolated sclera at different donor concentrations.

Steady state was reached after 2 hours of passive permeation. The fluxes, calculated from the slope of the regression line at steady state, increased linearly with the raise of cytochrome c concentration in the donor solution, as shown in Figure 10. Permeability coefficient resulted approximately $2.5*10^{-6}$ cm/s, in agreement with literature data obtained with molecules of comparable hydrodynamic radius [23].

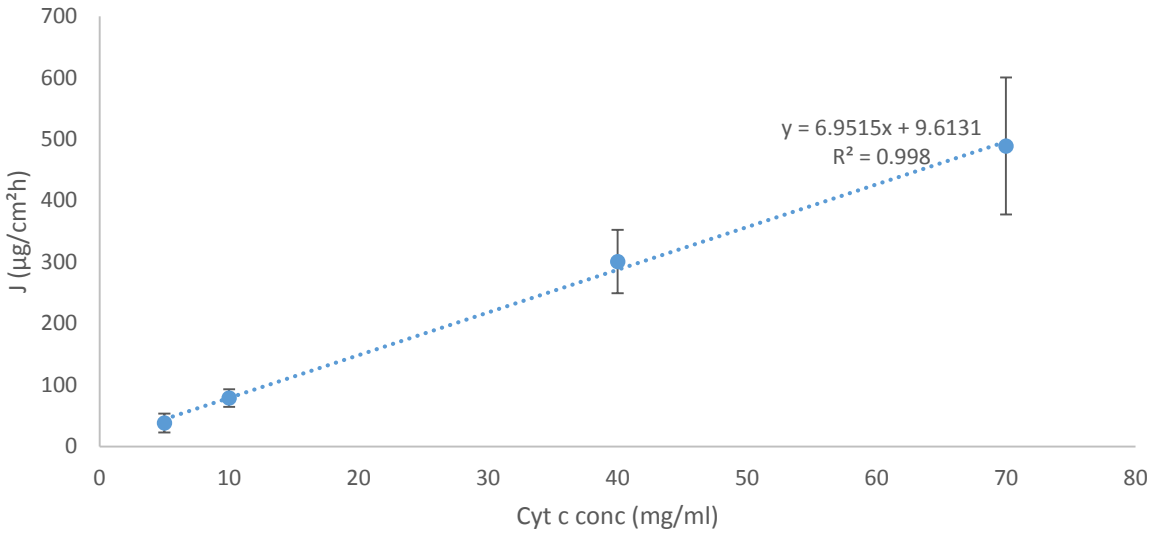

Figure 10 Passive fluxes of cytochrome c across isolated porcine sclera, calculated between 120 and 300 minutes from solutions at different concentrations.

Since the sclera is only the first barrier that molecules have to cross in order to reach the posterior segment, passive permeation was evaluated also across the trilayer (sclera-choroid and Bruch's membrane). The permeation profiles illustrated in Figure 11 show that the presence of choroid-Bruch's layer hindered cytochrome c permeation, as expected. No permeation was detectable at 5 mg/ml. Moreover, steady state was not reached, so it was impossible to calculate the fluxes and permeability coefficients. The presence of this further barrier brought to a 7-fold reduction in the amount permeated after 5 hours compared to isolated sclera.

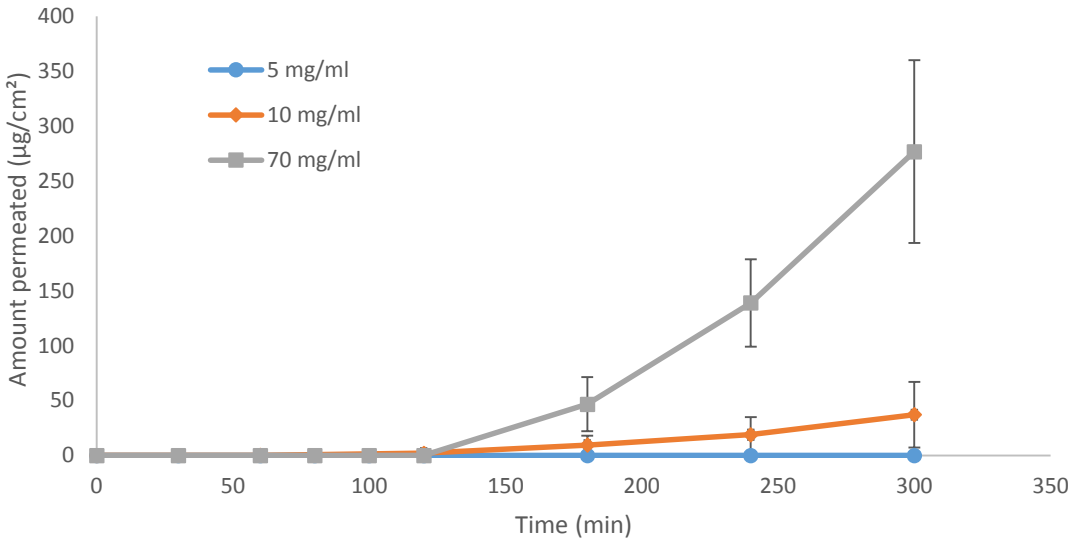

Figure 11 cytochrome c passive permeation across the trilayer (sclera-choroid-Bruch's membrane) from 5, 10 or 70 mg/ml donor solutions.

This effect can be ascribable to the barrier properties of the tissue itself [43, 46], but also to an unfavorable partition of the drug between the sclera and the choroid layer or the presence of non-aligned penetration pores in the two tissues. Another reason for the limited permeation is the consistent presence in the choroid of melanin, reported to be able to bind positively charged molecules with high affinity [47].

Given the results obtained from passive permeation across the trilayer, the affinity of cytochrome c for melanin was evaluated by comparing permeation across pigmented and not pigmented choroid-Bruch's bilayer [44]. Pigmented tissue is found in brown eyes and contains melanin, which is absent in the not pigmented one, that comes from light blue eyes. The steady state fluxes obtained (Figure 12) were similar, but when pigmented epithelium was used, time-lag raised to 80 minutes, thus suggesting an interaction of the molecule with melanin.

In order to further investigate the interaction between cytochrome c and melanin, binding studies were performed using two different vehicles (HEPES buffered saline and water) with concentrations of cyt c ranging from 0.8 to 40 µM.

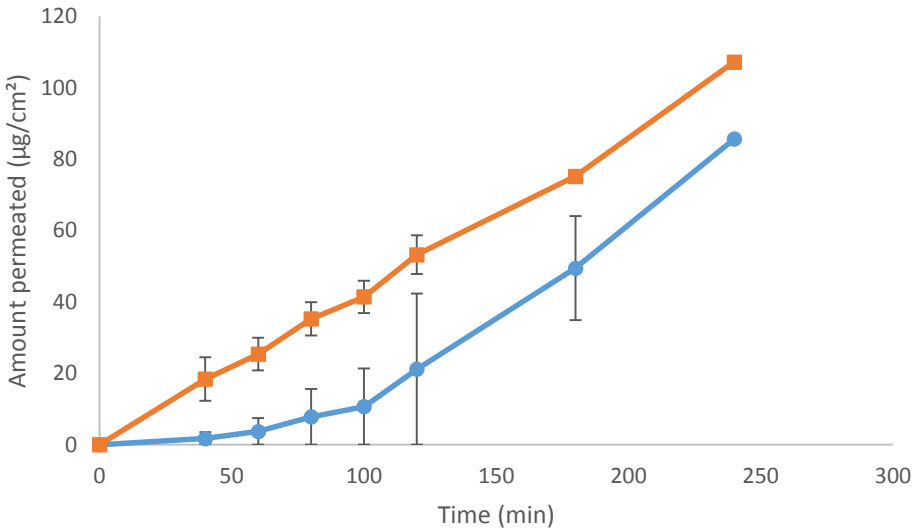

Figure 12 Permeation profiles of cytochrome c across pigmented (blue dots) or not pigmented (orange squares) isolated choroid.

4.4.4 Binding experiments

The results of binding studies, illustrated in Figure 13, show the direct interaction of the molecule with melanin. Even though it is known that melanin has several class of binding sites, data were fit to Langmuir equation assuming only one binding site. This was done because it is almost impossible to predict the different modes of interaction involved in the binding process [44].

The results of data processing also underline the dependence of the binding from the ionic strength of the vehicle: the interaction is in fact stronger in water (B_{max} 10.6 ng/mg; K_d 0.06 µM) than in HEPES buffered saline (B_{max} 4.2 ng/mg; K_d 1.49 µM). This result suggests that it could be possible to modulate the binding modifying the vehicle ionic strength, in order to maximize the extent of permeation.

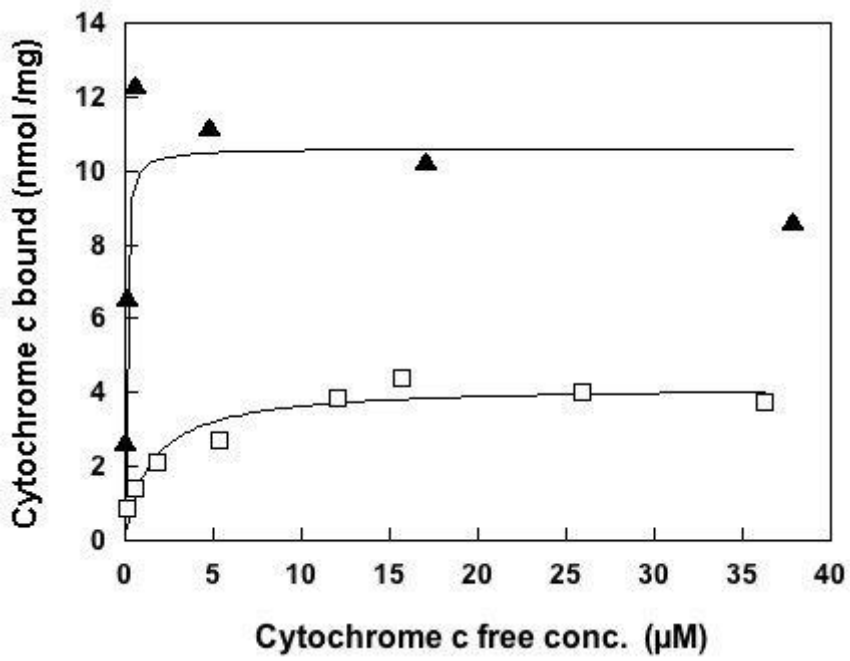

Figure 13 Binding curve of cytochrome c to spray dried melanin from *Sepia Officinalis* in water (full triangles) and HEPES buffered saline (void squares). The figure represents the amount of cytochrome c bound per mg of melanin as a function of the free cytochrome present in solution.

4.4.5 Current assisted experiments

Data presented hitherto suggest that trans-scleral administration of positively charged macromolecules is achievable. Nonetheless, other ocular barriers are present in vivo beyond the sclera and the choroid-Bruch's membrane, such as the choroidal circulation and the retinal pigmented epithelium. Thus, a high and sustained penetration across the sclera is required in order to reach a substantial concentration at the interface with the underlying barriers. Trans-scleral iontophoresis represents a possible enhancement approach.

4.4.5.1 Effect of donor solution concentration

Current assisted experiments were performed across isolated sclera. Cytochrome c is a polypeptide with 12 negatively charged aminoacidic residues (Glutamate and Aspartate) and 21 positively charged (Lysine and Arginine). Its isoelectric point is 10.0, and at pH 8.2 carries a net positive charge of +7.9, thus anodal iontophoresis was applied.

The effect of cytochrome c concentration in the donor solution on the extent of permeation was assessed applying 2.92 mA/cm² for 2 hours (Figure 14). Current application led to a remarkable increase in the protein permeation across isolated sclera at all the concentration tested.

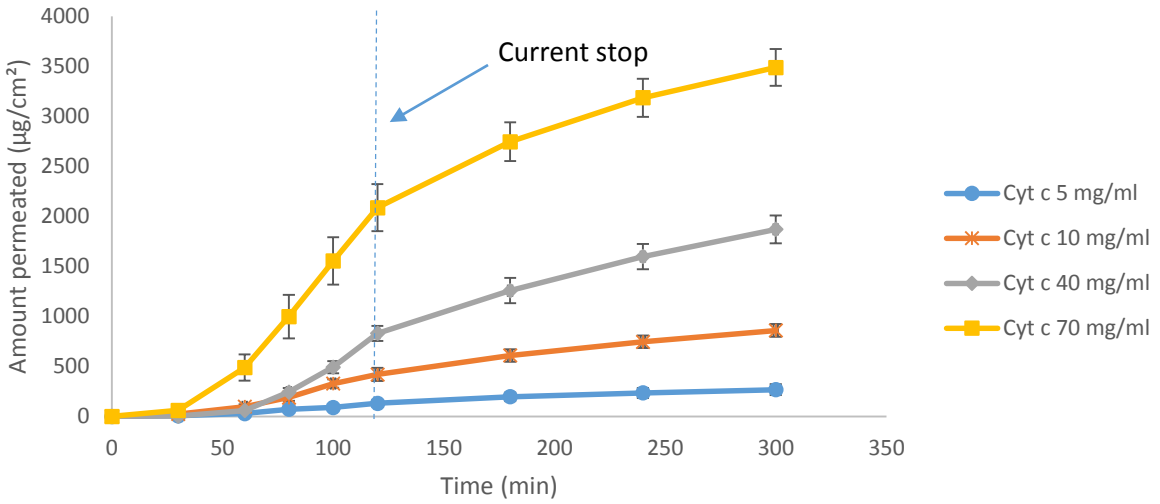

Figure 14 Effect of cytochrome c concentration on trans-scleral permeation. Current applied for 2 hours (2.92 mA/cm²)

Enhancement factors, calculated on the amount permeated after 2-hour iontophoresis, as well fluxes, permeability coefficients and time-lag values, determined at steady state, are shown in Table 4.

Table 4 Steady state parameters and enhancement factors as a function of donor concentration.

Donor concentration (mg/ml)	J (µg/cm²h)	P*10⁻⁶ (cm/s)	Time-lag (min)	EFq
5	101.12 ±26.3	5.62 ±1.46	49 ±8	5.3±3.8
10	389.28± 21.57	1.09±0.03	40±5	10.6±4.1
40	876.80± 55.11	6.09± 3.83	64 ±2	8.9±1.4
70	1635± 40.44	6.49± 1.60	43 ±8	12.3±2.5

Figure 15 illustrates the amount permeated as a function of cytochrome c concentration in the donor solution after 2 h iontophoretic permeation. The increase was not strictly proportional to the raise in concentration. This can be ascribable to the different relative contribution of the two iontophoretic transport mechanisms, electrorepulsion and electroosmosis, at different concentrations.

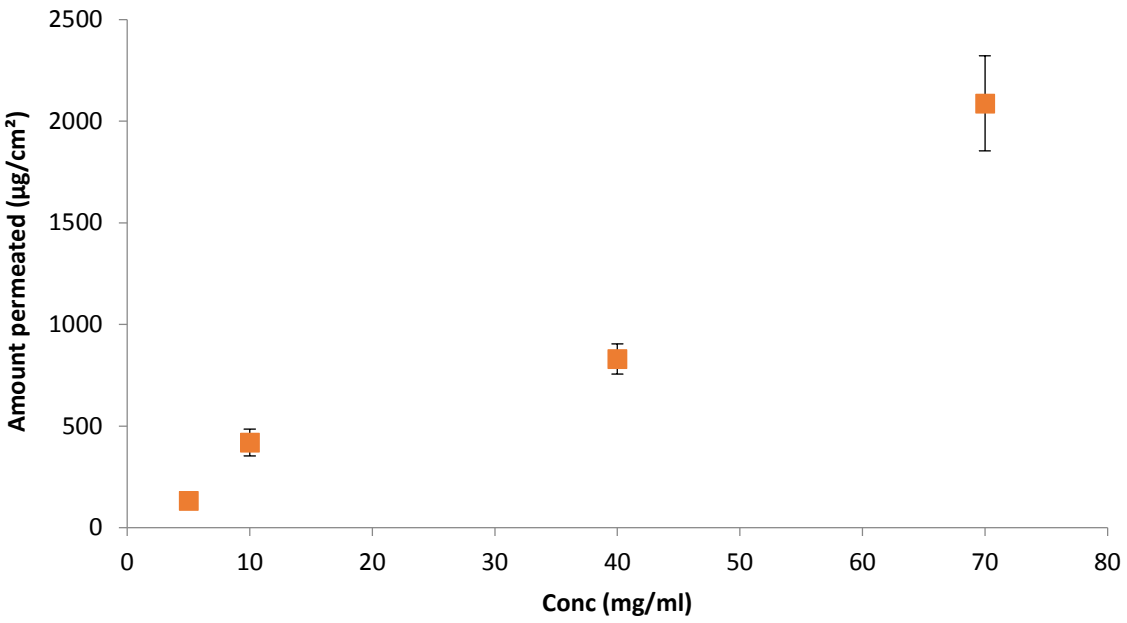

Figure 15 Amount permeated after 2-hour permeation (iontophoresis 2.92 mA/cm²) as a function of donor solution concentration.

After 2 hours current was stopped and the values of flux and permeability coefficients returned close to passive ones (Table 5). This result suggests that iontophoresis application caused neither an increase in scleral permeability nor a significant accumulation of cytochrome c in this tissue.

Table 5 Post iontophoretic fluxes and permeability coefficients

Donor concentration (mg/ml)	$J_{post\ ionto}$ (µg/cm²h)	J_{pass}(µg/cm²h)	$P_{post\ ionto}$ (cm/s) 10^{-6}	P_{pass} (cm/s) 10^{-6}
5	38.01± 6.2	38.39±15.42	1.95± 0.37	1.94±0.12
10	125.4±12	78.92±14.42	3.48±0.41	2.19±0.4
40	306.2 ±9.93	301.05±51.49	2.13 ±0.07	2.55±0.36
70	471 ±67.3	489.03±111.58	1.87± 0.27	2.13±0.44

4.4.5.2 Effect of vehicle composition

Vehicle composition is known to influence iontophoretic transport of macromolecules across the sclera for different reasons [46]. Indeed, the buffer can have a direct effect on the three-dimensional structure of cytochrome c, which could bring to exposure on the surface of more charges. Moreover, the presence in the vehicle of small ions, such as Na^+, with high electrophoretic mobility, can hinder the transport of bigger molecules. Thus, three vehicles, with different ionic strength, were tested to assess their effect on iontophoretic transport. Donor solutions of cytochrome c (10 mg/ml) were prepared in PBS (ionic strength 194 mM, pH=7.4), HEPES buffered saline (ionic strength 150 mM, pH=7.4) and distilled water (absence of co-ions, possible presence of K^+ and Cl^- deriving from leakage from the salt bridges, pH=9).

Figure 16 illustrates the permeation profiles obtained after current assisted permeation of cytochrome c. Despite the differences in buffer and ionic strength, no statistically significant difference was noticed.

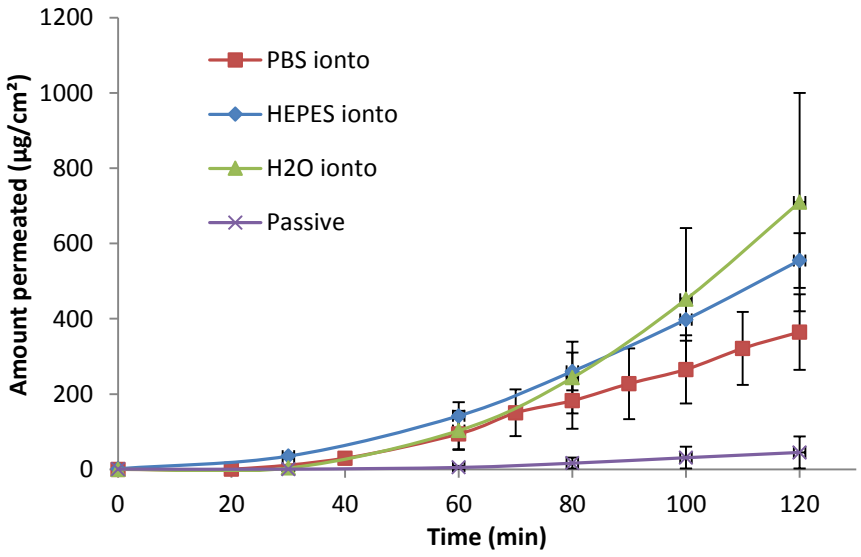

Figure 16 Permeation profiles of cytochrome c (10 mg/ml) from water, HEPES buffer and water. Current applied for 2 hours (2.92 mA/cm²).

Table 6 shows the fluxes, permeability coefficients and time-lag values calculated at steady state for the different vehicles tested.

Table 6 Fluxes (J), Permeability coefficients (P) and Time lag values calculated for different vehicles at steady state (80-120 min)

Vehicle	J (µg/cm²h)	P (cm/s) (*10^{-6})	Time-lag (min)
Water	578.53±40.99	16.1±5.05	57.08±5.30
HEPES	389.28±21.57	10.8±0.6	45.19±5.45
PBS	298.20±60.95	8.28±1.69	45.15±13.81

The fluxes and permeability coefficients result higher in distilled water, even though the difference is not statistically significant. Two different explanations to this trend can be hypothesized: first of all, the presence in the buffers of competitor ions with higher electrophoretic mobilities, but also the different charge of cytochrome c in different vehicles. It has been demonstrated, in fact, that its charge varies as a function of vehicle ionic strength, and in distilled water is higher than in buffered solutions [48].

In order to further evaluate the effect of buffers, also borate and citrate, both 25 mM, were used as donors in iontophoretic permeation of cytochrome c (40 mg/ml). The pH of the borate buffer was 6.4, while the pH of citrate buffer was 6.1. Permeation from citrate buffer is significantly higher than from borate (Figure 17). After 120 min, the amount permeated were respectively 1835.23±376.26 and 589.77±135.27 µg/cm², thus from citrate the amount permeated is 3 times higher.

The lower iontophoretic permeation of cytochrome c from borate buffer can be explained considering that this protein binds the tetrahedral borate anion. This interaction takes place at three different sites, and involves Lysine residues on the surface [49, 50]: in this way, part of the surface positive charge of the molecule is neutralized, reducing the electromigratory contribution. Moreover, binding of tetraborate can increase cyt c hydrodynamic radius, thus further reducing its mobility. Another possible explanation is linked to the effect of the citrate on electroosmotic flow. It has in fact been shown, in iontophoretic experiments across the skin, that citrate buffer gives higher electroosmotic flows across the skin compared to other buffers, such as phosphate or bicarbonate. This has been attributed to interactions of its organic backbone with the tissue and subsequent lining of the surface with negative charges that produce an increase in electroosmotic flow [51]. A similar mechanism can be hypothesized also for the sclera.

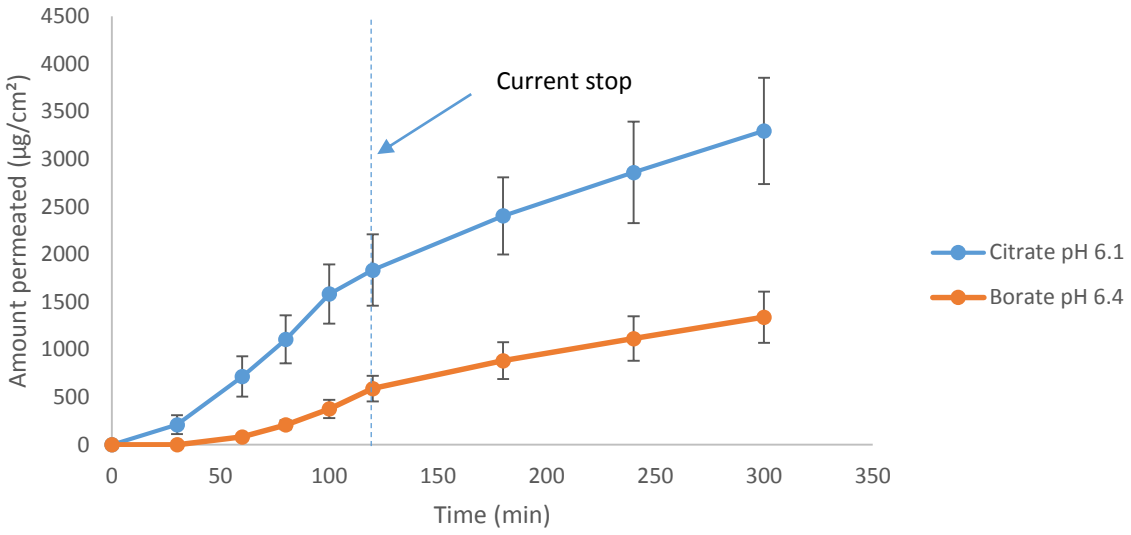

Figure 17 Effect of buffer composition on trans-scleral permeation of cytochrome c (40 mg/ml; iontophoresis applied for 2 hours 2.92 mA/cm²).

The effect of different pH on trans-scleral iontophoresis of cytochrome c was as well evaluated. A 40 mg/ml solution of cytochrome c in citrate buffer (25 mM) at different pH was used as donor solution. At pH 4, the calculated charge is +20, while at pH 6 is +11.6 and at pH 8 only +7.9 (www.protcalc.sourceforge.net). Figure 18 shows the permeation profiles obtained for the different pH. The lowest profile is obtained with the highest pH: this can be explained by the variation in absolute charge of cytochrome c as a function of pH. Quite surprisingly, despite the remarkable difference in calculated charge, there is no difference between the permeation profiles obtained at pH 4 and 6. However, the calculated charge refers to the primary structure, thus it could be inaccurate for folded proteins. Another explanation may be found in the effect of the variation of pH on electroosmotic flow extent. In fact, at pH 4 the contribution of EO flow could be limited or even not present, since it is a value close to the sclera isoelectric point [9, 52].

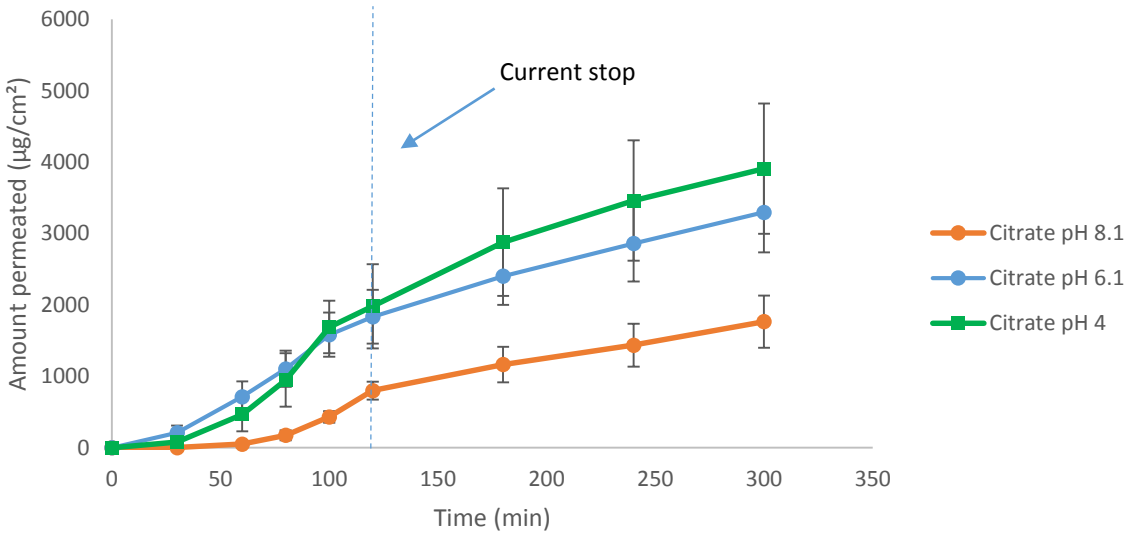

Figure 18 Effect of pH on cytochrome c current assisted permeation (2.92 mA/cm²).

4.4.5.3 Effect of polymers

In this part of the study, different polymers [53] were tested to evaluate their effect on cytochrome c permeation. The first step involved compatibility studies, mixing 1:1 a polymer solution with a cytochrome c solution in water.

The first polymer tested was Eudragit® FS 30 D, an aqueous dispersion of a metacrylic, methyl metacrilate and metacrilic-based anionic copolymer. It is insoluble in acid, while it dissolves at pH 7.

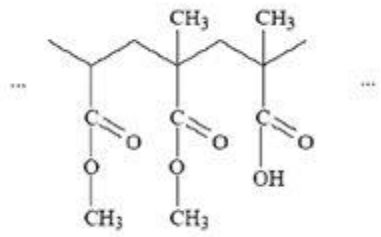

Figure 19 Eudragit® FS 30 D forming unit

After mixing this polymer with cytochrome c solution, a pink mixture formed, but after 5 minutes the 2 phases separated. The second polymer tested was Acritamer® 940, a high molecular weight copolymer of acrylic acid cross-linked with allylsaccarose or allylpentaerithrol. Three different concentrations were tested (0.25, 0.5 and 1%) and were mixed with cytochrome c solution. At all the concentrations tested a dark red precipitate was

formed. The colour of the precipitate was probably due to the acidic pH (=3), while the precipitation depended on the presence of the polymer itself, since it endured even after pH raise. Alginic acid, a blend of polyuronic acids composed by D-mannuronic and glucuronic acid residues, produced again a precipitation and was therefore discarded.

Sodium alginate, on the contrary, did not pose any stability issues. Thus, a 0.75% solution was used as donor solution for cytochrome c.

Neutral polymers were then tested. Kollidon® K90 (Figure 20) is essentially a linear chain of 1-vynyl-2-pyrrolidone residues. A 5% solution did not cause any visible degradation and had a viscosity similar to a water solution.

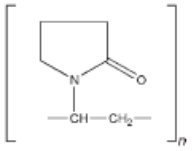

Figure 20 Forming unit of Kollidon® K90

The second neutral polymer was Lutrol® F127 (Poloxamer 407) (Figure 21), a block co-polymer of ethylene oxide and propylene. It has a molecular weight of 12200 and it contains 73% of polyossiethylene. An 8.35% solution was used.

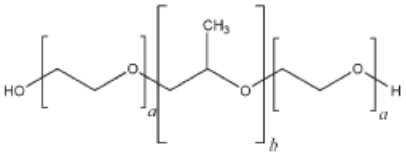

Figure 21 Forming unit of Lutrol 127

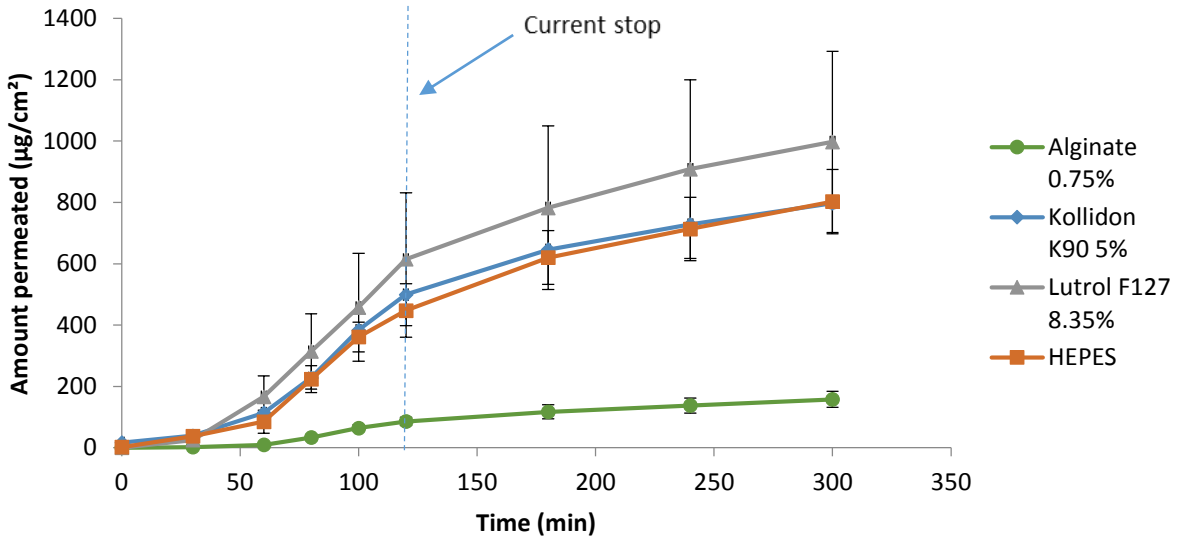

Figure 22 Permeation profiles of cytochrome c (10 mg/ml) from polymer solutions. Current applied for 2 h (2.92 mA/cm²).

Figure 22 shows the effect of the presence of polymer in the donor solution on the current assisted permeation of cytochrome c (10 mg/ml). Neutral polymers had substantially no effect, since the profiles are superimposable with the one obtained from HEPES buffered saline, while alginate, negatively charged, hindered cytochrome c permeation, probably due to charge interactions with the positively charged protein. The cumulative amount permeated after 2 hours, as shown in Figure 23, was 5 times lower for the solution containing alginate, and it was comparable to passive permeation from a buffered solution without polymers.

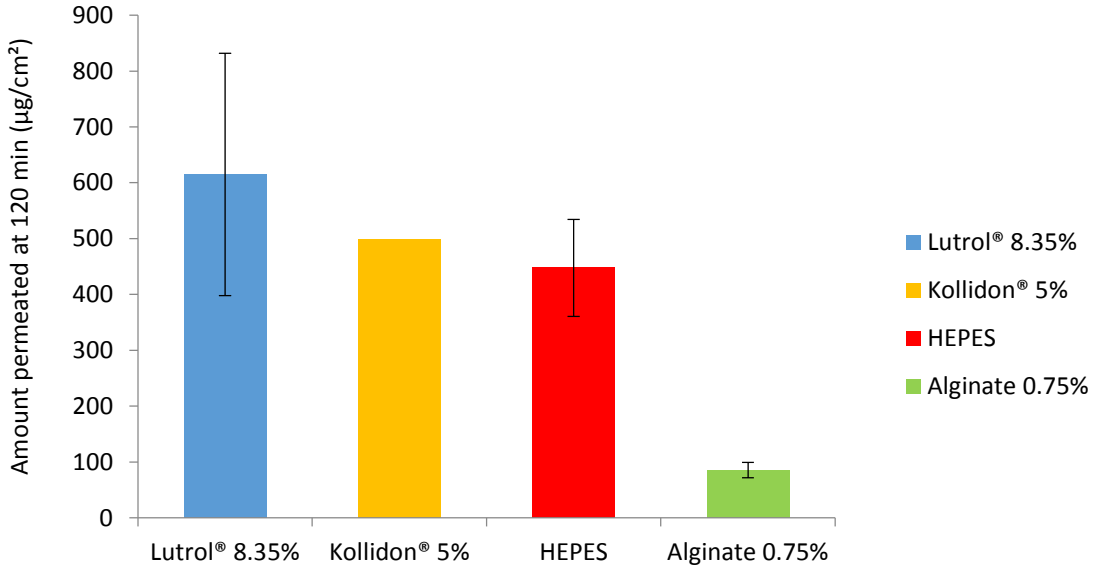

Figure 23 Cumulative amount permeated from polymer solutions after 2 hours anodal iontophoresis (2.92 mA/cm²)

4.4.5.4 FD-150 permeation

Porcine sclera has an isoelectric point between 3 and 4, thus it carries fixed negative charges at physiological pH [9, 52]. This means that, in presence of iontophoresis, there is a convective solvent flow, electroosmotic flow, which is directed from anode to cathode. This flow is the only responsible for the iontophoretic transport of neutral molecules, and can be particularly relevant in the case of macromolecules [9, 37]. However, it has been proposed that negatively [54] and positively [52] charged molecule can interact with the membrane, thus modifying the extent of electroosmotic flow.

The effect of cytochrome c on electroosmotic flow was then assessed using FD-150, a neutral fluorescent marker (M.W. 120 kDa), in passive and current assisted (2.92 mA/cm², 2 h) experiments, with or without cytochrome c. FD-150 was chosen as electroosmotic flow marker by reason of its high M.W. and consequent low passive permeation across the sclera. In absence of cyt c, the amount permeated after 2 h iontophoresis is 25 times higher than passive permeation (Figure 24). This enhancement, as previously stated, is completely ascribable to electroosmotic flow.

FD-150 permeation was then evaluated in the presence of 1, 5 and 70 mg/ml of cytochrome c. The permeation profiles, shown in Figure 24, clearly illustrate that the presence of cytochrome c hindered iontophoretic transport. No inhibition was noticed when 1 mg/ml cytochrome c was present in the donor solution, while inhibition factors were respectively 2.4±0.5 and 3.6±0.3 when cytochrome c was present at the concentrations of 5 and 70 mg/ml.

This behavior can be explained by the adsorption on cytochrome c on the scleral tissue, which implies a reduction of the charge, or even a reversal. Adsorption takes place at 5 mg/ml, while at 1 mg/ml is not significant, as was suggested by the partitioning experiments (section 4.4.2) and was recently demonstrated by streaming potential measurements on bovine and porcine sclera [55].

The experiments have demonstrated that iontophoresis is very effective in enhancing cytochrome c permeation across the sclera. Since it has been demonstrated that its presence strongly inhibits electroosmotic flow, it can be affirmed that the main transport mechanism for cytochrome c in this tissue is electromigration, and not electroosmosis. This result is consistent with what has been obtained in iontophoretic transdermal delivery of cytochrome

c [56], and also with other macromolecules, such as ribonuclease A and ribonuclease T1 [57, 58].

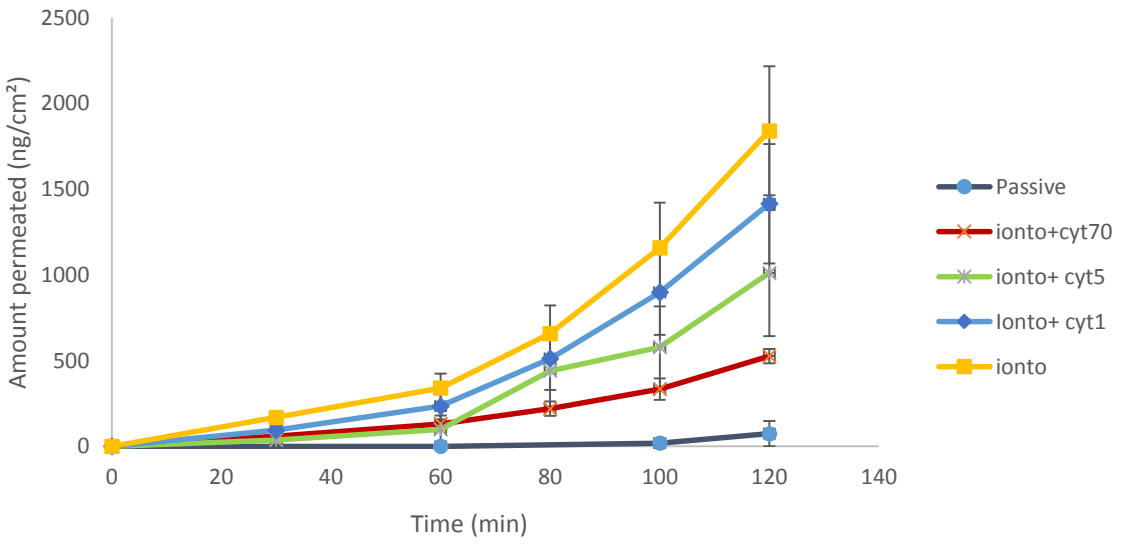

Figure 24 Permeation profiles of FD-150 (1 mg/ml) in passive and iontophoretic (2.92 mA/cm²) conditions in absence and presence of 1, 5 and 70 mg/ml of cytochrome c.

Figure 25 shows the post-iontophoretic phase of FD-150 permeation. In contrast to what happened with cytochrome c, where the permeation profiles quickly decreased after current stop, in the case of FD-150 a sustained release takes place. The explanation could be linked to a high FD-150 accumulation in the tissue during current application. This "reservoir effect" has been demonstrated also for another dextran, FD-40 [46] and is probably due to the hydrophilic nature of both the permeant and the sclera.

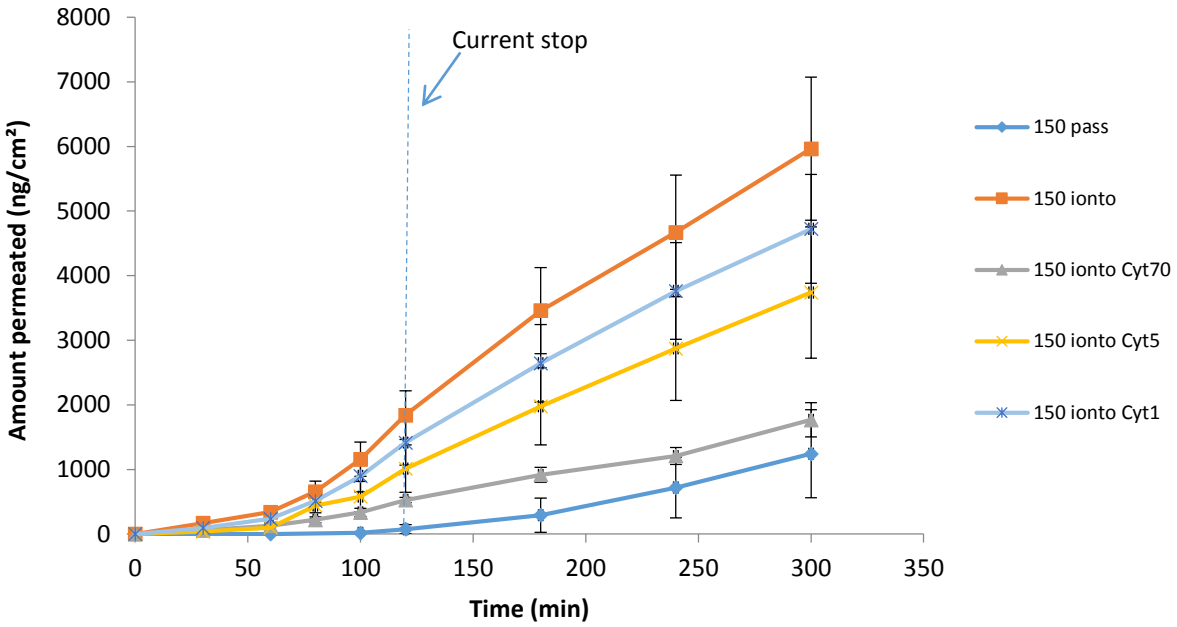

Figure 25 Effect of cytochrome c concentration on FD-150 permeation.

4.4.5.5 *Effect of current density*

Current density is one of the main factors that influence iontophoretic transport; therefore, cytochrome c permeation was evaluated at different current densities (1.51, 2.92 and 5.83 mA/cm²). Figure 27 illustrates the permeation profiles as a function of current density. It can be noticed that even the lowest current applied, 1.51 mA/cm², gives a significant enhancement of the permeation. The fluxes and permeability coefficients, shown in Table 7, raise proportionally with the raise in current density.

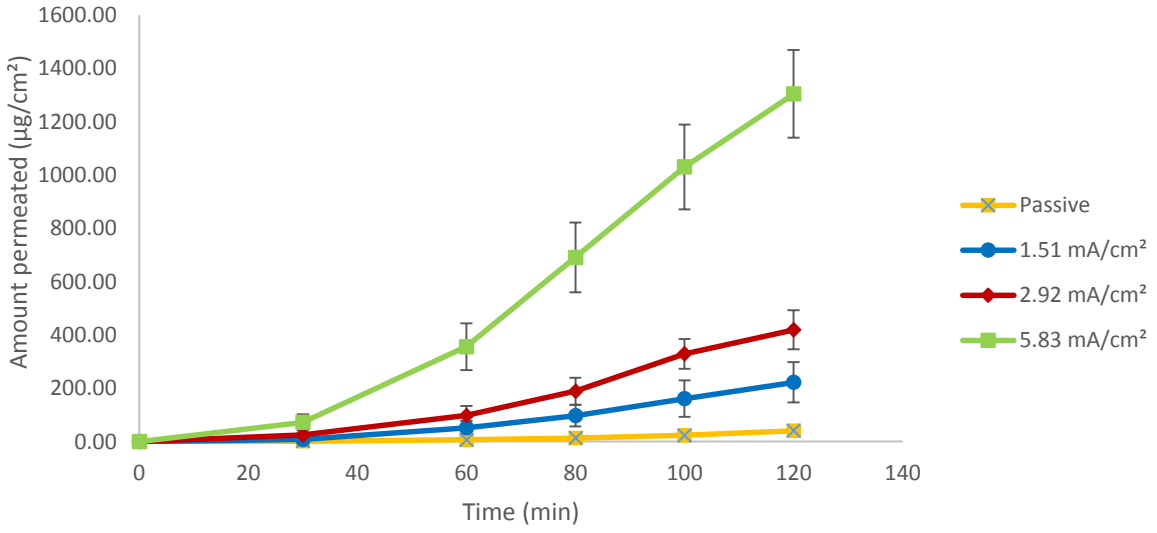

Figure 26 Permeation profiles of cytochrome c as a function of current density (anodal iontophoresis applied for 2 hours).

Table 7 Steady state parameters for different current densities

Current density (mA/cm²)	J iono (µg/cm²h)	P_{iono} (cm/s) *10^{-6}	Time-lag (min)
0	78.92±14.44	2.14±0.4	116±12
1.5	201.42 ±55.98	5.59±1.55	62±7
2.92	389.28± 21,57	10.81±0.60	40±5
5.83	1011.98 ±75.82	28.11±2.11	31±12

The EF (enhancement factors), calculated as the ratio between the amount permeated after 2 hours in iontophoretic and passive permeation resulted 6.0±4.3, 10.6±4.1 and 33.2±8.3 for 1.51, 2.92 and 5.83 mA/cm² respectively. In particular, the application of 5.83 mA/cm² resulted in the delivery of about 3 mg after 5 hours. Moreover, time-lag was significantly reduced from 112 to 31 minutes.

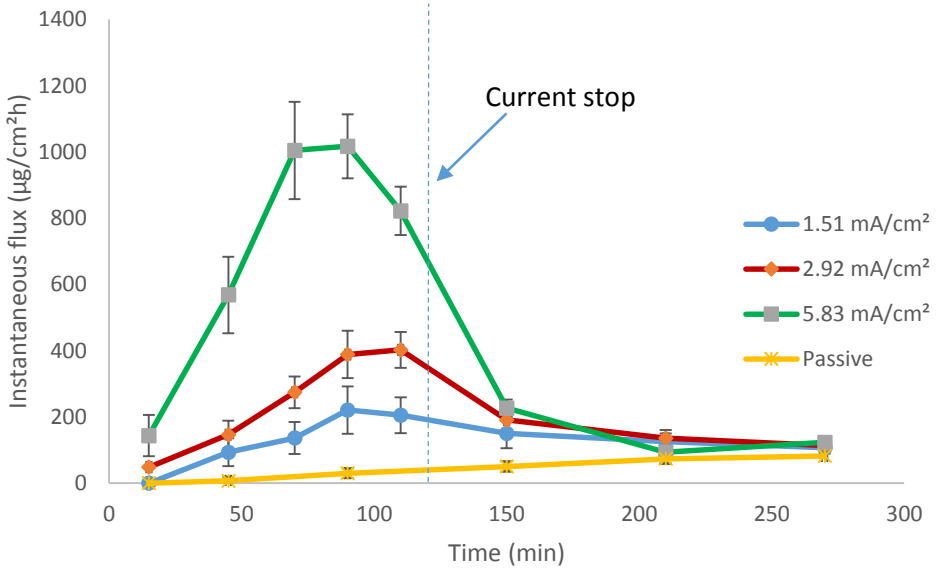

Figure 27 Effect of current density on cytochrome c (10 mg/ml) permeation: instantaneous fluxes in iontophoretic and iontophoretic phase and comparison with passive permeation

Figure 26 shows the instantaneous flux values as a function of current density, and a comparison with passive permeation.

After current stop, the fluxes returned rapidly to values not so different from passive ones for all the current densities tested. As previously stated, this not only indicates the absence of a

permanent modification of permeability due to application of iontophoresis, but also that cytochrome c does not accumulate significantly in the scleral tissue, in contrast to what happens for other molecules such as FD-150. However, the different concentrations used for cytochrome c (10 mg/ml) and FD-150 (1 mg/ml) could contribute to this different post-iontophoretic behavior.

4.4.6 Modulation of the release

The opportunity of a fine tuning of the release was further investigated. Experiments performed alternating anodal iontophoresis and passive permeation showed that a quick modulation of the release was possible (Figure 28).

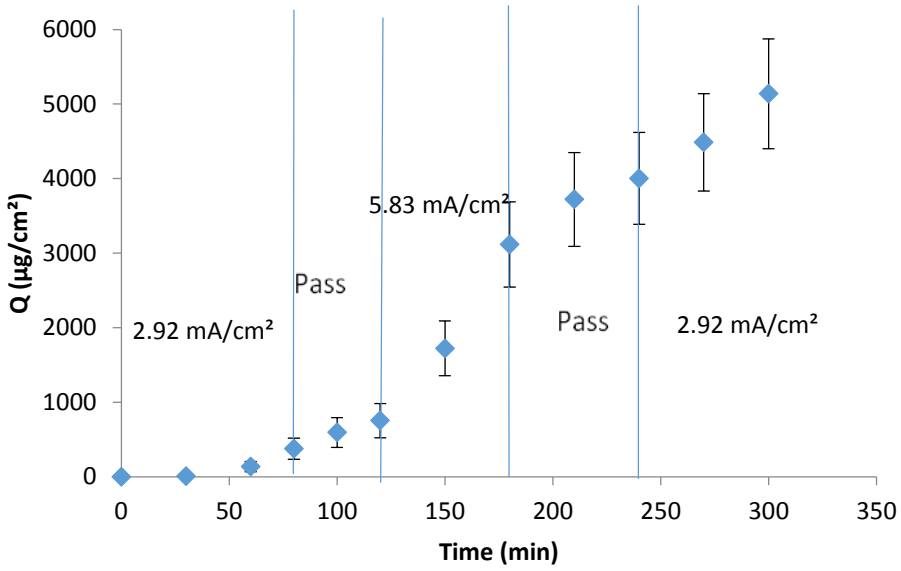

Figure 28 Permeation profile obtained by alternating anodal iontophoresis and passive permeation (cyt c concentration: 70 mg/ml)

Instantaneous fluxes, reported in Figure 29, confirm that, after an initial time necessary to load the tissue, quick changes can be obtained to finely modulate cytochrome c trans-scleral delivery. This result is quite promising, since a system like this could allow for example the physician to increase the dose of the drug when needed or to interrupt immediately the delivery in case of unwanted dose-related effects.

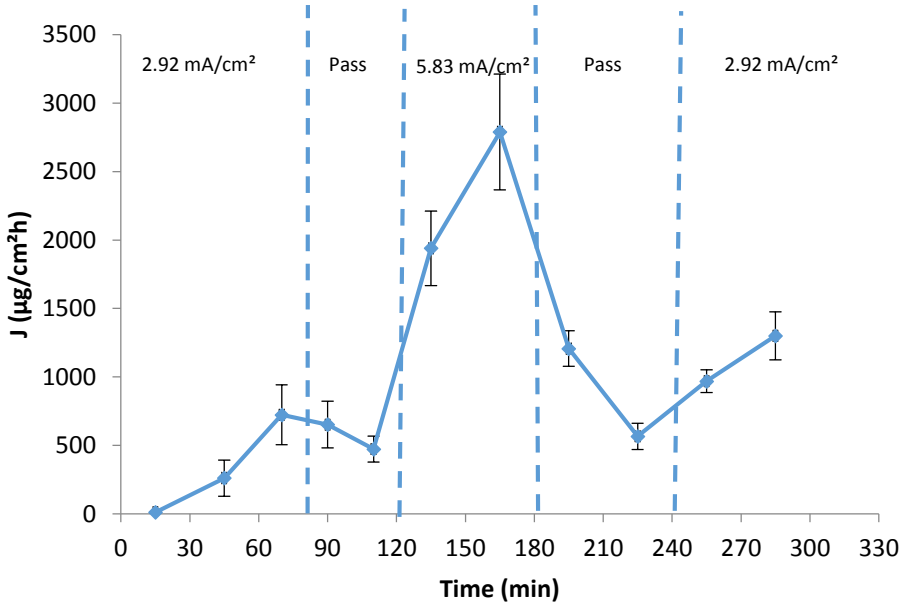

Figure 29 Instantaneous fluxes obtained with a 70 mg/ml cytochrome c solution, alternating constant current and iontophoresis.

4.5 Conclusions- Trans-scleral delivery

Passive permeation of cytochrome c across the sclera was directly proportional to donor solution concentration, and the permeability coefficient was comparable to other molecules of similar radius. The presence of choroid-Bruch's membrane layer represented a significant barrier to permeation, reducing by 7-fold the amount permeated after 5 hours. This was also ascribable to the presence, in the choroid, of melanin, which is able to bind cytochrome c. Anodal iontophoresis greatly enhanced cytochrome c permeation, and the effect was directly proportional to current density applied. An enhancement of 33 times was obtained with the highest current applied, so relevant amounts of drug (up to a few mg) could be delivered. A reduction in the ionic strength of the vehicle did not have a significant effect on cytochrome c, while changing the nature of buffer resulted in a 3-fold increase in the amount permeated. Neutral polymers did not have any effect on cytochrome c transport, while alginate, negatively charged, suppressed cytochrome c permeation. Experiments performed with FD-150 demonstrated that, despite the high molecular weight, the main transport mechanism was electromigration and that cytochrome c hindered electroosmotic flow. Finally, a quick and precise modulation of the release could be obtained by alternating passive permeation and iontophoresis in the same experiment.

Certainly these results are specific for this protein and linked to its properties, such as the high charge/MW ratio, but they can be probably extended to other proteins with similar M.W. and isolelectric point, and more therapeutic interest [59], such as basic fibroblast growth factor (M:W. 17-23 kDa, pI 9.6), interferon γ (M.W. 16 kDa, pI 9.5) and interleukin-10 (M.W. 16 kDa, pI 8.45).

5 Buccal delivery

5.1 State of the art

5.1.1 Anatomy of the mouth

The oral cavity comprises the lips, the cheeks, the tongue, hard and soft palate and floor of the mouth. Each part of the oral cavity is upholstered with mucosal tissue, which can be classified into buccal, sublingual, palatal, gingival and labial mucosa.

There are three histological types of mucosa, depending on their function. The lining mucosa, which accounts for almost 60% of the total surface, is composed by a non-keratinized epithelium that is supported by a thin and elastic lamina propria and submucosa. The specialized gustatory mucosa, 15% of the total surface, presents papillated surfaces, either keratinized or non-keratinized. It is located on the dorsal part of the tongue. The masticatory mucosa can be found on the hard palate and the gums. It has to be resistant to the mechanical stress deriving from mastication, so its superficial cells are keratinized. Moreover, it binds to the periosteum with a thick lamina propria [60].

The primary function of oral epithelium, except for specialized mucosa, is to protect the underlying tissue from fluid loss and to prevent the permeation of potentially harmful substances and microorganisms [61, 62].

The protective function is guaranteed by a stratified epithelium composed of multiple layers of cells. The thickness of the epithelium varies from 100 µm in the sublingual part to a maximum of 600 µm in the buccal part [60]. A fibrous connective tissue gives mechanical support and nourishment to the epithelium.

In addition to keratinocytes, the epithelium contains a small percentage (10%) of different cells, known collectively as nonkeratinocytes. These cells are melanocytes, Langerhans' cells, Merkel cells and inflammatory cells (mainly lymphocytes).

In the cheeks, the lips and in some parts of the hard palate, the connective tissue is elastic, alternatively fatty or glandular, and contains the major blood vessels and nerves. On the contrary, in the gums the mucosal tissue is in direct contact with the underlying bone.

Salivary glands, mainly found in the submucosa, secrete saliva through small ducts. Their role is to maintain a moist surface. Saliva contains mucins, some antimicrobial substances and epidermal growth factor (EGF), and it is a weak buffer (pH 5.5-7).

The volume of saliva secreted daily is between 0.5 and 2 l; however, the volume constantly present in the mouth is only 1 ml. Its main functions are to lubricate the oral cavity, to facilitate swallowing and to prevent demineralization of the teeth. Moreover, talking about administration of drugs, saliva is responsible for the determination of the residence time (saliva wash out).

The effective permeability barrier is represented by groups of lipid lamellae located in the intercellular spaces of the most superficial layer. This material is probably derived from MGMs (membrane coating granules), spherical organelles (100-300 nm) present in both keratinized and non keratinized epithelium. The cells of the oral epithelium are surrounded by intercellular mucus, made of complexes of proteins and carbohydrates. Mucus is secreted as part of the saliva. It is considered a non-stirred liquid layer and has an estimated thickness of 70 µm [63]. It contains mucins, which are glycoproteins with a molecular weight from 0.5 to 20 MDa, made up of basic units (400-500 kDa) linked in linear arrays. These mucins, such as MG1 , bind to mucosal tissue and contribute to the maintenance of hydration, they provide lubrication and prevent the attachment of microrganisms [64]. At physiological pH mucus carries a net negative charge, thanks to sialic acid residues and sulfate. Moreover, it has a gel structure that binds to the epithelial cells [60].

5.1.2 Buccal administration of drugs

Buccal administration could represent an attractive alternative to other administration routes, due to the peculiar structural and physiological properties of this tissue. In fact, the high vascularization allows direct access to the systemic circulation via capillaries, avoiding at the same time hepatic first pass effect. Moreover, in contrast to the relatively harsh environment that a molecule undergoes through the GI tract, the oral cavity has a constant pH, maintained by the salivary fluid, and there are less mucins and a limited enzymatic activity, without proteases [65].

Drugs can permeate across buccal mucosa by passive diffusion across lipid membranes via transcellular or paracellular route [60].

Buccal mucosa is more permeable than skin: its permeability has been estimated to be 4-4000 times greater than that of skin. This high variability can be ascribed to the fact that there are considerable differences in permeability among the regions of the oral cavity, depending on the thickness and degree of keratinization: the sublingual mucosa is relatively thin and non-keratinized, thus it is the most permeable part. Buccal mucosa exhibits an intermediate permeability, being non-keratinized but thicker (500-800 μm). Palatal mucosa, on the contrary, is the less permeable, because of the keratinization [65, 66].

Despite the advantages, buccal administration has some limitations: for significant drug absorption, the formulation needs to stay in contact with the mucosa for a relatively long time. This can be obtained either with repeated administration or with mucoadhesive dosage form. Moreover, due to the barrier properties of the tissue, only drugs with high potency seem to be good candidates for buccal administration.

Drugs like peptides and proteins, for example, have a very low bioavailability (5%), because of their physicochemical properties: they have high molecular weights and high hydrophilicity, factors that impede passive permeation [67].

A wide range of permeation enhancement techniques has been developed to overcome these limitations. Among them, iontophoresis represents an innovative enhancement strategy.

In fact, due to the good results obtained with the transdermal application of this technique, recently it has been proposed the application to the buccal route.

5.1.3 Buccal iontophoresis

Compared to transdermal iontophoresis, data regarding buccal iontophoresis are scarce. Research is still focusing on mechanistic studies aiming at the characterization of the membrane, more than on the development of therapeutically active device.

J. Jacobsen's study on buccal iontophoretic delivery of atenolol is the first one regarding the application of this technique on buccal tissue [68]. The study implied the application of a low current density (0.4 mA/cm^2) for 8 hours. It investigated the effect of concentration in the donor solution and of current density. It demonstrated that the iontophoretic approach was feasible, and it elucidated that electric factors were more important than initial donor concentration in determining the permeation enhancement.

Other studies, more recently, regarded galantamine [69], ondansetron HCl [70], naltrexone [71, 72], nicotine, lidocaine [73] and some model macromolecules [74].

In the study on ondansetron, current ranging from 0.1 to 0.3 mA/cm^2 was applied for 24 hours, and a linear correlation between current density and ondansetron flux was established. They also investigated the histomorphology of the tissue before and after iontophoresis, and they found no major morphological changes after 8 h iontophoresis at 0.3 mA/cm^2.

In the study on model macromolecules, passive and iontophoretic permeation of two dextrans and parvalbumin were investigated. The results obtained confirmed that iontophoresis was able to enhance drug permeation. Moreover, in this case current was applied for 1 hour, a more realistic application time in real life situations.

Moscicka and co-workers conducted a more mechanistic study in order to investigate the properties of buccal mucosa as a semipermeable membrane under the influence of an electric field [75]. They measured the electroosmotic flow across the membrane, and compared the results obtained with the skin. The results showed that a volume solvent flow is present and goes from anode to cathode (same as skin). Thus, buccal mucosa is negatively charged at physiological pH. Moreover, they reported a higher permeability if compared to skin (intuitive-lack of stratum corneum).

Interestingly, cytopathic effects were observed only after application of 2 mA/cm^2 for 2 hours in the permeation of Naltrexone [71].

Short duration iontophoresis (20 min) was recently investigated by Gratieri et al. for the topical delivery of 5-fluorouracil and leucovorin [76]. The results demonstrated that even short application was sufficient to allow the deposition of clinically relevant amounts of drugs.

Almost all these studies were conducted using porcine buccal mucosa as a model for buccal mucosa. However, this model poses practical problems: the surface area is limited, the excision procedure can be time consuming and the masticatory process can ruin the tissue.

Since oral mucosa and esophageal tissue exhibit many common features [62], porcine esophageal mucosa has also been used as a model for buccal mucosa [77, 78]. It has been characterized for passive permeation and the results obtained confirmed the goodness of the model. Moreover, it offers the advantages of a big surface area, and the isolation of the

epithelium is quite easy. However, there are no data about its behavior under the application of an electric field.

5.1.4 Sumatriptan succinate

Sumatriptan succinate (M.W. 413.15 Da) was chosen as model molecule for permeation experiments across porcine esophageal epithelium. It is a selective agonist for 5HT1 serotonin receptors and it is used for the treatment of migraine. It has been successfully administered across the skin with an iontophoretic patch (NuPathe®), because of its physicochemical properties that facilitates iontophoresis.

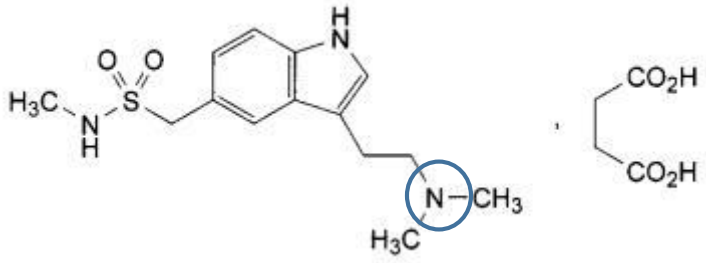

Figure 30 Sumatriptan succinate structure

It is, in fact, soluble in water, and the tertiary amine has a pk_a of 9.63, thus positively ionizes at physiological pH [79].

5.2 Aim of the study

The aim of this study was the characterization of porcine esophageal epithelium, a well-known model for buccal epithelium, upon the application of low density current. Sumatriptan succinate, a small molecule used for the treatment of migraine, whose iontophoretic behavior across the skin has been well characterized, was used as a model molecule. The effect of current density and donor solution concentration, factors known to influence iontophoretic transport, was investigated.

5.3 Materials and methods

5.3.1 Materials

Sumatriptan succinate was a kind gift from GlaxoSmithKline Manufacturing S.p.A. (S. Polo di Torrile, PR, IT), Acetaminophen was from ACEF (Fiorenzuola d'Arda, PC, I), HEPES (2-[4-(2-hydroxyethyl)piperazin-1-yl]ethanesulfonic acid), was from Sigma-Aldrich (St. Louis, MO, USA).

All other reagents were of analytical grade.

5.3.2 Buffers

PBS (phosphate buffered saline) had a concentration of 150 mM NaCl, 17 mM Na_2HPO_4 and 1.4 mM KH_2PO_4. pH was adjusted to 7.4.

HEPES buffered saline contained NaCl 150 mM and HEPES 20 mM. pH was adjusted to 7.4.

5.3.3 Tissue preparation

Pig esophagus was obtained from a local slaughterhouse (Annoni S.p.A., Madonna dei Prati, Busseto (PR), Italy) and epithelial tissue was isolated according to [77].

The esophagus was separated from the surrounding muscular tissue with the help of a scalpel (Figure 31 A and B). After that, it was cut longitudinally and then in square pieces of approximately 4 cm^2 (Figure 31, C and D). Then, heat separation was performed: the pieces were immersed for 60 s in distilled water kept at 60 °C. The epithelium was then isolated from the underlying connective tissue by gently peeling it off with a spatula (Figure 31, E and F).

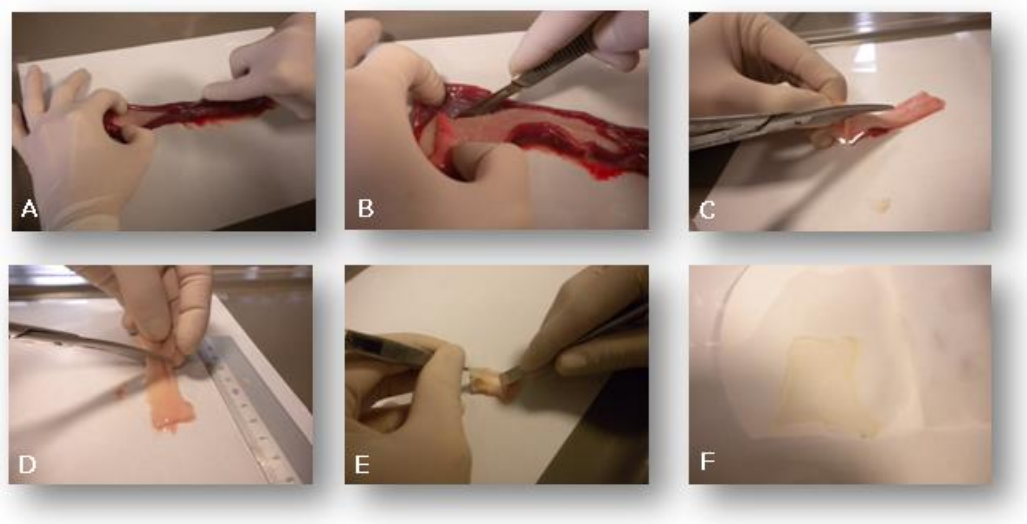

Figure 31 Isolation of pig esophagus epithelium

The so obtained pieces were then frozen at -20 °C. The tissue was thawed in physiological solution for 30 minutes prior to use.

5.3.4 Permeation experiments

Permeation experiments were performed with Franz-type vertical diffusion cells using porcine esophageal epithelium as a membrane. A regenerated cellulose filter, soaked for 20 min in boiling water, served as a support for the membrane. The donor compartment contained 0.4 ml of a sumatriptan succinate solution in PBS (pH 7.4), while the receiver was filled with 4 ml of HEPES buffered saline (20 mM, pH 7.4) and kept under constant magnetic stirring. All the experiments were performed at room temperature and in dark conditions.

Samples of 0.3 ml were taken at predetermined time intervals (0, 30, 60, 80, 100, 120, 180, 240 and 300 min), topping up after that with the same amount of fresh buffer.

Passive permeation experiments were performed applying 3 different concentrations: 2.5, 5 and 10 mg/ml of sumatriptan succinate (corresponding respectively to 1.79, 3.57 and 7.14 mg/ml of sumatriptan base- M.W. 295.4 Da) in the donor solution.

In current assisted experiments, anodal iontophoresis was applied with a constant current generator (Cosmic 1, Iono, Pesaro, IT). Silver/Silver chloride electrodes were connected to the donor and receiving chamber via salt bridges (Agar 2% in KCl 1 M). The effect of donor concentration and current density on sumatriptan succinate permeation were evaluated.

Table 8 summarizes the experimental conditions tested.

Table 8 Experimental conditions tested in current assisted experiments

Donor concentration (expressed as sumatriptan succinate, mg/ml)	Current density (mA/cm²)
2.5 (1.79)	0
	0.75
5 (3.57)	0
	0.38
	0.75
	1
	1.5
	5.83
10 (7.14)	0
	0.75

Values reported in brackets are the concentrations expressed as sumatriptan base.

One current assisted experiment (0.75 mA/cm²) was performed using a 5 mg/ml acetaminophen solution in PBS as donor. Acetaminophen flux was determined in presence and absence of 5 mg/ml sumatriptan succinate (3.57 mg/ml sumatriptan base).

5.3.5 Analytical methods

5.3.5.1 Analytical method for Sumatriptan Succinate

All the samples were analyzed via HPLC-UV. Pump was a Series 200 LC (Perkin-Elmer, Norwalk, CT, USA), autosampler was a ProStar 410 (Varian, Walnut creek, CA, USA), detector was an SPD 20A (Shimadzu, Kyoto, Japan). The software used was Turbochrom Workstation (Perkin-Elmer, Norwalk, CT, USA).

The column used was a NovaPak C18, 150*3.9 mm (Waters, Milford, MA, USA). A mixture of $NH_4H_2PO_4$ 50 mM, pH 3.3 and acetonitrile in the ratio 85:15 (V/V) was used as mobile phase.

Flux was set at 1 ml/min, detection wavelength was 283 nm and retention time was 2.4 min. The analyses were conducted at room temperature.

Limit Of Detection (LOD) and Limit Of Quantification (LOQ) were respectively 1.57 and 5.25 µg/ml of sumatriptan succinate (corresponding to 1.12 and 3.75 µg/ml of sumatriptan base).

5.3.5.2 Analytical method for Acetaminophen

The apparatus was the same used for Sumatriptan Succinate, as well as the column. The mobile phase was a 92:8 (V/V) mixture of CH_3COONa 10 mM, pH 4 and acetonitrile. Detection wavelength was set at 254 nm, with a retention time of 2.6 min.

The analytical methods were both validated according to USP 37.

5.3.6 Data analysis

The results obtained from the permeation experiments were plotted as cumulative amount (µg/cm^2) as a function of time. From the profiles obtained it was possible to calculate the steady state flux (from the linear part of the profile). The flux (µg/cm^{2}h) was the slope of the regression line, while the permeability coefficient (P, cm/s) was calculated as J/c_d, where c_d is sumatriptan concentration in the donor solution (µg/ml). Enhancement factors (EF) were calculated as the ratio between the flux obtained with iontophoresis and that obtained with passive permeation. Instantaneous fluxes were calculated from the slope for all time points ($\Delta Q/\Delta t$) were ΔQ is the change in the cumulative amount permeated in the time interval Δt.

Equation 11 gives the total flux of sumatriptan succinate across porcine esophageal mucosa:

$$J_{tot} = J_{pass} + J_{EM} + J_{EO}$$

Equation 11

Where J_{pass} is the passive flux of sumatriptan succinate at a given concentration, J_{EM} express the electromigratory contribution and J_{EO} represents the electroosmotic flow.

Electroosmotic flow can be calculated as follows:

$$J_{EO} = V_W \times c_{sum}$$

Equation 12

Where V_W is the solvent permeability coefficient, which can be estimated from:

$$V_W = \frac{J_{ACE}}{c_{ACE}}$$

Equation 13

J_{ACE} is the flux of acetaminophen, electroosmotic flow marker, and c_{ACE} its concentration in the donor solution. J_{EM} is determined by subtracting passive and electroosmotic contributions from the total flux.

Statistically significant differences were assessed by ANOVA followed by Bonferroni correction or t-test.

Each experiment was performed at least in triplicate.

5.4 Results and discussions

Pig esophageal mucosa is a well-characterized model for buccal mucosa [78], and it has been proposed as an alternative model for buccal epithelium instead of porcine buccal mucosa, mainly because of the ease in the supply and isolation of the tissue. The permselectivity properties of porcine buccal mucosa during iontophoresis have been, to a certain extent, investigated [3, 75]. On the contrary, the same information, necessary for the optimization of iontophoretic delivery, for porcine esophageal epithelium are lacking. Data previously obtained in our laboratory (I. Telò, Unpublished data) with two different techniques confirmed that that porcine esophageal epithelium is negatively charged at physiological pH, having an isoelectric point between 3 and 3.5. Thus, it behaves as a cation permselective membrane, and, when iontophoresis is applied, an electroosmotic flow directed from anode to cathode is established. The solvent flow for the esophageal epithelium resulted to be about 1.7 µl/cm²h. In this study, the aim was to give further insight on porcine esophageal epithelium during and after application of iontophoresis, examining the permeation of sumatriptan succinate, a positively charged drug chosen as model molecule. Passive and current assisted permeation across porcine esophageal epithelium was investigated. The effect of different parameters, such as donor solution concentration and current density, on sumatriptan permeation, were evaluated.

5.4.1 Passive permeations

Passive permeation of sumatriptan was evaluated at 3 different concentrations (1.79, 3.57, 7.14 mg/ml sumatriptan base). The results (Figure 32) show that the permeation increases as a function of concentration of drug in the donor solution. Moreover, steady state is reached after 2 hours of permeation.

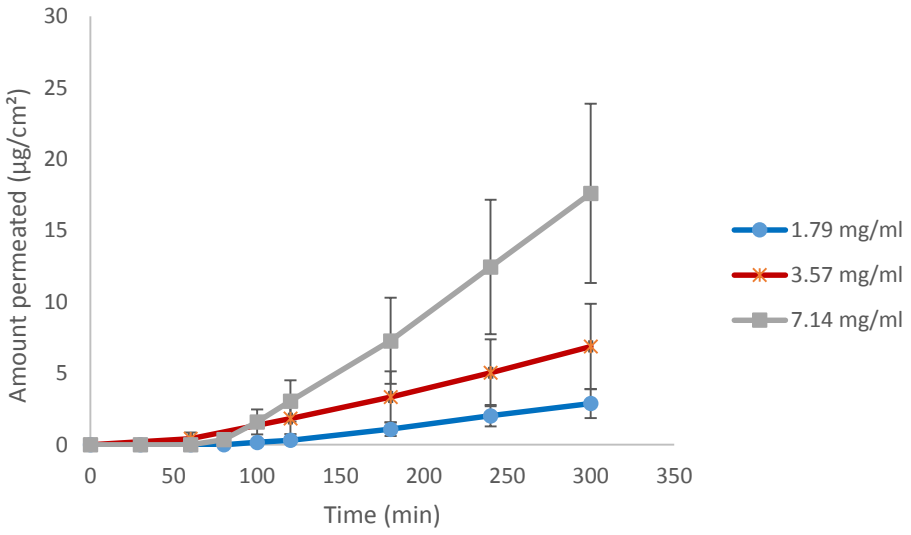

Figure 32 Passive permeation of sumatriptan succinate at different concentrations in the donor solution

Table 9 illustrates fluxes, permeability coefficients and lag time values calculated at steady state for the different donor concentrations. Fluxes increase linearly with the raise in sumatriptan concentration in the donor solution. In particular, sumatriptan flux, calculated at 3.57 mg/ml, resulted 1.73±0.6 µg/cm²h. This result is consistent with literature data [80] obtained in similar experimental conditions across porcine sublingual tissue (reported flux was 2.71±1.00 µg/cm²h). Permeability coefficient P resulted an order of magnitude larger than that reported for skin [81]. This last result can be explained by the different barrier properties of the two tissues. The skin is in fact thicker than esophageal mucosa, and in addition, it is keratinized.

Table 9 Fluxes (J), permeability coefficients (P) and time lags calculated for passive permeation at different donor concentrations. Donor concentration expressed as sumatriptan base (corresponding to 2.5, 5 and 10 mg/ml sumatriptan succinate).

Sumatriptan concentration (mg/ml)	J (µg/cm²h)	P (cm/s)*10^{-7}	Time lag (min)
1.79	1.06±0.6	1.65±0.45	108.25±43.37
3.57	1.73±0.6	1.31±0.47	82.01±47.14
7.14	4.79±0.92	1.86±0.36	117.52±55.78

Tukey-Kramer post hoc test demonstrated a statistically significant difference between the fluxes at 1.79 and 7.14 and also 3.57 and 7.14. The high variability is probably responsible for the lack of difference between the lowest concentrations.

5.4.2 Current assisted experiments

5.4.2.1 Effect of donor concentration

In order to evaluate the effect of donor concentration on iontophoretic permeation of sumatriptan, current assisted experiments were performed at 0.75 mA/cm^2 testing the same sumatriptan concentrations used for passive permeation (1.79, 3.57, 7.14 mg/ml). After 2 hours, current was stopped and passive permeation was allowed for 3 more hours. Figure 33 shows the permeation profiles of sumatriptan at different donor solution concentrations.

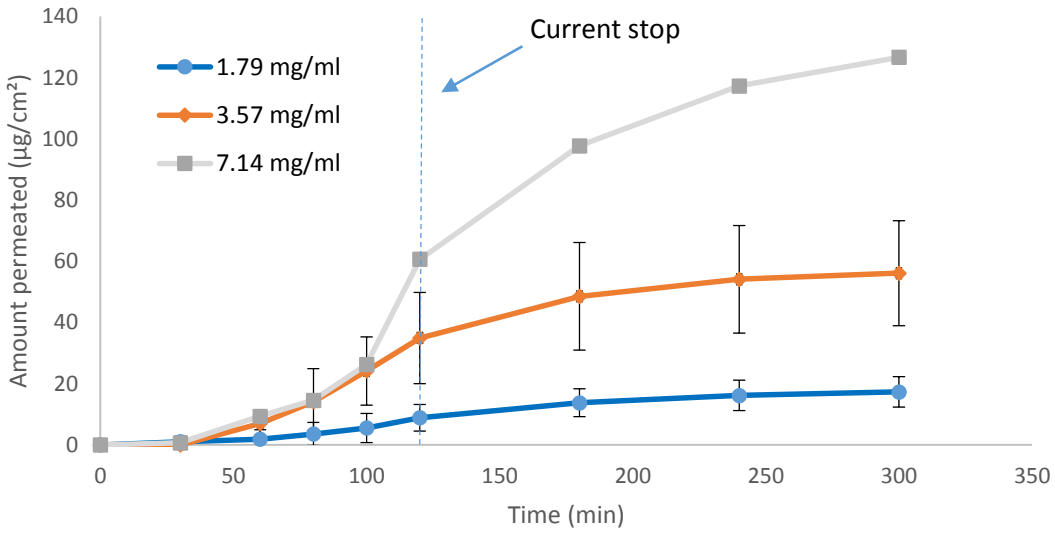

Figure 33 Permeation profiles for sumatriptan at different donor concentration. Current applied for 2 hours (0.75 mA/cm^2).

It can be seen that there is an increase in the amount permeated as a function of donor solution concentration. Moreover, after current stop the profiles decrease rapidly, returning similar to passive ones. This indicates the absence of a considerable accumulation of drug in the tissue, as well as of irreversible permeability impairment of the membrane upon the application of iontophoresis.

As shown in Figure 34, the fluxes calculated at steady state increase proportionally as a function of sumatriptan succinate concentration in the donor solution, in accordance to Nernst-Planck equation.

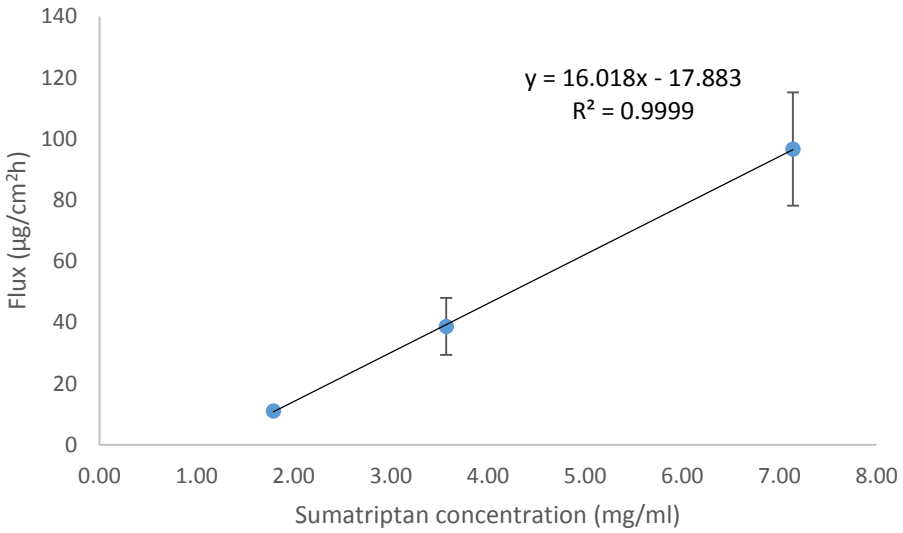

Figure 34 Fluxes at steady state as a function of concentration in the donor solution

5.4.3 Effect of current density

Current density plays a major role in driving iontophoretic transport, especially in buccal iontophoresis [3]. An increase in current density usually brings to a corresponding raise in fluxes and in the amount permeated.

In order to investigate the effect of different current densities on sumatriptan succinate permeation, ascending current densities, in the range 0.38-5.83 mA/cm² were applied for 2 hours, using a sumatriptan succinate solution in PBS pH 7.4 (5 mg/ml, corresponding to 3.57 mg/ml sumatriptan base) as donor solution. Passive permeation was then followed up to 5 hours. Figure 35 shows the permeation profiles of sumatriptan, during the application of iontophoresis, at different current densities.

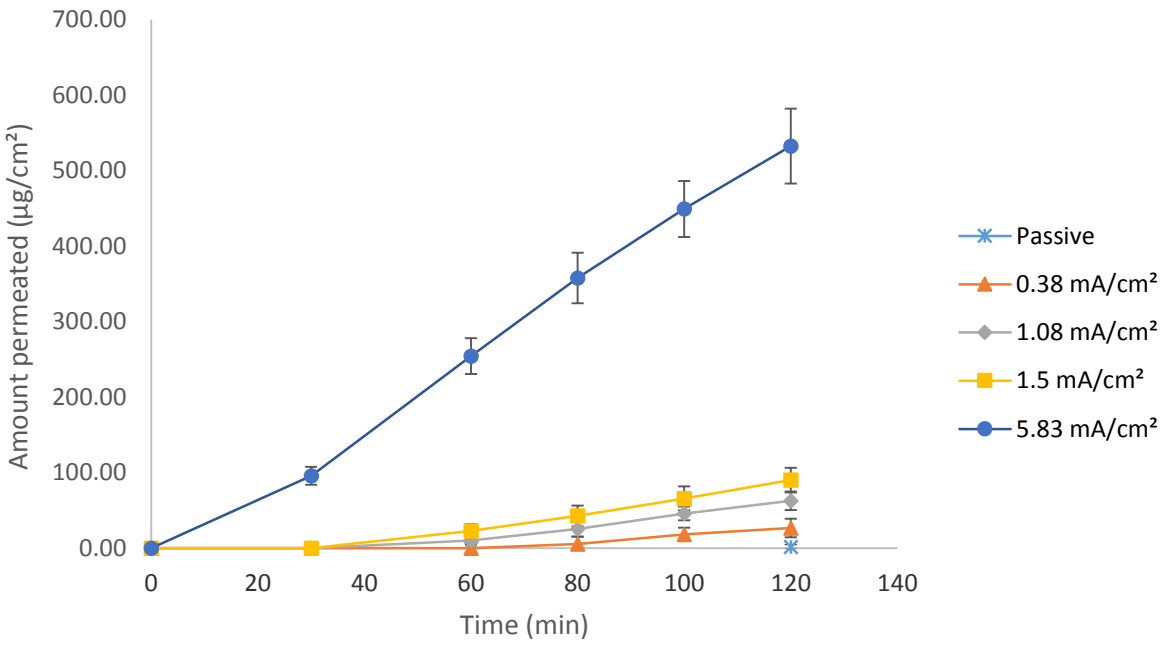

Figure 35 Effect of current density on the permeation profiles of sumatriptan (donor concentration: 3.57 mg/ml sumatriptan base).

Even the application of the lowest current density resulted in an enhancement of sumatriptan permeation. When 5.83 mA/cm² were applied, the amount permeated after 2 hours was 250 times greater compared to passive permeation (respectively 1.84±1.10 and 532.49±49.72 µg/cm² for passive and current assisted permeation). Table 10 illustrates fluxes, permeability coefficients and time-lag values calculated at steady state, as well as enhancement factors calculated as the ratio between the average current assisted and passive flux.

Table 10 Sumatriptan permeation parameters (results reported as average±SD)

Current density (mA/cm²)	Flux (J, µg/cm²h)	Permeability coefficient (P, cm/s)*10⁻⁶	Time lag (min)	EF_j
0	1.73±1.26	0.131±0.098	82.01±47.14	1
0.38	32.12±26.84	2.5±2	63.37±9.99	18.58
0.75	28.29±10.12	2.2±0.79	44.12±6.52	16.37
1.05	56.16±7.17	4.37±0.56	52.97±13.71	32.5
1.5	71.11±6.86	5.53±0.53	30.27±28.01	41.14
5.83	261.96±49.76	22.8±3.97	8.96±0.91	151.6

Enhancement factors ranged from 19 to 152. Remarkably, time lag exhibited a 10-fold reduction at 5.83 mA/cm² when compared to passive permeation. Permeability coefficients P follow the same trend as the fluxes.

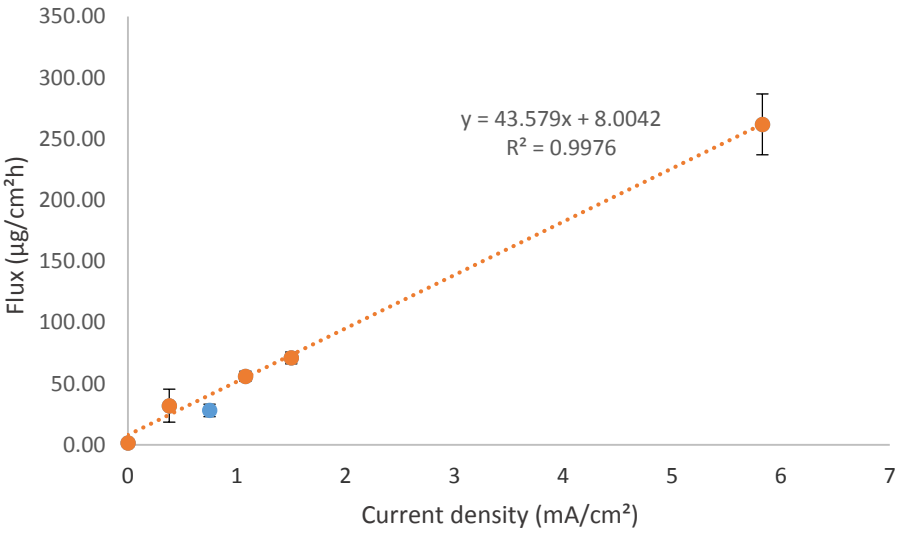

Figure 36 variation of the fluxes as a function of current density applied.

Figure 36 illustrates the fluxes calculated at steady state as a function of current density, and suggests a direct proportionality relation. The only exception is the flux obtained when 0.75 mA/cm² is applied, whose value is equivalent to the one at 0.38 mA/cm² (blue dot).

This particular behavior may be explained with the variation of the relative contribution of electromigration and electroosmosis to the transport of sumatriptan succinate at different current densities.

Relative contributions of electromigration and electroosmosis, when 0.75 mA/cm² was applied, were calculated in previous experiments according to Equation 12 and Equation 13. Acetaminophen was used as electroosmotic flow marker. Passive, electroosmotic and electromigratory contribution for sumatriptan permeation resulted to be respectively 6, 21 and 73%, thus in these iontophoretic conditions the contribution of electroosmosis is not negligible. It has been demonstrated for other tissues, such as the sclera [54], that the presence of charged molecules can reduce the extent of electroosmotic flow, probably because of a direct interaction of the positively charged molecule with the negative charges of the tissue. In order to verify whether the absence of difference between the permeation at 0.38 and 0.75 mA/cm² could be ascribable to a reduction of electroosmotic flow due to the

presence of sumatriptan succinate itself, acetaminophen iontophoretic permeation was investigated in presence and absence of sumatriptan succinate (5 mg/ml) in the donor solution. The presence of sumatriptan succinate effectively reduced acetaminophen flux from 45.43 µg/cm²h to 39.68 µg/cm²h, thus confirming the hypothesis done. This difference, although not huge, is statistically significant.

Another possible explanation could be that electroosmotic flow, at low current densities, does not raise in a strictly proportional way with current density, thus influencing the overall transport. This was observed by Moscicka-Studzinska and coworkers [75] in porcine buccal mucosa for current densities ranging from 0.2 to 1 mA/cm², and could contribute to explain the result obtained.

After two hours, current was stopped, and passive permeation was followed up to 5 hours. Instantaneous fluxes (Figure 37), calculated between 2 time points, show that, after current stop, flux returned quickly to values close to passive ones. As stated before, this demonstrates that the membrane is not permanently damaged by the application of current, since its permeability is not impaired. This observation is valid also for the highest current applied (5.83 mA/cm^2).

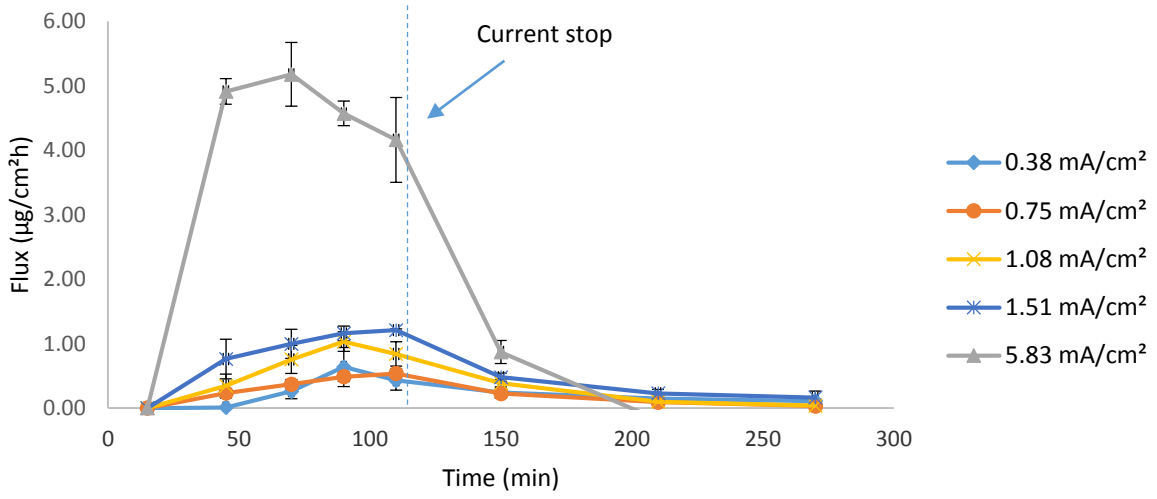

Figure 37 Instantaneous fluxes at different current densities. Results shown as average±SD

5.5 Conclusions- Buccal delivery

Porcine esophageal epithelium can be considered a good model for buccal epithelium for in vitro permeation experiments. However, there is a lack of data in its characterization as for iontophoresis. In this study, passive and current assisted experiments were performed using sumatriptan succinate as a model molecule. Sumatriptan succinate passive permeation confirmed the similarities between porcine esophageal and buccal epithelium, since the results obtained were similar in terms of flux and permeability coefficients to data reported in the literature. The evaluation of different donor solutions concentrations and the application of different current densities gave a further insight on iontophoretic behavior of this membrane. Iontophoresis was able to enhance sumatriptan transport without causing a permanent damage to the membrane.

Finally, the effect of current density was evaluated: sumatriptan permeation increased linearly with the raise of current density, except for one point (0.75 mA/cm^2). Current assisted experiments performed with acetaminophen in the presence and absence of sumatriptan succinate suggested that the presence of this molecule could hinder electroosmotic flow, thus giving a possible explanation for the result obtained.

6 Transdermal delivery

6.1 State of the art

6.1.1 Structure of the skin

The skin is the largest organ of the human body. It is primarily intended as a protection from unwanted influences from the surrounding environment. The outermost layer of the epidermis, stratum corneum, carries out the protective function, while the underlying tissue generates the components of the stratum corneum.

The dermis, that forms the bulk of the skin, is constituted by connective tissue elements: collagen, elastin and glycosaminoglycans form the so called extracellular matrix, which is elaborated by fibroblasts [82]. While the epidermis is avascular, the dermis is highly vascularized. Dermis is divided into 2 principal components: the papillary layer is in contact with the epidermis. It is made up of connective tissue and contains capillaries and the sensing elements of the skin. Under the papillary layer there is the reticular layer, composed of dense, irregular connective tissue that embeds blood vases, hair follicles, nerves, sweat glands and sebaceous glands. The fibers of the reticular layer intertwine with the underlying hypodermis. It contains, apart from the connective tissue, many fat cells [83].

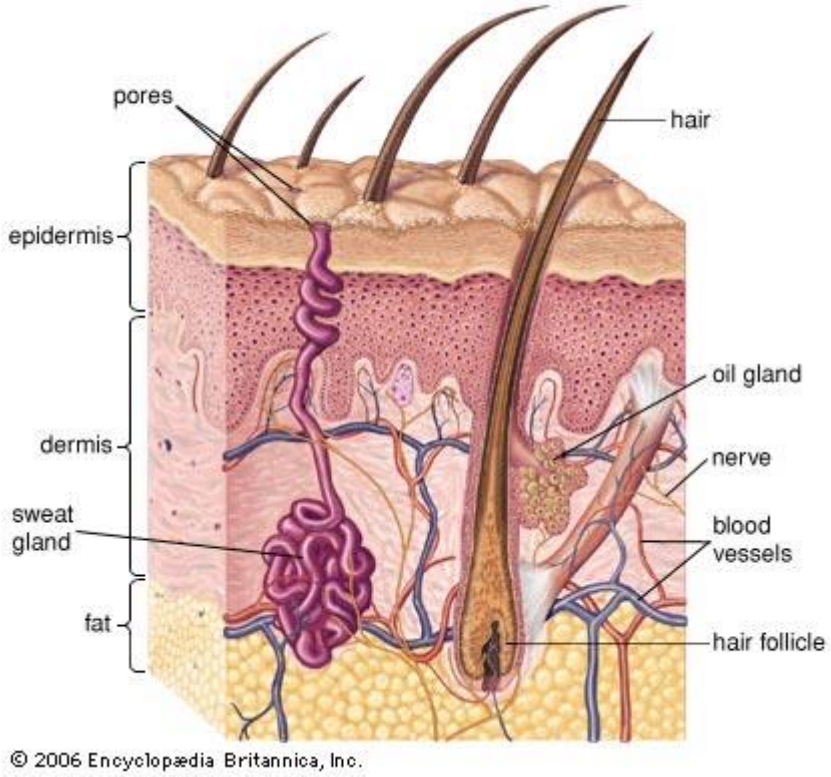

Figure 38 Anatomy of human skin

The epidermis (100 to 150 µm thick) is divided into 4 layers: the stratum basale, stratum spinosum, stratum granulosum and stratum corneum.

The stratum basale is made up of columnar epidermal stem cells and transiently amplifying cells derived from them. They interconnect via desmosomes and show a high nucleus-cytoplasm ratio, cell organelles and keratin filaments. These cells connect to the basal membrane via hemi desmosomes.

The Stratum spinosum shows the presence of lipid enriched lamellar bodies (Odland bodies), keratinosomes and membrane coating granules. In the upper layers the cells begin to flatten and elongate, grading to the stratum granulosum.

In this layer, the keratin synthesis increases. Keratin filaments are highly phosphorylated and have extensive disulfide bonds. The uppermost cells display a unique structural and functional organization, since they are ready to differentiate into corneocytes, and to secrete the lamellar bodies to the extracellular domain.

The stratum corneum is a composite of corneocytes and contents of the lamellar bodies. It has a “brick and mortar” structure, which creates a tortuous path that drugs have to traverse

in order to cross the horny layer. In human skin, it has 18-20 layers of corneocytes. These cells have a diameter of 20-40 μm, significantly bigger than the basal cells (6-8 μm). They also exhibit differences in thickness and number of desmosomes, depending on the body site and location in the stratum corneum. These features may influence their degree of hydration that varies from 10 to 30%, along with the rate of proteolysis. In fact, filaggrin breakdown leads to the formation of a blend of aminoacids known as natural moisturizing factors (NMF).

The corneocytes, considered as bricks, impart physical protection to the horny layer, probably due to the orientation of keratin filaments that may help the lateral propagation of the stress. The hydrophobic lipids, organized in tight lamellar structures, provide a watertight barrier property. There are several theories concerning the structural organization of the matrix: the lipids were proposed to be organized as liquid crystalline, as a blend of liquid crystalline and gel phase or a single coherent gel phase [82].

In the extracellular matrix ceramides, cholesterol and fatty acids are present roughly in equimolar ratio, along with small amounts of triglycerides, glycosphingolipids and cholesterol sulphate. Ceramides are the most crucial components for the lipid organization of the barrier, and they can be classified in 9 subclasses that differentiate by the head group architecture (sphingosine, phytosphingosine or 6-hydroxysphingosine), linked to a non-hydroxylated or α-hydroxylated fatty acid of varying hydrocarbon chain length[84]. Cholesterol, on the other way, promotes the intermixing of different lipid species. Cholesterol sulfate, although present in only small amounts (2-5%) plays a very important role in the desquamation process of the stratum corneum [85].

The epidermis contains also immunocompetent cells, which can be defined as a real immune system. The immucompetent cells of the epidermis include Langerhans cells and T cells that may initiate a potent immune response when the skin is exposed to antigens. Langerhans cells constitute 20% of the surface area of the skin and are antigen presenting cells. They can be found as immature cells in the basal layer of the epidermis, and become mature while migrating to the paracortical T cell areas of the draining lymph nodes, where they present the antigen to naïve T cells. In this case, the skin behaves as a mucosal surface [86].

The skin has always been considered poor in drug metabolism. However, it has been demonstrated that most of the enzymes present in the human body occur also in the skin,

even if they are less specific. Among them, cytochromes P450 (CYP, many subspecies), Flavin dependent monooxigenases, alcohol dehydrogenases, aldehyde dehydrogenases, esterases and amidases, that are highly active in human skin, and epoxide hydrolase. Although their specific activity is just 10% compared to liver enzymes, their presence has to be accounted for in the development of transdermal drug delivery systems.

There are also Phase II enzymes, such as glutathione-S-Transferase, glucurunosyltransferase, sulfotransferase, acetyltransferase and methyltransferase [87].

6.1.2 Transdermal iontophoresis of peptides and proteins

Peptides and proteins have become important options for the treatment of a variety of diseases. Moreover, the fast developments in the field of biotechnology have made available many pure recombinant proteins, which are easier to commercialize (safer for the patient).

Since they are complex molecules that pose many stability issues, they have always been considered bad candidates for any delivery route other than parenteral [88]. However, because of their short half-life, proteins and peptides usually require repeated administrations, with low patient compliance. Furthermore, with this route of administration it is noticeable a variability in blood concentrations [89], which can lead to unwanted side effects. Thus, a less invasive administration technique, such as transdermal delivery, may improve the therapeutic outcome.

The advantages of transdermal administration systems, in addition to the lower invasiveness, are that they can be easily self-administered; they can provide release over a long period (up to one week). Moreover, they can improve the pharmacokinetic avoiding unwanted plasma peaks. However, they also have limitations: in fact, due to the barrier properties of the stratum corneum, only small (<500 Da) and lipophilic molecules can penetrate easily through the skin [90].

Iontophoresis has been widely investigated as enhancement technique both for local and systemic administration of peptides and proteins [88, 91].

This technique has many advantages, since it is non-invasive, and it allows modulating the permeation of the drug varying the current density, the duration of current applied and the area of application. Moreover, it gives faster onset and offset timings, making it possible to customize the rate and extent of delivery on the needs of the single patient [91].

Transdermal iontophoresis has been widely investigated for the administration of small molecules, leading also to marketed product such as LidoSite®, a lidocaine patch for local anesthesia, Nupathe®, that contains sumatriptan succinate and it is used for the treatment of migraine, and Ionsys®, loaded with Fentanyl for the treatment of postoperative pain.

Although investigation on peptide iontophoresis dates back to the 80s, with the first studies on transdermal administration of insulin [92, 93], with the latest technical improvements more compact and easier to use iontophoretic systems became available, thus giving opening new opportunities for this technique.

Proteins and peptides are particularly challenging molecules for iontophoretic administration, and their permeation, depending on a wide number of different factors, is far less predictable if compared to small molecules. For a long time it was believed that charge/mass ratio was the main factor affecting transdermal iontophoretic transport. However, recent findings have demonstrated that this parameter is not sufficient to describe the transport of complex molecules, since other factors such as volume, shape and charge distribution can influence electrophoretic mobility and thus permeation [91]. Talking about the mechanisms involved, intuitively, due to the lower charge/mass ratio, compared to small molecules, electroosmotic flow should dominate over electromigration. However, studies conducted on small polypeptides [94] and on cytochrome c [56] suggest on the contrary that electromigration remains the most important mechanism.

Moreover, complex biomolecules are more likely to interact with the skin transport pathways, since they can expose regions with a more pronounced hydrophobic or hydrophilic character [95]. In addition, Li et al. demonstrated that a polyelectrolyte assumes different conformations depending on the concentration of the background electrolyte. This fact can also have an effect on its diffusivity [96].

Thus, even if the flux is proportional to the current applied, according to Faraday's law, drug delivery is affected by so many other factors that only a specific investigation on the molecule is able to determine the extent to which iontophoresis enhances permeation [88].

There are many examples of in vitro and in vivo iontophoretic administration of macromolecules. The most investigated one is for sure insulin [91]. Because of its unrivaled therapeutic interest, it has been thoroughly investigated for iontophoretic delivery, despite

having physicochemical properties not suitable for iontophoretic transport. Indeed the insulin monomer (5800 Da) is a 51 amino acids peptide with an isoelectric point of about 5.3, very close to the isoelectric point of the skin. This means that when it gets in contact with the skin it tends to become neutral, while when it reaches the inner layers (pH > 5.3) it becomes negatively charged, thus hindering its anodal transport. On the contrary, during cathodal iontophoresis, the electroosmotic flow goes in the opposite direction. Moreover, it has been proved that insulin forms hexamers at low concentrations, which further complicates the iontophoretic transport.

These results led to new approaches to overcome these obstacles: new insulin analogues, with different isoelectric points [97] were investigated, as well as monomeric human analogues with reduced tendency to aggregation [98].

Calcitonin (M.W. 3500 Da), polypeptide used for the treatment of osteoporosis and Paget's disease, was investigated in numerous studies. This peptide has to be administered by multiple subcutaneous injections, due to its short half-life, and this leads to poor patient compliance. This peptide carries a positive charge at physiological pH, so anodal iontophoresis was tried. In in vivo studies in rats the amount delivered were sufficient to reach a therapeutic effect [99-102]. In these studies, moreover, it was noticed that the fluxes were not proportional to the current densities applied.

Studies on human parathyroid hormone (hPTH, 4117 Da) [103, 104] found a linear correlation between donor concentration and plasma levels. In addition, it was noted that the main transport pathway was via the hair follicles.

Another widely investigated peptide is the luteinizing hormone-releasing hormone (LHRH, 1182 Da): it is released in a pulsatile manner from the hypothalamus, and activates the release from the pituitary gland of the luteinizing hormone. Studies conducted both in vivo and in vitro demonstrated that the flux increased linearly with the increase of current density, and that the molecule retained its pharmacological activity after iontophoresis [105, 106]. Therapeutically active concentrations were achieved for Triptorelin (1311 Da) [107, 108], Vasopressin (1084 Da) [109], and Vapreotide [108], even if in this case the molecule was found to bind irreversibely to the skin.

In studies with somatorelin (3929 Da) [110] and octreotide (1019 Da) [111] the flux increased as a linear function of current density.

At last, Botulinum toxin was delivered iontophoretically to relieve the symptoms of hyperhidrosis [112]. The molecule was found in hair roots, sebaceous glands and arrector pili muscle fibers.

More recently, iontophoresis has been used to enhance transdermal permeation of bigger molecules, such as cytochrome c [56], ribonuclease A and T1[57], human basic fibroblast growth factor, and lysozyme [113]. In all these studies, the major contribution to the transport was due to electromigration, and not, as was previously believed for proteins, to electroosmosis. Only in another study about daniplestim (M.W. 12.76 kDa, pI 6.2) [114] electroosmosis seemed to be predominant over electromigration. These findings led to the hypothesis that physicochemical properties that enhanced electrophoretic mobility were the determinants of eletrotransport rates.

6.1.3 Laser microporation

Laser microporation is a physical enhancement technique that consists in the ablation of the stratum corneum. Laser emits monochromatic light in parallel rays. When the rays hit the skin, part of the energy is absorbed and converted to heat. The most used lasers for transdermal application are CO_2 laser and Er:YAG laser. The latter has been preferred because it causes less thermal damage compared to CO_2.

Er:YAG laser is a solid state laser that emits at 2.94 µm, which corresponds to the maximum absorbance of water. The laser beams hit the skin and cause the water molecules to evaporate explosively, thus forming an array of micropores. The skin contains 77% of its weight in water, thus it is an ideal substrate for Er:YAG laser.

Emission of the laser can be either continuous or pulsed, with latter being safer for dermal application. Further developments have led to fractional ablative lasers, which rely on a series of small parallel beams (diameter 150 µm) instead of one single bigger beam [115]. This diminishes the thermal damage allowing a faster healing.

The parameters to be controlled during laser application are fluence (J/cm^2), Fractional Ablative Area (FAA, %), pulse width (µs) and frequency (Hz).

Fluence, expressed as J/cm^2, is the energy applied per unit area, and it controls pore depth. Increasing fluence leads to deeper pores. Thus, a variation in the fluence applied can be useful for the targeting of different skin layers.

Fractional Ablative Area (%) defines the percentage of the treated area that results microporated after laser application. An increase in FAA should lead to an increase in cumulative permeation, since more pores are created.

Pulse width is the time during which the laser output remains above half of its maximum power [116]. It should be lower than thermal relaxation time, which can be defined as the cooling time of the tissue.

Frequency, number of pulses emitted per second (Hz), should be optimized with respect to the heat conductance properties of the tissue [117].

Initially, these lasers were used for skin resurfacing: they cause a controlled thermal damage and stimulate the repairing processes of the skin [118]. They are also used in cancer treatment, with 5-FU being the most studied molecule in this field [119, 120]. It was demonstrated that the application of Er:YAG laser gave a 133 fold higher permeation if compared to passive permeation. Another anticancer drug was methotrexate, whose permeation was increased by 80 folds compared to passive permeation. Imiquimod administration was also investigated: interestingly, a low fluence was sufficient to allow a 10 fold reduction in the dose that needed to be applied to achieve the therapeutic effect [121].

A very interesting application is in photodynamic therapy for the targeted delivery of 5-ALA (5-aminolaevulinic acid). This prodrug, used for the treatment of non-melanoma skin cancer, is a hydrophilic zwitterion at physiological pH, thus is scarcely absorbed in the stratum corneum. Different physical enhancement techniques were tried, and among them Er:YAG laser was the most powerful method (300-fold increase compared to passive permeation) [122]

This technique can be an interesting strategy for the delivery of polypeptides and proteins into and across the skin. An Er:YAG laser was used to successfully deliver FSH and triptorelin to women that were doing in vitro fertilization.

In vitro studies, conducted on microporated porcine skin, investigated the effect of fluence and pore number (FAA %) variation, as well as formulation factors on transdermal delivery of four different proteins: cytochrome c (12.4 kDa), recombinant human growth hormone (hGH, 22kDa), urinary follicular stimulating hormone (FSH, 32 kDa) and FITC- labelled bovine serum albumin (FITC-BSA, 70 kDa). The results obtained for cytochrome c and FITC-BSA demonstrated a linear dependence of the permeation from pore number. On the contrary, only delivery of FITC-BSA was proportional to the increase in pore depth. This result can be explained by the fact that the impact of fluence is dependent also on the physicochemical properties of the proteins, which can interact with the material present in the micropore [95].

Laser microporation has been extensively studied, both in vitro and in vivo, for the intradermal administration of vaccines. In fact, as previously underlined, the skin has unique immunological features that can provide good therapeutic outcomes both for vaccination and immunotherapy [123]. Vaccination studies performed in mouse models [124, 125], using model antigens like lysozyme and OVA, showed enhanced immunological response for the laser treated groups. One of the hypotheses was that the micropores could act as reservoir that supplied the immune system with antigens for a long period of time.

Transcutaneous immunotherapy, for the treatment of allergic asthma, was also evaluated: in a study Phl p 5, a grass pollen allergen, was administered with adjuvants (TLR agonists) via laser microporated skin and the results were compared to subcutaneous injection. The results obtained showed that laser microporation was superior to subcutaneous injection. Interestingly, the immune responses were different for the two approaches: in fact, with intradermal administration there was no induced systemic boost of TH-2 associated cytokines and IgG1 antibodies, which are associated with the unwanted side effects of this therapy and are common with subcutaneous injection. This finding furthermore highlights the unique characteristics of the skin-associated immune system [126, 127].

It was also attempted to deliver DNA and RNA based vaccines [123], but no immune response was elicited, probably due to rapid degradation of the plasmid DNA or RNA by skin derived or cytoplasmic nucleases.

6.1.4 Thymosin α1

Thymosin α1 is a member of the family of Thymosins, biologically active substances produced by the human body. It was first isolated in 1966 and characterized by Goldstein et al. [128, 129]. Thymosin α1 derives from the thymus, and is one of the several present in thymosin fraction 5, which is a potent immunopotentiating preparation that was used to reconstitute the immune function in thymus deprived individuals [128, 129]. Thymosins were classified based on isoelectrofocusing pattern: All the peptides were divided into three regions (α, β and γ). Peptides in the α regions are highly acidic, with isoelectric points below 5.0. Thymosin α1 is the asparaginyl endopeptidase cleavage product of prothymosin α, a nuclear polypeptide consisting of 109 aa. In particular, thymosin α1 is a heat stable, 28 amino acids peptide with an estimated isoelectric point of 4.32 (protcalc.sourceforge.net), and an estimated charge at physiological pH of -5. It has a quite peculiar structure, since it has a high aspartic and glutamic acid content, and it does not contain any histidine, arginine, proline, glycine, cysteine, methionine, tyrosine, and phenylalanine or tryptophan residues. Thus, it exhibit a marked hydrophilicity. In aqueous solution it is unfolded, and can be classified as an "intrinsically unfolded protein", while it assumes a α-helix conformation in membrane like environment [130].

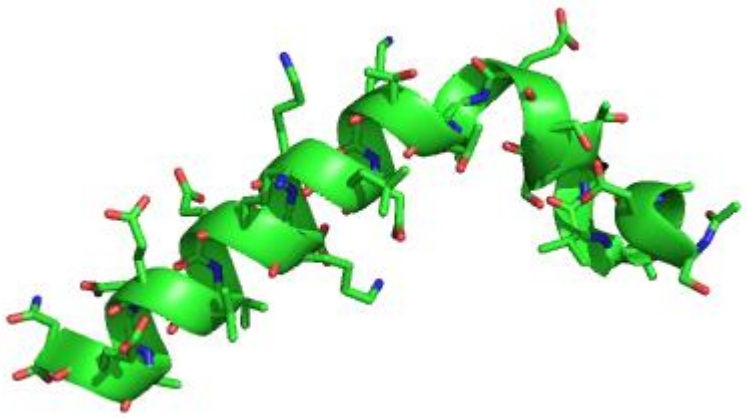

Figure 39 3-D structure of Thymosin α1 in membrane-environment

It is higly conserved and is mainly found in thymic epithelial cells, but also in lymphoid tissue like spleen and lymphnodes, and in non-lymphoid tissue, for example in the lungs, kidneys and brain (Rif. J.Li).

Its secretion is not regulated by hormones or regulating factors, and it is considered a potent biological modifier, thus it can be useful in the treatment of a variety of diseases. The immunoregulatory activity of Tα1 has not been fully explained yet. It has been shown, for example, that it increases the efficiency of T-cells maturation [131], and it can stimulate the differentiation in CD4+ and CD8+ lymphocytes [132], that can explain its antiviral activity, at the same time regulating the balance between these lymphocytes and peripheral monocytes [133]. It has also an effect on sensitivity of receptors to IL-2 and directly depresses viral replication. Moreover, it has been shown that it increases the expression of viral antigens on the infected cells: they become more visible to the immune system and are eliminated more easily [134]. The immunoregulatory mechanism probably involves the action on multiple targets. A direct modulation on cytokines, MHC I, MHC II related genes, as well as other not well known genes.

Tα1 has been used as experimental therapy to treat different kinds of cancer [135], such as hepatocarcinoma, lung and adenocarcinoma, breast cancer, glioblastoma and colorectal cancer, either as a monotherapy or in combination with other drugs. Its efficacy could be linked either to the stimulation of the immune system or to a direct inhibition of the tumor growth.

Tα1 has also been used in clinical trial for Hepatitis b therapy. It gave a complete response (normalization of alanine transaminase) in HBeAg negative patients, while it showed less promising results in HBeAg positive patients. When used in combination with lamivudine, it demonstrated to be particularly efficient [136]. In the treatment of hepatitis c the combination of Tα1 and pegylated interferon α2a showed a better therapeutic outcome if compared to interferon monotherapy. A triple therapy (Peg IFN+ ribavirin +Tα1) was developed for particularly difficult cases [137]. Moreover, Tα1 showed to be safe and well tolerated by patients [138].

Probably one of the most interesting field of application is HIV therapy [135]. As stated before, Tα1 stimulates the differentiation of stem cells in CD4+ and CD8+. HIV targets these cells, bringing to a collapse of the entire immune system. Thus, maintaining a significant immune response can be helpful to avoid the onset of AIDS (acquired immunodeficiency syndrome). Tα1 was used in combination with HAART (highly active antiretroviral therapy) [139] or with zidovudine (AZT) and IFN-α [140]. In both cases, the results obtained were promising.

Tα1 is approved in Europe as a co-adjuvant for influenza vaccine (Zadaxin™, SciClone Pharmaceuticals) for the vaccination of immunocompromised patients, since it can help to improve the vaccine response. Indeed, it can enhance the production of specific antibodies. Thus, it could also be useful for the preparation of a cheaper and quicker vaccine, useful for example in case of pandemic outbreaks.

Given the broad spectrum of application of this molecule, and the fact that, in any case, it needs multiple injections to exert its therapeutic effect, it was considered worth investigating the possibility of an alternative route of administration such as the transdermal route.

6.2 Aim of the study

The aim of this study was to evaluate the effect of two physical enhancement techniques on transdermal permeation and deposition of the polypeptide Thymosin α1. Laser microporation, a minimally invasive enhancement technique that causes the ablation of the stratum corneum, and iontophoresis were investigated. The objective was to compare the different effects of these techniques, both widely used, and to give further insight on the transdermal permeation and deposition of thymosin α1 under the application of iontophoresis, clarifying the preferential route of permeation.

This part of the work has been performed at the University of Geneva, School of Pharmaceutical Sciences, under the supervision of Prof. Yogeshvar N. Kalia.

6.3 Materials and methods

6.3.1 Materials

Thymosin α1 was purchased from ChinaPeptides Co.,Ltd, Shanghai, China.

MES (2-(N-morpholino)ethanesulfonic acid hydrate) (MW 213.25 Da), as well as NaCl, Na_2HPO_4, KH_2PO_4, TRIS hydrochloride (tris(hydroxymethyl)aminomethane) (MW 157.6Da) and HEPES ((4-(2-hydroxyethyl)-1-piperazineethanesulfonic acid) were from Sigma, Saint-Louis, MO, USA. Ultrapure water (MilliQ®, from Merck-Millipore). All the other reagents were of analytical grade.

6.3.2 Buffers

Buffers used for the different experiments were prepared as follows:

PBS (Phosphate Buffered Saline): NaCl 150 mM, Na_2HPO_4 17 mM, KH_2PO_4 1.4 mM; pH adjusted to 7.4 with NaOH 1 M.

PB (Phosphate Buffer): 57.7% Na_2HPO_4 25 mM, 42.3% NaH_2PO_4 25 mM; pH adjusted to 7

HEPES-TRIS: HEPES (4-(2-hydroxyethyl)-1-piperazineethanesulfonic acid) 25 mM, TRIS (tris(hydroxymethyl)aminomethane) 25 mM; pH adjusted to 7

MES: MES ((2-(N-morpholino)ethanesulfonic acid hydrate) 25 mM; pH adjusted to 6.5 with HCl 1M

6.3.3 Tissue preparation

Pig ears were obtained from a slaughterhouse (CARRE, Rolle, Switzerland). The outer skin was excised with a scalpel. Hair were removed with a hair trimmer (Philips). Pieces of 2 cm^2 were punched, after that subcutaneous fat was removed with scissors, in order to obtain full-thickness skin samples.

Human skin from abdominoplasty (Figure 40, panels A and B) was a courtesy of the HUG (Hôpitaux Universitaires de Genève). Subcutaneous fat was removed (Figure 40, panel C), obtaining samples of 1 mm thickness (Figure 40, panel D).

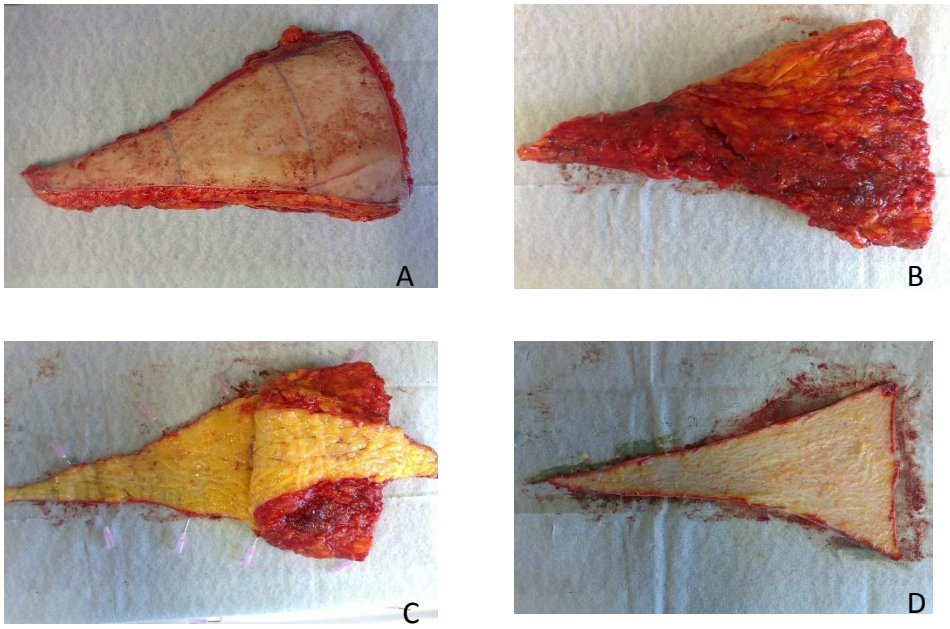

Figure 40 Full-thickness human skin preparation

6.3.4 Experimental set-up

All experiments, either passive or current-assisted, were performed in custom-made Franz type vertical diffusion cells, with an additional arm for the placement of the salt bridge in the receiving compartment. The membrane was full-thickness porcine or human skin, with a permeation area of 2 cm^2.

The donor solution consisted of a buffered solution (different buffers-see below) of Thymosin α1 1mg/ml (322 μM), while the receiving compartment contained 11 ml of degassed PBS at pH 7.4. All experiments were thermostatted at 37 °C and under constant magnetic stirring.

Samples of 0.5 ml were taken at predetermined time points, replenishing the receiver with the same volume of fresh buffer.

Samples were then analysed using a UHPLC-MS/MS method.

6.3.5 Analytical method

A UHPLC with tandem mass spectrometry method was developed to quantify Tα1 in permeation samples.

UHPLC conditions:

An Acquity UPLC system was used (Waters, Milford, MA, USA). The column was an Acquity BEH300 C18 1.7 µm equipped with a protective precolumn of the same brand (Waters, Milford, MA).

Flow was set at 0.2 ml/min, with a retention time of 0.9 min. No matrix effect was noticed. Isocratic elution was performed, using 80% water+0.1% formic acid and 20% CH_3CN+0.1% formic acid. Injection volume was set at 5 µl.

MS/MS conditions:

The mass spectrometer was a Xevo™ TQ MS detector (Waters, Milford, MA, USA), a tandem quadrupole. The source was a ZSpray (ESI source). Positive ionization mode was chosen. Under these conditions Thymosin α1 forms a triple-charged species $(M+3H)^{3+}$ whose m/z ratio is 1037. Using this as precursor ion, the product-ion scan produced an intense response for the 316 fragment. These 2 ions were chosen to represent Tα1 in the MRM experiment.

Lower Limit of Quantification (LLOQ) was 78.9 ng/ml, while Lower Limit of Detection (LLOD) was 23.68 ng/ml.

6.3.6 Laser microporated skin permeation experiments

Porcine skin samples were equilibrated in Physiological solution (NaCl 0.9%) for 30 minutes prior to microporation. Laser microporation was performed using a solid state Er:YAG laser (P.L.E.A.S.E.® Professional, Pantec Biosolution, Ruggel, Liechtenstein). After microporation the tissue was clamped in a Franz cell and passive permeation of Tα1 (1mg/ml in PBS buffer) was allowed for 24 hours. Samples were taken at 0, 2, 3, 4, 5, 6, 7, 8 and 24 hours.

The effect of both fractional ablative area (FAA%) and fluence (J/cm^2) applied were tested (Table 11):

Table 11 Laser conditions applied to porcine skin

FAA (%)	J (J/cm^2)
5	23.7
15	
5	7.9
	23.7
	39.5

After the experiments, the donor solution was removed, the tissue was rinsed with physiological solution and then deposition (total amount deposited in the skin) or biodistribution (distribution of the compound within the different layers of the skin) of the drug were assessed.

6.3.7 Biodistribution assessment

The skin samples were mounted on an appropriate holder and snap-frozen in isopentane cooled in liquid nitrogen. Slicing of the samples was carried out using a cold knife cryomicrotome (Microm HM 560, Histocom AG, Switzerland). 10 slices of 40 µm thickness were obtained from each sample. In addition, the remaining dermis was analysed. Fractional extraction of Tα1 was carried out with 0.2 ml of extraction mixture (H_2O:CH_3CN 80:20). Samples were agitated for 1 hour, the mixture was replaced with 0.2 ml of fresh liquid, then after another hour the 2 fractions were collected, mixed and filtered with 0.45 µm syringe filters.

6.3.8 Total deposition assessment

To assess total deposition, the skin sample was cut in small pieces after having dismantled the cell and Tα1 was extracted with 2 ml of extraction mixture. After 1 hour the mixture was replaced with 2 ml fresh solution. At the end of the two hours the fractions were mixed, filtered and analysed by UHPLC-MS/MS.

6.3.9 Thymosin stability in presence of human skin

A solution of Tα1 100 µg/ml was placed in contact with defrost porcine skin, both with the epidermal and dermis side, for 24 hours. Samples were taken hourly for the first 8 hours, and then at hour 24.

6.3.10 Thymosin stability to current

Tα1 stability to current intensity was assessed applying 1 mA for 6 hours to a solution of Tα1 in MES buffer, the most harsh condition tested in permeation experiments. Samples were taken each hour and analysed. Two different concentrations were tested, 10 and 100 µg/ml. Aliquots of the same solutions, without the passage of current, were used as control.

6.3.11 Current assisted permeation experiments

Current assisted experiments were performed in order to evaluate the effect of different composition of the donor solution and of different current densities.

Cathodal iontophoresis was applied for 6 h using Ag/AgCl electrodes connected to the Franz cell with salt bridges. Samples were taken at 1, 2, 3, 4, 5, 6 h. Three buffers were tested: PB 25 mM (pH 7), MES buffer 25 mM (pH 6.5) and HEPES-TRIS buffer 25 mM (pH 6.5). These pH values were chosen because they are dermocompatible and there are studies that demonstrate that at these pH Tα1 stability is higher (studio cinese). At this pH value more than 2 pH units above its isoelectric point, the polypeptide is completely negatively charged, thus improving the conditions for a successful iontophoresis.

To evaluate the effect of current density, 0.15, 0.3 and 0.5 mA/cm^2 were applied.

At the end of the experiments either Tα1 deposition or biodistribution were assessed.

One set of experiments (0.5 mA/cm^2, Tα1 in MES buffer) was carried out also using full-thickness human skin as membrane.

6.3.12 Fluorescent labelling of Tα1

In order to visualize the pathway of penetration of Tα1, the peptide was labelled with a fluorescent dye. An Alexa Fluor® 488 kit was used (Life Technologies, Carlsbad, CA, USA). Briefly, a 2 mg/ml solution of Tα1 was prepared in water. The pH was adjusted with a sodium bicarbonate solution. The solution was the added to the dye, and the reaction was carried out

for 1 hour under constant magnetic stirring. After that, the labelled protein was purified on a purification column, using MES buffer as mobile phase.

The obtained Tα1 solution was used as a donor in a current assisted experiment (0.5 mA/cm^2). At the end of the experiment the porcine skin sample was cut in vertical slices (approximatively 1 mm thick) and mounted on a glass slide. The confocal images were obtained with an Achroplan 20x or Fluar 5x air objective and analysed with Image J. Each image was the average of 4 repeated scan.

6.3.13 Statistical analysis

All the experiments were performed at least in triplicate. The results obtained were compared using ANOVA followed by a Bonferroni correction (α=0.05).

6.4 Results and discussions

The aims of this project were to evaluate and compare the effect of two widely used enhancement techniques for the transdermal permeation of a 28 aa polypeptide, Thymosin α1. This polypeptide is used as an adjuvant for the vaccination of immunocompromised patients, and also as an experimental therapy for different types of cancer and hepatitis b. Passive transdermal permeation and deposition of Tα1 are negligible. In this study transdermal permeation and deposition of thymosin α1 were assessed on porcine skin, following laser microporation of the skin or during iontophoresis. The experimental condition that gave the best results was chosen for a comparison with human skin samples. Moreover, the penetration pathway of this molecule across intact skin during iontophoresis was studied via confocal laser microscopy visualization (CLSM).

6.4.1 Thymosin α1 stability

Tα1 stability to current was tested applying 1 mA for 6 hours via salt bridges to a solution of Tα1 in MES buffer. The loss of Tα1 was about 25% for both the concentration tested.

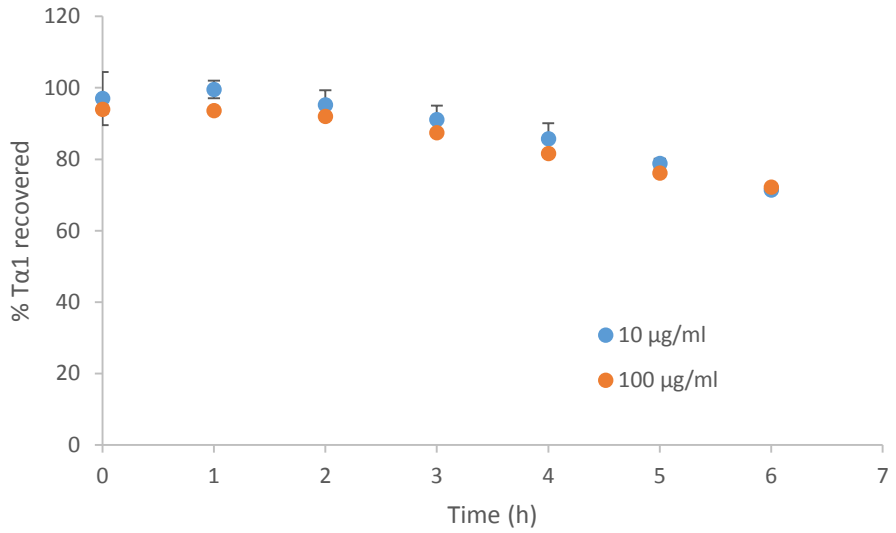

Figure 41 Tα1 stability to current application. Current applied for 6 h, 0.5 mA

Stability to skin was also assessed, and no significant variation in the concentration was noticed after a contact time of 24 hours with defrost porcine skin.

6.4.2 Laser microporation

6.4.2.1 Effect of fluence

The variation of fluence can be useful to control the depth of the pores obtained with laser microporation. Three different fluences were tested (7.9, 23.7 and 39.5 J/cm^2) while keeping the FAA constant at 5%.

Histology studies on microporated porcine skin have shown that low energies (4.53-13.58 J/cm²) are sufficient for a selective removal of the stratum corneum (20-30 µm), usually considered the main barrier to permeation. The application of 22.65 and 45.3 J/cm² produced pores that reached respectively a depth of 50 and 100 µm [141]. Increase in pore depth reduces the diffusional pathway of the molecule across intact skin, thus it could be hypothesized an increase in drug permeation as a function of fluence [95].

Figure 42 shows the cumulative amount permeated after 24 h of passive permeation across microporated skin. At all fluences applied, the permeation is small. When fluence raises from from 23.7 to 39.5 J/cm² there is a significant increase in the amount permeated, while there is no statistical difference between 7.9 J/cm² and 23.7 J/cm^2.

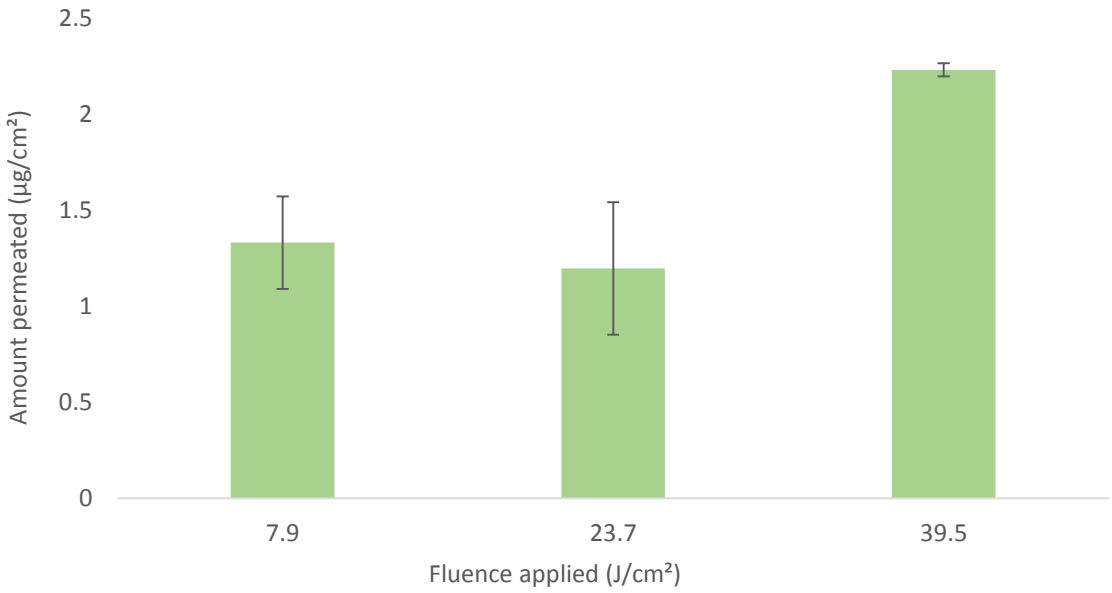

Figure 42 Amount permeated after 24 h passive permeation across microporated skin (results are shown ±SEM)

Thymosin α1 is a strongly hydrophilic molecule, thus stratum corneum should represent the main barrier to transdermal passive permeation. However, the limited extent of permeation,

if compared to even bigger molecules (for example cytochrome c) [95], would suggest that stratum corneum is not the only barrier to permeation. It has to be underlined that the micropores created with the laser contain elements of desiccated epidermis, which can interact with the permeant. The extent and nature of this interaction would depend on the physicochemical properties of the molecule itself [95]. It is possible that the polypeptide interacts with the tissue along the penetration pathway: thymosin α1 behaves, in fact, as an "intrinsically disordered protein"[130], and the prediction of its interactions (intermolecular and with the local environment) turns out to be quite challenging. These observations can also explain the low deposition values obtained (Figure 43).

For the lower fluences applied, it resulted negligible, respectively 0.03±0.01 and 0.06±0.05 µg/cm² when 7.9 and 23.7 J/cm² were applied. The application 39.5 J/cm^2 resulted in an increase in the amount deposited (0.34±0.07 µg/cm²) remained anyhow very low.

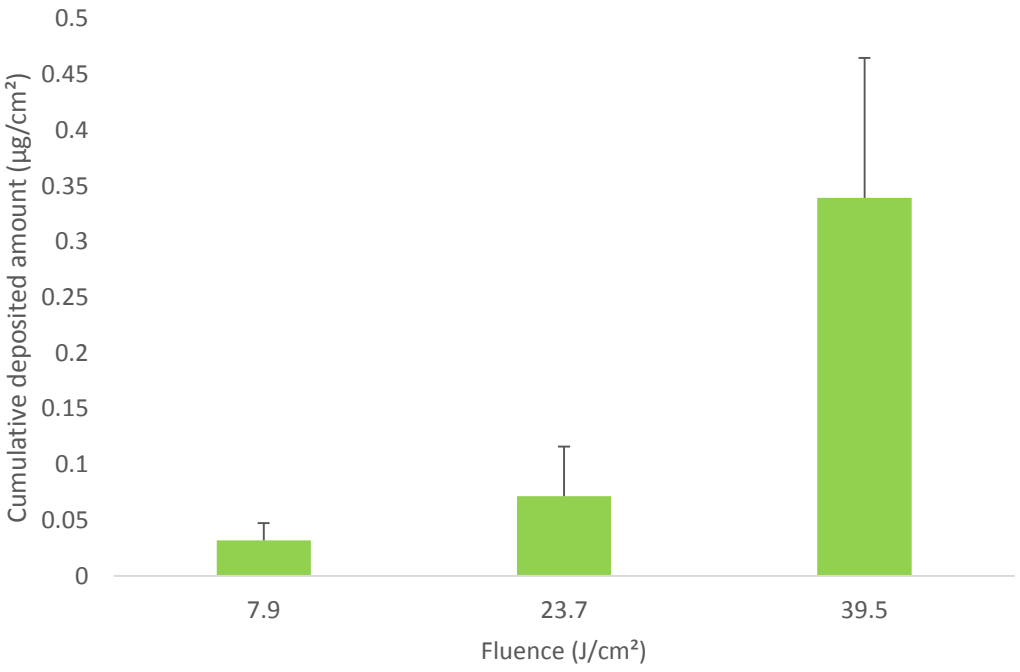

Figure 43 Cumulative amount deposited after 24 h permeation (FAA 5%)

Biodistribution (distribution of the drug in the different layers of the skin) was also assessed (Figure 44), and it showed that, with the application of 39.5 J/cm^2, most of the Thymosin α1 deposited accumulated in the epidermis.

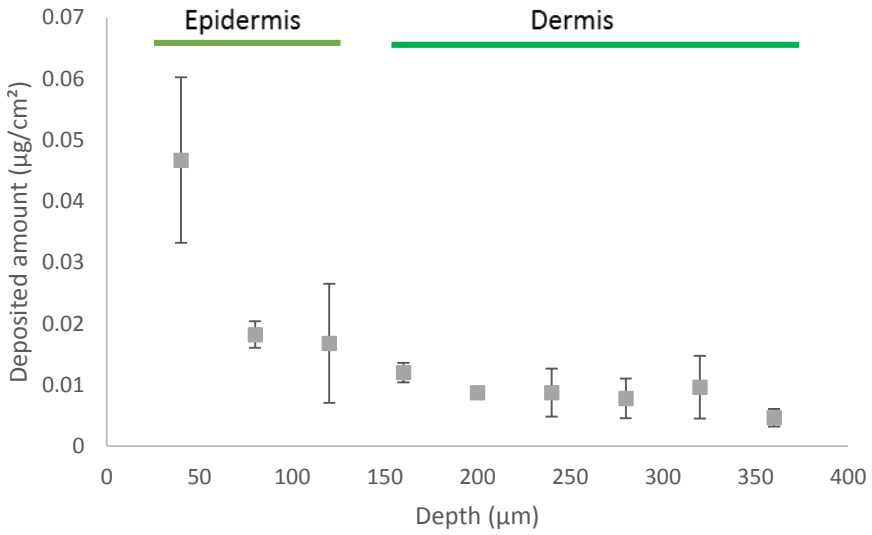

Figure 44 Biodistribution profile of Thymosin α1 in the different layers of the epidermis (39.5 J/cm², FAA 5%)

6.4.2.2 Effect of Fractional Ablative Area

The P.L.E.A.S.E.® system microporates the skin with many small parallel beams (Φ=150 µm) instead of one larger beam [119]. This allows a reduction in the tissue damage due to the laser. Fractional Ablative Area (FAA %) value indicates the percentage of treated skin that results microporated, in other words it gives the number of pores per unit area, and usually varies from 5 to 15 %. Increasing the number of pores should result in a raise in the amount permeated.

In these experiments, fluence applied was at 23.7 J/cm^2, and 5% and 15% FAA were applied.

As shown in Figure 45, no statistical difference was noticeable up to 8 h, while after 24 h the amount permeated with the highest FAA was 5 times higher if compared to a FAA of 5%. The cumulative amount permeated was 5.67±0.27 µg/cm².

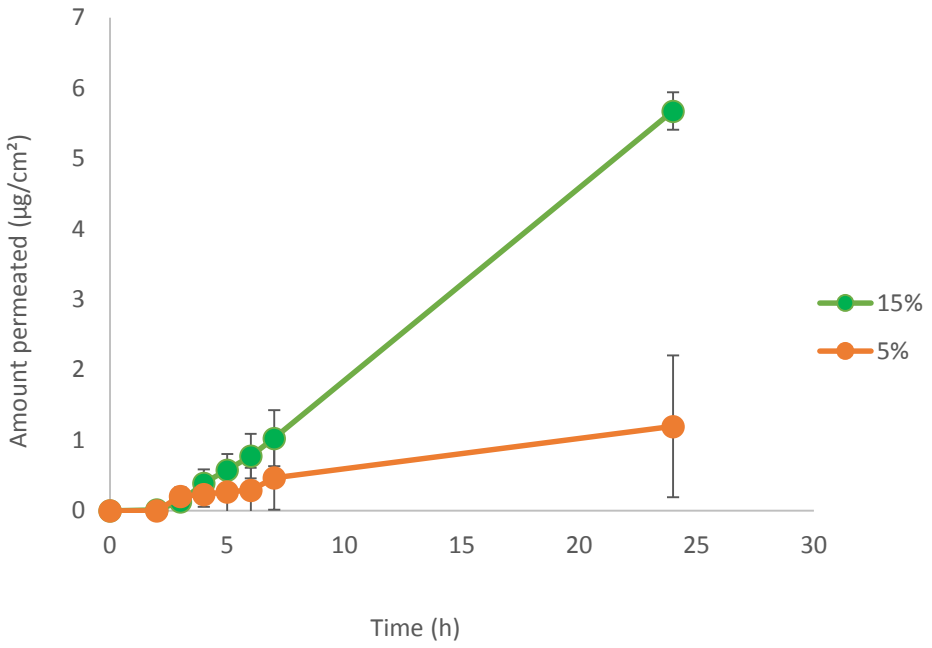

Figure 45 Comparison of the permeation profiles of Tα1 as a function of FAA (%). 24 hours permeation, donor concentration 1 mg/ml, Fluence 23.7 J/cm².

Instantaneous fluxes, calculated between 8 and 24 hours, were respectively 0.131±0.04 and 0.270±0.03 µg/cm²h for a fractional ablative area of 5 and 15%. The estimated permeability coefficients were instead $1.72\pm1.00*10^{-8}$ and $7.51\pm0.83*10^{-8}$ cm/s.

Increasing the fractional ablative area, thus the number of pores per unit area, was more efficient than producing deeper pores for the enhancement of Thymosin α1 permeation. This would suggest that permeation takes place only across the micropores.

Biodistribution evaluation (Figure 46) showed that when 5% FAA was applied Tα1 accumulated mainly in the epidermis, while with 15% it could reach the dermis. The total amounts deposited were respectively 0.06±0.05 and 0.28±013 µg/cm² for 5 and 15 % FAA, thus triplicating the number of pores resulted in 4-fold increase in the amount deposited.

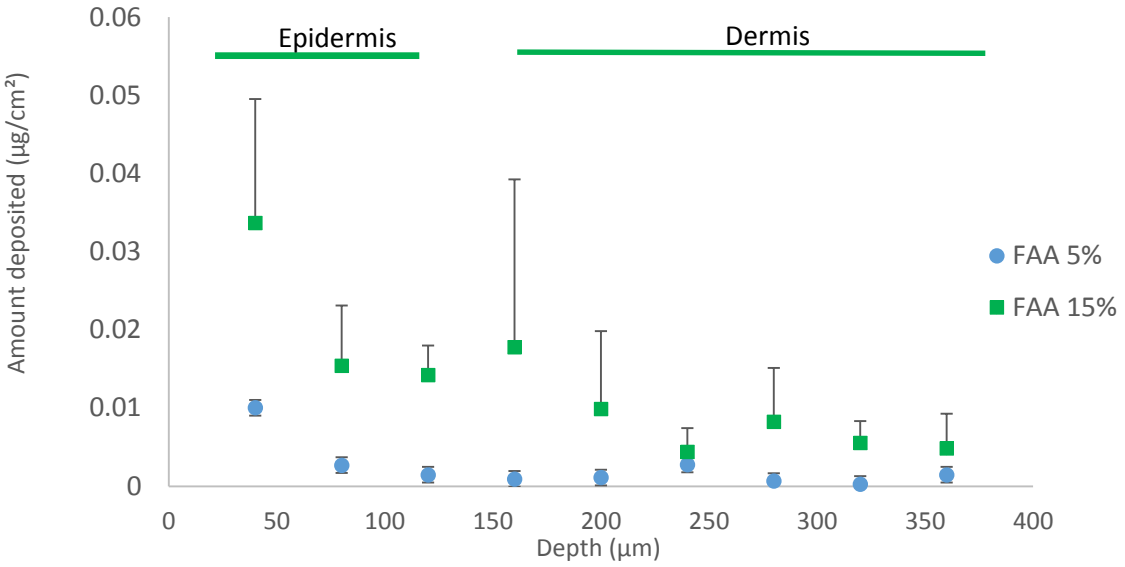

Figure 46 Biodistribution profile of T1 as a function of FAA

6.4.3 Iontophoresis

Thymosin α1 is a hydrophilic peptide that contains 9 negatively charged aminoacidic residues (6 glutamate and 3 aspartate), and 4 positively charged lysine residues. Its isoelectric point is 4.2, and at pH 6.5 it carries a net negative charge of -5. Given these properties, it may be a good candidate for cathodal iontophoretic transport.

6.4.3.1 Effect of vehicle composition

Differences in the donor composition can influence the iontophoretic transport of the molecules. Three different buffers were tested, in order to choose the best one for the following experiments.

As stated before, Tα1 has an isoelectric point of 4.2, so the pH of the donor solutions were adjusted to be at least 2 pH units above this point. Cathodal iontophoresis was applied for 6 hours (0.5 mA/cm²).

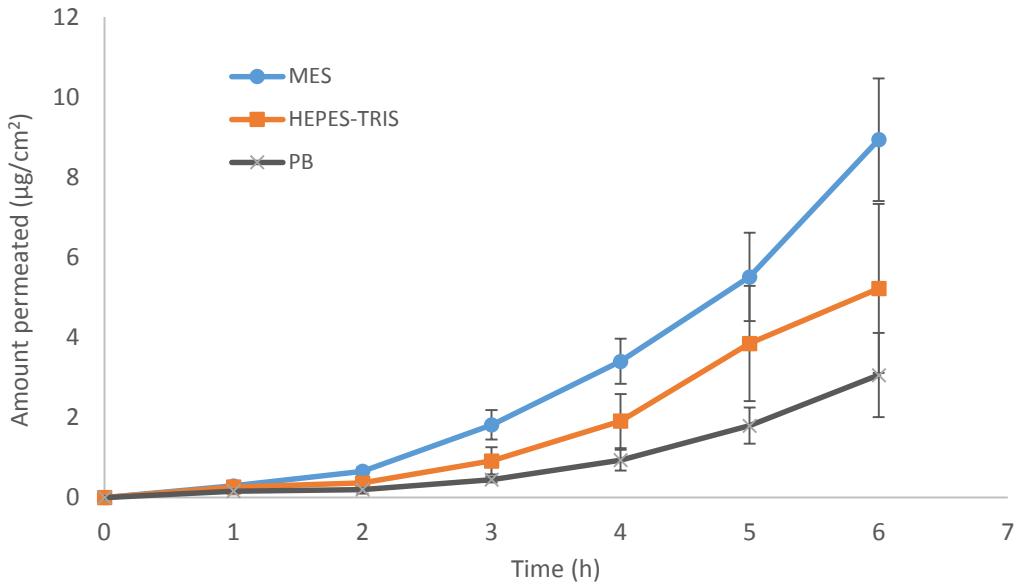

Figure 47 Permeation profiles obtained after 6 h cathodal iontophoresis of T1 in different buffers (Tα1 1 mg/ml, cathodal iontophoresis 0.5 mA/cm²)

As shown in Figure 47 MES buffer gave the highest permeation profile. The difference compared to PB was statistically significant. This is probably due to the presence in PB of phosphate ions with high electrophoretic mobility that can compete with Tα1 for the transport of current. Another possible explanation can be found in the differences in ionic strength of the vehicles that can modify iontophoretic transport. MES buffer also allowed the highest deposition.

Up to 6 hours, steady state was not reached.

Figure 48 shows the cumulative permeated and deposited amount of Thymosin α1 from different vehicles. A twofold increase can be seen in the total amount delivered from MES buffer compared to HEPES-TRIS buffer, while it is 4 times higher than phosphate buffer.

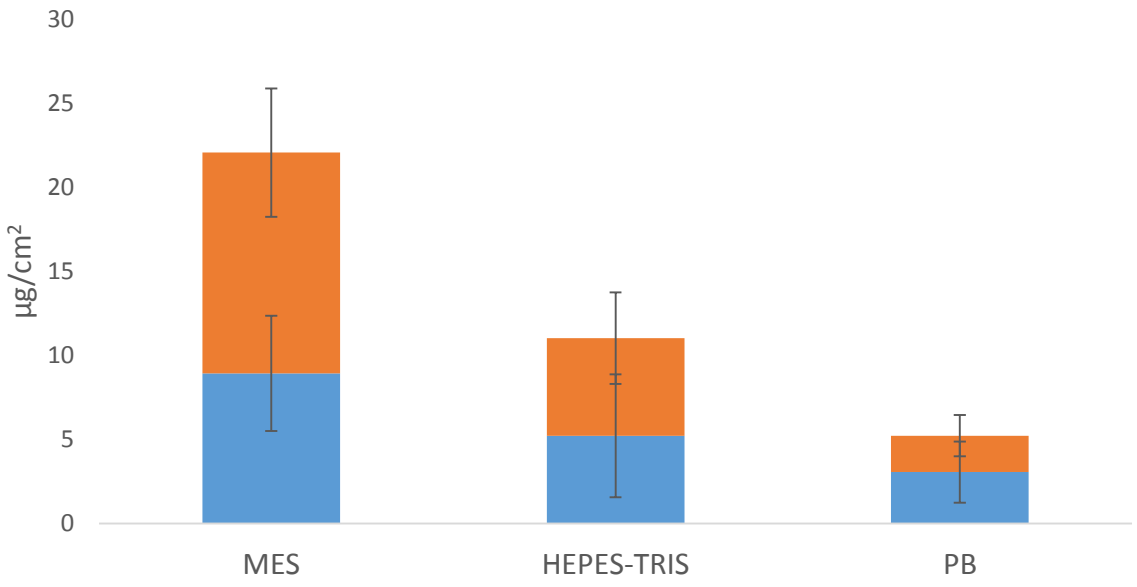

Figure 48 Cumulative permeated (blue) and deposited (orange) amount after 6 h iontophoresis from the different vehicles

6.4.3.2 Effect of current density

The effect of current density on the transdermal permeation and deposition of Tα1 was investigated using a donor solution of Tα1 in MES (pH 6.5). 0.15, 0.3 and 0.5 mA/cm² were applied for 6 hours.

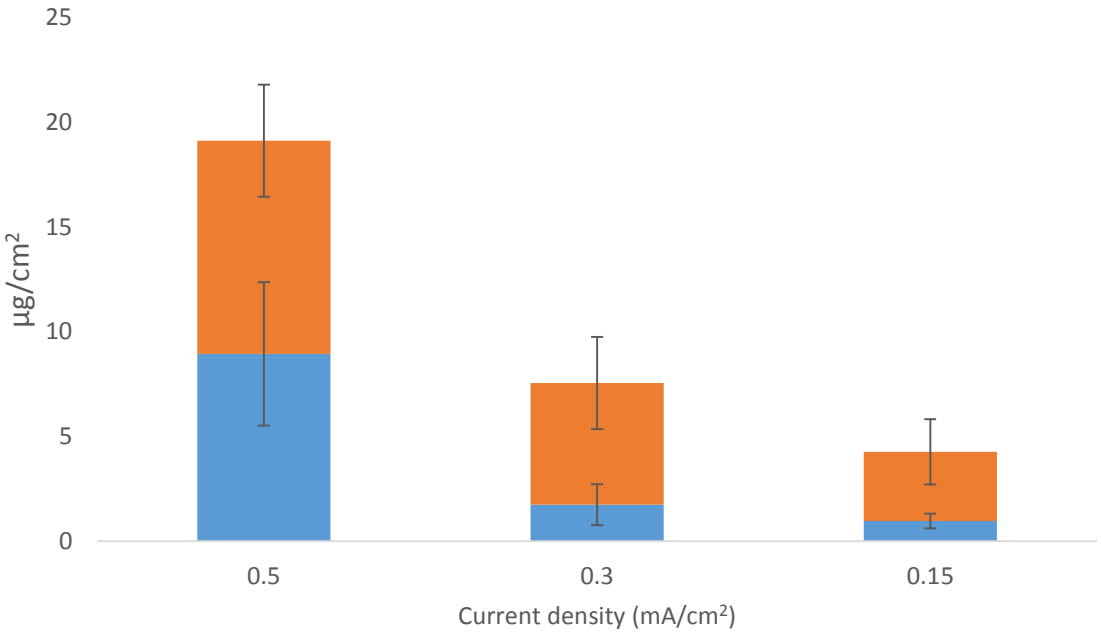

Figure 49 Effect of current density on transdermal permeation (blue bar) and deposition (orange bar) of Tα1. Donor solution was a 1 mg/ml Tα1 in MES buffer (pH 6.5).

Raising the current density from 0.15 to 0.5 mA/cm^2 resulted in a significant increase in both the amount permeated and deposited, but not in a proportional way, as shown in Figure 49.

Given the fact that steady state was not reached, it was not possible to calculate the flux and permeability coefficient, instead instantaneous fluxes (calculated between 5 and 6 h) and apparent permeability coefficients are reported in Table 12.

As Table 12 shows, the application of 0.5 mA/cm^2 resulted in a 10-fold increase in the instantaneous flux when compared to 0.15 mA/cm^2. On the contrary, there is no statistical difference between 0.15 and 0.3 mA/cm^2. To explain this behavior the mechanisms involved in transdermal iontophoresis need to be considered: in particular, due to the application of cathodal iontophoresis, electrorepulsion between Tα1 negative charges and the cathode promotes drug transport. On the other hand, electroosmosis is directed from anode to cathode, thus hindering Tα1 iontophoretic delivery. It is possible that the relative contributions of these two opposing mechanism vary with the increase of current density, thus explaining the lack of proportionality.

Table 12 Instant Fluxes and apparent permeability coefficients calculated between 5 and 6 h for different current densities (average±SD)

Current density (mA/cm^2)	Instantaneous flux (5-6 h) (J, µg/cm^{2}h)	Apparent permeability coefficient (5-6 h) (P, cm/s) *10^{-7}
0.15	0.30±0.07	0.84±0.2
0.3	0.56±0.08	1.56±0.45
0.5	2.61±0.48	7.25±1.30

The values of permeation and deposition obtained in this work are low if compared to the iontophoretic permeation of another negatively charged protein, RNAase T1 (11.7 kDa) [57]. One possible explanation for this relatively low enhancement could be the fact that Thymosin α1 could exist in solution as an oligomer (possibly a trimer- M.W. 11000) [142]. This, as in the case of insulin, could contribute to lower the efficacy of iontophoretic transport.

Moreover, in that study dermatomed skin (250 µm thick) was used, a much thinner membrane compared to full thickness skin used here.

Data on cathodal iontophoresis of macromolecules give variable results, for example in a study on negatively charged oligonucleotides [143] the values of fluxes obtained were very low, considering the highly favourable m/z. Moreover, no relationship could be established between iontophoretic permeation enhancement and mass/charge ratio.

In another study, cathodal iontophoresis of Daniplestim (12.76 kDa, pI 6.2) was performed, but no molecule was detectable in the receiving compartment [114].

It has to be also realized that the charge number of a macromolecule in the solution, due to ion binding, is different from that calculated from its pK_a value.

Studies about transdermal iontophoresis of peptides and proteins confirm that it is not possible to establish a common behavior, but each polypeptide has to be investigated separately. This can be due to the complex structure and nature of interaction of this kind of molecules between themselves and the environment.

Cathodal iontophoresis (0.5 mA/cm^2) was then applied using human skin as a membrane. The results obtained, reported in Figure 50, show no significant difference between the two profiles, confirming that porcine ear skin is a good model for human tissue.

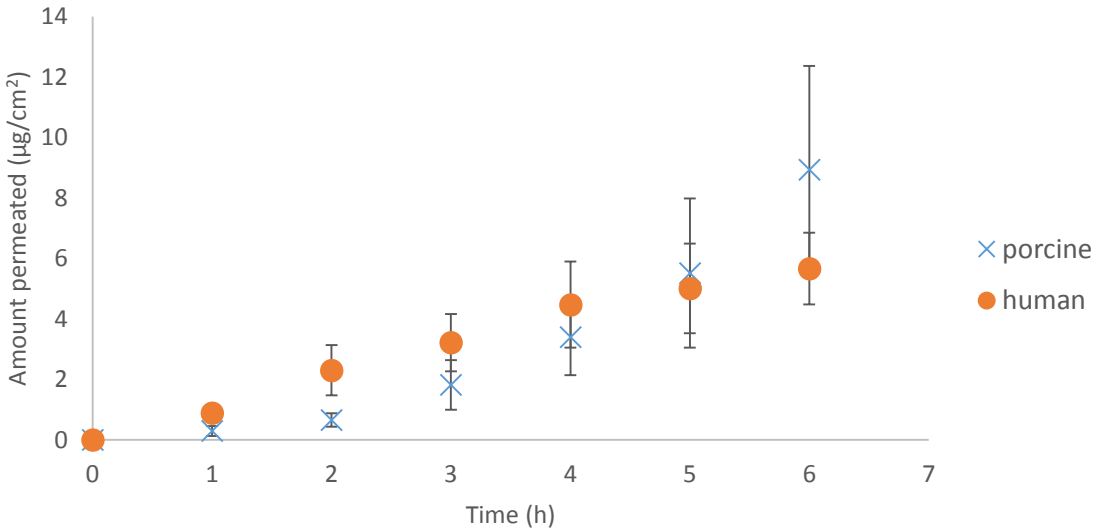

Figure 50 Comparison between iontophoretic permeation of Thymosin alpha 1 (0.5 mA/cm²in MES buffer) across human and porcine skin.

6.4.3.3 Visualization of the penetration pathways

A solution of fluorescently labelled Tα1 was used as donor in an iontophoretic experiment (0.5 mA/cm^2, 6 h) across porcine skin. After the experiment, the cell was dismantled and the skin sample was observed with a confocal microscope. Figure 51 shows the skin sample firstly observed under a UV-lamp. Fluorescence spots can be noticed around the hair follicles. In confocal images (Figure 52) it is more clearly visible an accumulation of fluorescence around the hair shaft, suggesting that the annexial route could be preferential for the iontophoretic permeation of Thymosin α1.

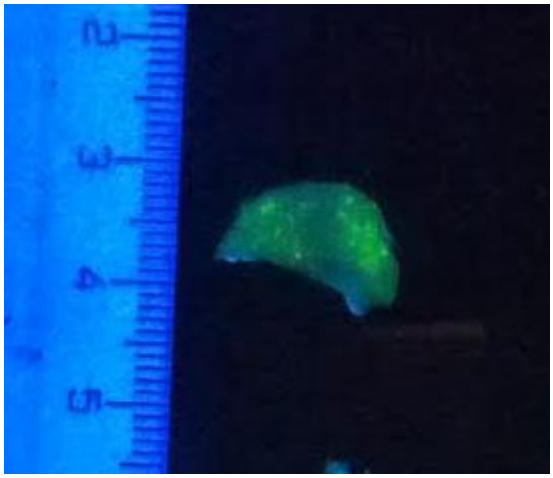

Figure 51 Skin sample after iontophoretic permeation of labelled Tα1, observed under UV lamp. It is visible an accumulation of drug around the hair follicles

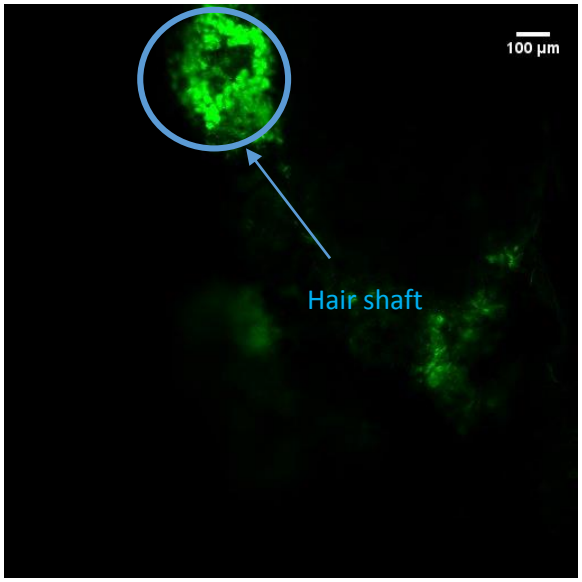

Figure 52 Confocal image of skin sample after iontophoretic permeation of Tα1 (planar visualization)

6.4.4 Comparison between laser microporation and iontophoresis

From the data obtained it is possible to compare the two techniques. Considering the best condition for laser microporation (23.7 J/cm², FAA 15%) and iontophoresis (0.5 mA/cm² in MES buffer), iontophoresis proved to be superior to laser microporation to enhance transdermal delivery of Thymosin α1.

In fact, the amount permeated after only 6 hours of iontophoretic permeation was 10.67±2.67 µg/cm², 2 times higher than 24 hours of passive permeation across microporated skin. Instantaneous flux, calculated between 5 and 6 hours, as well as apparent permeability coefficient, resulted 10 times smaller in laser microporated skin than after iontophoresis application (Table 13).

Table 13 Instantaneous flux and apparent permeability coefficient values calculated between 5 and 6 hours for the best laser microporation condition and iontophoretic delivery

Enhancement technique	Instantaneous flux (µg/cm²h) (5-6 h)	Apparent permeability coefficient (cm/s)*10^{-7} (5-6 h)
Laser microporation (23.7 J/cm²; FAA 15%)	0.19±0.08	0.5±0.22
Iontophoresis (0.5 mA/cm², 6 h)	2.61±0.48	7.25±1.3

These results are consistent, in terms of difference in enhancement effectiveness, to the ones obtained with cytochrome c [95], where iontophoresis gave a 10-fold enhancement compared to laser microporation.

6.5 Conclusions- Transdermal delivery

These experiments demonstrated that physical enhancement techniques, such as laser microporation and iontophoresis, could be useful to promote permeation and deposition of Tα1, a negatively charged polypeptide (M.W. 3108 Da). Iontophoresis was more promising than laser microporation for this purpose, in fact, it allowed a 10-fold greater permeation compared to the best condition for laser microporation and the amount deposited was almost 40 times higher.

Moreover, the results obtained with human skin confirmed that porcine skin is a convenient model for the human tissue.

Finally, studies carried out using a fluorescently labelled derivative of Tα1 showed that the preferential iontophoretic penetration pathway was across the hair shafts.

Even though the amounts deposited and permeated obtained either with laser microporation or with iontophoresis are probably too low to elicit a therapeutic response, these experiments helped giving further insight on the iontophoretic behavior of a negatively charged polypeptide.

7 General conclusions

The results obtained in this work confirm that iontophoresis is a promising enhancement technique for the permeation of drugs across the three membranes tested, and give a further insight into the mechanisms involved in iontophoretic transport.

Indeed, iontophoresis proved to effectively enhance cytochrome c permeation across the sclera. In fact, it allowed the permeation of significant amounts of cytochrome c (up to a few mg) without causing evident damage to the sclera. Moreover, the possibility of a subtle modulation of the release throughout iontophoresis was demonstrated.

As for buccal iontophoresis, the experiments performed using sumatriptan succinate indicated that iontophoresis greatly enhanced its permeation across porcine esophageal epithelium, and the enhancement was proportional to both the current applied and the drug concentration in the donor solution.

Transdermal iontophoresis of thymosin alpha 1 showed that iontophoresis was more effective than laser microporation to enhance thymosin permeation and deposition. In fact, after only six hours the amount permeated was double compared to passive permeation across microporated skin, and the amount deposited was 40 times more.

8 Presentation of the results

8.1 Publications

- E. Tratta, S. Pescina, C. Padula, P. Santi, S. Nicoli, *In vitro* permeability of a model protein across ocular tissues and effect of iontophoresis on the transscleral delivery, European Journal of Pharmaceutics and Biopharmaceutics, Volume 88, Issue 1, September 2014, Pages 116-122, ISSN 0939-6411, http://dx.doi.org/10.1016/j.ejpb.2014.04.018.

- Paper in preparation: Telò, I., Tratta, E., Guasconi, B., Nicoli, S., Pescina, S., Santi, P., Padula, C. "Pig esophageal epithelium properties during iontophoresis"

8.2 Presentation of the results in Conferences and Doctoral Schools

1. E.Tratta, C. Padula, P.Santi "Development of Advanced Medications containing silver nanoparticles for the treatment of Chronic Skin Wounds", (2012 6th AItUN Annual Meeting, Parma, 08-09 March 2012)
2. E. Tratta, M.Martorano, P. Santi, S.Nicoli "Iontophoretic Trans-scleral Delivery of Cytochrome C", (XII Scuola Nazionale Dottorale per la formazione avanzata in discipline Tecnologico Farmaceutiche "I Medicinali Biotecnologici" Firenze, 10-12 September 2012).
3. Elena Tratta, Isabella Baldrighi, Maria Martorano, Patrizia Santi, Sara Nicoli "Effect of iontophoresis on trans-scleral permeation of cytochrome c", (7th AItUN meeting "New Frontiers in Cell Living Encapsulation", Perugia, 8-9 March 2013)
4. Elena Tratta, Sara Nicoli, Patrizia Santi, Cristina Padula "Trans-scleral delivery of cytochrome c: effect of iontophoresis", (ULLA Summer School, London, 7-12 July 2013)
5. E.Tratta, S.Nicoli, P.Santi, Y.N. Kalia "Comparison of iontophoresis and fractional laser ablation for the controlled delivery of thymosin α1: Quantification of transdermal permeation and skin biodistribution" (Prague, 14th Skin Forum Annual Meeting, 4-5 September 2014)
6. E. Tratta, B. Guasconi, C. Padula "Iontophoretic enhancement of in vitro permeation of sumatriptan succinate across porcine esophageal epithelium" (AAPS Annual Meeting, San Diego, 2-6 November 2014)

9 Bibliography

1. Singh, J. and H. Maibach, *Topical iontophoretic drug delivery in vivo: historical development, devices and future perspectives.* Dermatology, 1993. **187**(4): p. 235-238.
2. Green, P.G., *Iontophoretic delivery of peptide drugs.* Journal of controlled release, 1996. **41**(1): p. 33-48.
3. Ciach, T. and A. Moscicka-Studzinska, *Buccal iontophoresis: an opportunity for drug delivery and metabolite monitoring.* Drug discovery today, 2011. **16**(7): p. 361-366.
4. Gratieri, T. and Y. Kalia, *Topical Iontophoresis for Targeted Local Drug Delivery to the Eye and Skin*, in *Focal Controlled Drug Delivery*, A.J. Domb and W. Khan, Editors. 2014, Springer US. p. 263-284.
5. Naik, A., Y.N. Kalia, and R.H. Guy, *Transdermal drug delivery: overcoming the skin's barrier function.* Pharmaceutical science & technology today, 2000. **3**(9): p. 318-326.
6. Kalia, Y.N., et al., *Iontophoretic drug delivery.* Advanced Drug Delivery Reviews, 2004. **56**(5): p. 619-658.
7. Gratieri, T. and Y.N. Kalia, *Mathematical models to describe iontophoretic transport in vitro and in vivo and the effect of current application on the skin barrier.* Advanced Drug Delivery Reviews, 2013. **65**(2): p. 315-329.
8. Hu, L., et al., *CHAPTER 4 - Iontophoretic Transdermal Drug Delivery*, in *Handbook of Non-Invasive Drug Delivery Systems*, V.S. Kulkarni, Editor. 2010, William Andrew Publishing: Boston. p. 95-118.
9. Nicoli, S., et al., *In vitro transscleral iontophoresis of high molecular weight neutral compounds.* European Journal of Pharmaceutical Sciences, 2009. **36**(4–5): p. 486-492.
10. Kasting, G.B. and J. Keister, *Application of electrodiffusion theory for a homogeneous membrane to iontophoretic transport through skin.* Journal of controlled release, 1989. **8**(3): p. 195-210.
11. Geroski, D.H. and H.F. Edelhauser, *Transscleral drug delivery for posterior segment disease.* Advanced drug delivery reviews, 2001. **52**(1): p. 37-48.
12. Testut, L., A. Latarjet, and E. Allara, *Trattato di anatomia umana*. 1978: Utet.
13. Cassin, B., M.L. Rubin, and S. Solomon, *Dictionary of eye terminology*. 1984: Triad Publishing Company.
14. Fong, D.S., et al., *Retinopathy in diabetes.* Diabetes care, 2004. **27**(suppl 1): p. s84-s87.
15. Javitt, J.C., et al., *Detecting and Treating Retinopathy in Patients with Tyke I Diabetes Mellitus: Savings Associated with Improved Implementation of Current Guidelines.* Ophthalmology, 1991. **98**(10): p. 1565-1574.

16. Resnikoff, S., et al., *Global data on visual impairment in the year 2002.* Bulletin of the World Health Organization, 2004. 82(11): p. 844-851.
17. Zhang, K., et al., *Ciliary neurotrophic factor delivered by encapsulated cell intraocular implants for treatment of geographic atrophy in age-related macular degeneration.* Proceedings of the National Academy of Sciences, 2011. 108(15): p. 6241-6245.
18. Schwartz, S.G., et al., *Drug delivery techniques for treating age-related macular degeneration.* Expert opinion on drug delivery, 2014. 11(1): p. 61-68.
19. Katzung, B.G., S.B. Masters, and A.J. Trevor, *Basic & clinical pharmacology*. 2004.
20. Tsai, J.C. and E.M. Kanner, *Current and emerging medical therapies for glaucoma.* Expert Opinion on Emerging Drugs, 2005. 10(1): p. 109-118.
21. Kang-Mieler, J.J., C.R. Osswald, and W.F. Mieler, *Advances in ocular drug delivery: emphasis on the posterior segment.* Expert opinion on drug delivery, 2014. 11(10): p. 1647-1660.
22. Hughes, P.M., et al., *Topical and systemic drug delivery to the posterior segments.* Advanced Drug Delivery Reviews, 2005. 57(14): p. 2010-2032.
23. Pescina, S., et al., *Trans-scleral delivery of macromolecules.* Therapeutic delivery, 2011. 2(10): p. 1331-1349.
24. Kim, S.H., et al., *Transport Barriers in Transscleral Drug Delivery for Retinal Diseases.* Ophthalmic Research, 2007. 39(5): p. 244-254.
25. Amrite, A., et al., *Delivery of celecoxib for treating diseases of the eye: influence of pigment and diabetes.* Expert opinion on drug delivery, 2010. 7(5): p. 631-645.
26. Cheruvu, N.P., A.C. Amrite, and U.B. Kompella, *Effect of eye pigmentation on transscleral drug delivery.* Investigative ophthalmology & visual science, 2008. 49(1): p. 333-341.
27. Geng, J., et al., *Bacterial melanin interacts with double-stranded DNA with high affinity and may inhibit cell metabolism in vivo.* Archives of microbiology, 2010. 192(5): p. 321-329.
28. Pitkänen, L., et al., *Binding of betaxolol, metoprolol and oligonucleotides to synthetic and bovine ocular melanin, and prediction of drug binding to melanin in human choroid-retinal pigment epithelium.* Pharmaceutical research, 2007. 24(11): p. 2063-2070.
29. Eckhart, L., et al., *Melanin binds reversibly to thermostable DNA polymerase and inhibits its activity.* Biochemical and biophysical research communications, 2000. 271(3): p. 726-730.
30. Ban, Y. and L.J. Rizzolo, *A culture model of development reveals multiple properties of RPE tight junctions.* Mol Vis, 1997. 3: p. 18.

31. Pitkänen, L., et al., *Permeability of retinal pigment epithelium: effects of permeant molecular weight and lipophilicity.* Investigative ophthalmology & visual science, 2005. **46**(2): p. 641-646.
32. Duvvuri, S., S. Majumdar, and A.K. Mitra, *Role of metabolism in ocular drug delivery.* Current drug metabolism, 2004. **5**(6): p. 507-515.
33. Myles, M.E., D.M. Neumann, and J.M. Hill, *Recent progress in ocular drug delivery for posterior segment disease: emphasis on transscleral iontophoresis.* Advanced drug delivery reviews, 2005. **57**(14): p. 2063-2079.
34. Parkinson, T.M., et al., *Tolerance of ocular iontophoresis in healthy volunteers.* Journal of ocular pharmacology and therapeutics, 2003. **19**(2): p. 145-151.
35. Patane, M.A., et al., *Ocular iontophoresis for drug delivery.* Retina Today, 2011. **6**: p. 64-6.
36. Davies, J.B., et al., *Delivery of several forms of DNA, DNA-RNA hybrids, and dyes across human sclera by electrical fields.* Mol. Vis, 2003. **9**: p. 569-578.
37. Chopra, P., J. Hao, and S.K. Li, *Iontophoretic transport of charged macromolecules across human sclera.* International journal of pharmaceutics, 2010. **388**(1): p. 107-113.
38. Pescina, S., et al., *In-vitro permeation of bevacizumab through human sclera: effect of iontophoresis application.* Journal of Pharmacy and Pharmacology, 2010. **62**(9): p. 1189-1194.
39. Nelson, D.L., A.L. Lehninger, and M.M. Cox, *Lehninger principles of biochemistry*. 2008: Macmillan.
40. Jiang, X. and X. Wang, *Cytochrome C-mediated apoptosis.* Annual review of biochemistry, 2004. **73**(1): p. 87-106.
41. Kabanov, V., et al., *Sorption of proteins by slightly cross-linked polyelectrolyte hydrogels: kinetics and mechanism.* The Journal of Physical Chemistry B, 2004. **108**(4): p. 1485-1490.
42. Bertini, I., G. Cavallaro, and A. Rosato, *Cytochrome c: occurrence and functions.* Chemical reviews, 2006. **106**(1): p. 90-115.
43. Cheruvu, N.P. and U.B. Kompella, *Bovine and porcine transscleral solute transport: influence of lipophilicity and the Choroid–Bruch's layer.* Investigative ophthalmology & visual science, 2006. **47**(10): p. 4513-4522.
44. Pescina, S., et al., *Ex vivo models to evaluate the role of ocular melanin in trans-scleral drug delivery.* European Journal of Pharmaceutical Sciences, 2012. **46**(5): p. 475-483.
45. Zaidi, S., et al., *The role of key residues in structure, function, and stability of cytochrome-c.* Cellular and Molecular Life Sciences, 2014. **71**(2): p. 229-255.

46. Pescina, S., et al., *Effect of formulation factors on the trans-scleral iontophoretic and post-iontophoretic transports of a 40kDa dextran in vitro.* European Journal of Pharmaceutical Sciences, 2011. **42**(5): p. 503-508.
47. Leblanc, B., et al., *Binding of Drugs to Eye Melanin Is Not Predictive of Ocular Toxicity.* Regulatory Toxicology and Pharmacology, 1998. **28**(2): p. 124-132.
48. Kontturi, A.-K., et al., *The effective charge number and diffusion coefficient of cationic cytochrome c in aqueous solution.* Acta Chemica Scandinavica, 1992. **46**: p. 348-353.
49. Taler, G., A. Schejter, and G. Navon, *< sup> 1</sup> H and< sup> 11</sup> B NMR evidence for specific binding of borate ion to cytochrome< i> c</i>.* Inorganica chimica acta, 1998. **273**(1): p. 388-392.
50. Taler, G., G. Navon, and O.M. Becker, *The Interaction of Borate Ions with Cytochrome< i> c</i> Surface Sites: A Molecular Dynamics Study.* Biophysical journal, 1998. **75**(5): p. 2461-2468.
51. Tamada, J.A. and K. Comyns, *Effect of formulation factors on electroosmotic glucose transport through human skin in vivo.* Journal of pharmaceutical sciences, 2005. **94**(8): p. 1839-1849.
52. Güngör, S., et al., *Trans-scleral iontophoretic delivery of low molecular weight therapeutics.* Journal of Controlled Release, 2010. **147**(2): p. 225-231.
53. Rowe, R.C., et al., *Handbook of pharmaceutical excipients*. Vol. 6. 2009: Pharmaceutical press London.
54. Pescina, S., et al., *< i> In vitro</i> trans-scleral iontophoresis of methylprednisolone hemisuccinate with short application time and high drug concentration.* International journal of pharmaceutics, 2013. **451**(1): p. 12-17.
55. Murtomäki, L., et al., *Drug adsorption on bovine and porcine sclera studied with streaming potential.* Journal of pharmaceutical sciences, 2013. **102**(7): p. 2264-2272.
56. Cázares-Delgadillo, J., et al., *Transdermal Delivery of Cytochrome C—A 12.4 kDa Protein—Across Intact Skin by Constant–Current Iontophoresis.* Pharmaceutical Research, 2007. **24**(7): p. 1360-1368.
57. Dubey, S. and Y.N. Kalia, *Electrically-assisted delivery of an anionic protein across intact skin: Cathodal iontophoresis of biologically active ribonuclease T1.* Journal of Controlled Release, 2011. **152**(3): p. 356-362.
58. Dubey, S. and Y. Kalia, *Non-invasive iontophoretic delivery of enzymatically active ribonuclease A (13.6 kDa) across intact porcine and human skins.* Journal of controlled release, 2010. **145**(3): p. 203-209.

59. El Sanharawi, M., et al., *Protein delivery for retinal diseases: from basic considerations to clinical applications.* Progress in retinal and eye research, 2010. **29**(6): p. 443-465.
60. Patel, V.F., F. Liu, and M.B. Brown, *Advances in oral transmucosal drug delivery.* Journal of controlled release, 2011. **153**(2): p. 106-116.
61. Squier, C.A. and B.K. Hall, *The Permeability of Skin and Oral Mucosa to Water and Horseradish Peroxidase as Related to the Thickness of the Permeability Barrier.* J Investig Dermatol, 1985. **84**(3): p. 176-179.
62. Squier, C.A. and M.J. Kremer, *Biology of oral mucosa and esophagus.* JNCI Monographs, 2001. **2001**(29): p. 7-15.
63. Collins, L. and C. Dawes, *The surface area of the adult human mouth and thickness of the salivary film covering the teeth and oral mucosa.* Journal of dental research, 1987. **66**(8): p. 1300-1302.
64. Tabak, L.A., et al., *Role of salivary mucins in the protection of the oral cavity.* Journal of Oral Pathology & Medicine, 1982. **11**(1): p. 1-17.
65. Shojaei, A.H., et al., *Systemic drug delivery via the buccal mucosal route.* Pharmaceutical technology, 2001. **25**(6): p. 70-81.
66. Shojaei, A.H., *Buccal mucosa as a route for systemic drug delivery: a review.* J Pharm Pharm Sci, 1998. **1**(1): p. 15-30.
67. Madhav, N., et al., *Orotransmucosal drug delivery systems: a review.* Journal of Controlled Release, 2009. **140**(1): p. 2-11.
68. Jacobsen, J., *Buccal iontophoretic delivery of atenolol· HCl employing a new in vitro three-chamber permeation cell.* Journal of controlled release, 2001. **70**(1): p. 83-95.
69. De Caro, V., et al., *Galantamine Delivery on Buccal Mucosa: Permeation Enhancement an d Design of Matrix Tablets.* J Bioequiv Availab, 2009. **1**: p. 127-134.
70. Hu, L., et al., *Enhanced< i> in vitro</i> transbuccal drug delivery of ondansetron HCl.* International journal of pharmaceutics, 2011. **404**(1): p. 66-74.
71. Giannola, L.I., et al., *Diffusion of naltrexone across reconstituted human oral epithelium and histomorphological features.* European journal of pharmaceutics and biopharmaceutics, 2007. **65**(2): p. 238-246.
72. Giannola, L.I., et al., *Release of naltrexone on buccal mucosa: permeation studies, histological aspects and matrix system design.* European Journal of Pharmaceutics and Biopharmaceutics, 2007. **67**(2): p. 425-433.
73. Wei, R., et al., *Effects of iontophoresis and chemical enhancers on the transport of lidocaine and nicotine across the oral mucosa.* Pharmaceutical research, 2012. **29**(4): p. 961-971.

74. Patel, M.P., et al., *Electrically induced transport of macromolecules through oral buccal mucosa.* Dental Materials, 2013. **29**(6): p. 674-681.
75. Moscicka-Studzinska, A., E. Kijeńska, and T. Ciach, *Electroosmotic flow as a result of buccal iontophoresis – Buccal mucosa properties.* European Journal of Pharmaceutics and Biopharmaceutics, 2009. **72**(3): p. 595-599.
76. Gratieri, T. and Y.N. Kalia, *Targeted local simultaneous iontophoresis of chemotherapeutics for topical therapy of head and neck cancers.* International journal of pharmaceutics, 2014. **460**(1): p. 24-27.
77. Diaz del Consuelo, I., et al., *Evaluation of pig esophageal mucosa as a permeability barrier model for buccal tissue.* Journal of pharmaceutical sciences, 2005. **94**(12): p. 2777-2788.
78. Diaz-del Consuelo, I., et al., *Comparison of the lipid composition of porcine buccal and esophageal permeability barriers.* Archives of oral biology, 2005. **50**(12): p. 981-987.
79. Van der Bijl, P., L. Penkler, and A. Van Eyk, *Permeation of sumatriptan through human vaginal and buccal mucosa.* Headache: The Journal of Head and Face Pain, 2000. **40**(2): p. 137-141.
80. Vrbata, P., et al., *Electrospun drug loaded membranes for sublingual administration of sumatriptan and naproxen.* International Journal of Pharmaceutics, 2013. **457**(1): p. 168-176.
81. Femenía-Font, A., et al., *Iontophoretic transdermal delivery of sumatriptan: effect of current density and ionic strength.* Journal of pharmaceutical sciences, 2005. **94**(10): p. 2183-2186.
82. Menon, G.K., *New insights into skin structure: scratching the surface.* Advanced Drug Delivery Reviews, 2002. **54, Supplement**(0): p. S3-S17.
83. Martini, Timmons, and Tallitsch, *Anatomia Umana*. II ed, Napoli: EdiSes.
84. Bouwstra, J.A. and M. Ponec, *The skin barrier in healthy and diseased state.* Biochimica et Biophysica Acta (BBA) - Biomembranes, 2006. **1758**(12): p. 2080-2095.
85. Sato, J., et al., *Cholesterol sulfate inhibits proteases that are involved in desquamation of stratum corneum.* Journal of investigative dermatology, 1998. **111**(2): p. 189-193.
86. Huang, C.-M. *Topical vaccination: the skin as a unique portal to adaptive immune responses*. in *Seminars in immunopathology*. 2007: Springer.
87. Oesch, F., et al., *Drug-metabolizing enzymes in the skin of man, rat, and pig.* Drug metabolism reviews, 2007. **39**(4): p. 659-698.
88. Kalluri, H. and A. Banga, *Transdermal Delivery of Proteins.* AAPS PharmSciTech, 2011. **12**(1): p. 431-441.

89. Chaturvedula, A., et al., *In vivo iontophoretic delivery and pharmacokinetics of salmon calcitonin.* International Journal of Pharmaceutics, 2005. **297**(1–2): p. 190-196.
90. Prausnitz, M.R. and R. Langer, *Transdermal drug delivery.* Nat Biotech, 2008. **26**(11): p. 1261-1268.
91. Gratieri, T., D. Kalaria, and Y.N. Kalia, *Non-invasive iontophoretic delivery of peptides and proteins across the skin.* Expert opinion on drug delivery, 2011. **8**(5): p. 645-663.
92. Siddiqui, O., et al., *Facilitated transdermal transport of insulin.* Journal of Pharmaceutical Sciences, 1987. **76**(4): p. 341-345.
93. Stephen, R., T. Petelenz, and S. Jacobsen, *Potential novel methods for insulin administration: I. Iontophoresis.* Biomedica biochimica acta, 1983. **43**(5): p. 553-558.
94. Abla, N., et al., *Effect of Charge and Molecular Weight on Transdermal Peptide Delivery by Iontophoresis.* Pharmaceutical Research, 2005. **22**(12): p. 2069-2078.
95. Bachhav, Y., A. Heinrich, and Y. Kalia, *Controlled intra-and transdermal protein delivery using a minimally invasive Erbium: YAG fractional laser ablation technology.* European Journal of Pharmaceutics and Biopharmaceutics, 2013. **84**(2): p. 355-364.
96. Li, S.K., et al., *Iontophoretic transport of oligonucleotides across human epidermal membrane: A study of the Nernst–Planck model.* Journal of Pharmaceutical Sciences, 2001. **90**(7): p. 915-931.
97. Langkjær, L., et al., *Iontophoresis of monomeric insulin analogues in vitro: effects of insulin charge and skin pretreatment.* Journal of Controlled Release, 1998. **51**(1): p. 47-56.
98. Kanikkannan, N., J. Singh, and P. Ramarao, *Transdermal iontophoretic delivery of bovine insulin and monomeric human insulin analogue.* Journal of Controlled Release, 1999. **59**(1): p. 99-105.
99. Chang, S.-L., et al., *Transdermal iontophoretic delivery of salmon calcitonin.* International journal of pharmaceutics, 2000. **200**(1): p. 107-113.
100. Chaturvedula, A., et al., *In vivo iontophoretic delivery and pharmacokinetics of salmon calcitonin.* International journal of pharmaceutics, 2005. **297**(1): p. 190-196.
101. Santi, P., et al., *Transdermal iontophoresis of salmon calcitonin can reproduce the hypocalcemic effect of intravenous administration.* Farmaco (Societa chimica italiana: 1989), 1996. **52**(6-7): p. 445-448.
102. Nakamura, K., et al., *Transdermal administration of salmon calcitonin by pulse depolarization-iontophoresis in rats.* International journal of pharmaceutics, 2001. **218**(1): p. 93-102.

103. Suzuki, Y., et al., *Prevention of bone loss in ovariectomized rats by pulsatile transdermal iontophoretic administration of human PTH (1–34).* Journal of pharmaceutical sciences, 2002. **91**(2): p. 350-361.
104. Suzuki, Y., et al., *Iontophoretic pulsatile transdermal delivery of human parathyroid hormone (1–34).* Journal of Pharmacy and Pharmacology, 2001. **53**(9): p. 1227-1234.
105. Chen, L.-L.H. and Y.W. Chien, *Transdermal iontophoretic permeation of luteinizing hormone releasing hormone: characterization of electric parameters.* Journal of controlled release, 1996. **40**(3): p. 187-198.
106. Heit, M.C., et al., *Transdermal Iontophoretic Delivery of Luteinizing Hormone Releasing Hormone (LHRH): Effect of Repeated Administration.* Pharmaceutical research, 1994. **11**(7): p. 1000-1003.
107. Schuetz, Y.B., et al., *Transdermal iontophoretic delivery of triptorelin in vitro.* Journal of pharmaceutical sciences, 2005. **94**(10): p. 2175-2182.
108. Schuetz, Y.B., et al., *Transdermal Iontophoretic Delivery of Vapreotide Acetate AcrossPorcine Skin in Vitro.* Pharmaceutical research, 2005. **22**(8): p. 1305-1312.
109. Banga, A.K., M. Katakam, and R. Mitra, *Transdermal iontophoretic delivery and degradation of vasopressin across human cadaver skin.* International journal of pharmaceutics, 1995. **116**(2): p. 211-216.
110. Kumar, S., et al., *Effect of iontophoresis on in vitro skin permeation of an analogue of growth hormone releasing factor in the hairless guinea pig model.* Journal of pharmaceutical sciences, 1992. **81**(7): p. 635-639.
111. Lau, D.T.-W., et al., *Effect of Current Magnitude and Drug Concentration on Iontophoretic Delivery of Octreotide Acetate (Sandostatin®) in the Rabbit.* Pharmaceutical research, 1994. **11**(12): p. 1742-1746.
112. Pacini, S., et al., *Transdermal delivery of< i> Clostridium botulinum</i> toxin type A by pulsed current iontophoresis.* Journal of the American Academy of Dermatology, 2007. **57**(6): p. 1097-1099.
113. Dubey, S. and Y.N. Kalia, *Understanding the poor iontophoretic transport of lysozyme across the skin: When high charge and high electrophoretic mobility are not enough.* Journal of Controlled Release, 2014. **183**(0): p. 35-42.
114. Katikaneni, S., et al., *Molecular charge mediated transport of a 13 kD protein across microporated skin.* International Journal of Pharmaceutics, 2009. **378**(1–2): p. 93-100.
115. Fang, J.-Y., et al., *Transdermal delivery of macromolecules by erbium:YAG laser.* Journal of Controlled Release, 2004. **100**(1): p. 75-85.
116. Dubey, S., *LASER MICROPORATION FOR THE DELIVERY OF DRUGS.* Bulletin of Pharmaceutical Research, 2012. **2**(3): p. 118-23.

117. Walsh, J.T., T.J. Flotte, and T.F. Deutsch, *Er: YAG laser ablation of tissue: effect of pulse duration and tissue type on thermal damage.* Lasers in surgery and medicine, 1989. 9(4): p. 314-326.
118. Caniglia, R.J., *Erbium: YAG laser skin resurfacing.* Facial plastic surgery clinics of North America, 2004. 12(3): p. 373-377.
119. Fang, J.-Y., et al., *Transdermal iontophoresis of 5-fluorouracil combined with electroporation and laser treatment.* International journal of pharmaceutics, 2004. 270(1): p. 241-249.
120. Lee, W.R., et al., *The effect of laser treatment on skin to enhance and control transdermal delivery of 5-fluorouracil.* Journal of pharmaceutical sciences, 2002. 91(7): p. 1613-1626.
121. Lee, W.-R., et al., *Laser-assisted topical drug delivery by using a low-fluence fractional laser: imiquimod and macromolecules.* Journal of Controlled Release, 2011. 153(3): p. 240-248.
122. Lee, W.-R., et al., *Fractional laser as a tool to enhance the skin permeation of 5-aminolevulinic acid with minimal skin disruption: a comparison with conventional erbium: YAG laser.* Journal of Controlled Release, 2010. 145(2): p. 124-133.
123. Scheiblhofer, S., J. Thalhamer, and R. Weiss, *Laser microporation of the skin: prospects for painless application of protective and therapeutic vaccines.* Expert opinion on drug delivery, 2013. 10(6): p. 761-773.
124. Chen, X., et al., *An update on the use of laser technology in skin vaccination.* 2013.
125. Lee, W.-R., et al., *Erbium: YAG laser enhances transdermal peptide delivery and skin vaccination.* Journal of Controlled Release, 2008. 128(3): p. 200-208.
126. Bach, D., et al., *Transcutaneous immunotherapy via laser-generated micropores efficiently alleviates allergic asthma in Phl p 5–sensitized mice.* Allergy, 2012. 67(11): p. 1365-1374.
127. Hessenberger, M., et al., *Transcutaneous delivery of CpG-adjuvanted allergen via laser-generated micropores.* Vaccine, 2013. 31(34): p. 3427-3434.
128. Goldstein, A.L., et al., *Thymosin alpha1: isolation and sequence analysis of an immunologically active thymic polypeptide.* Proceedings of the National Academy of Sciences, 1977. 74(2): p. 725-729.
129. Low, T. and A. Goldstein, *Thymosins: structure, function and therapeutic applications.* Thymus, 1983. 6(1-2): p. 27-42.
130. Grottesi, A., et al., *The conformation of peptide thymosin α1 in solution and in a membrane-like environment by circular dichroism and NMR*

spectroscopy. a possible model for its interaction with the lymphocyte membrane. Peptides, 1998. **19**(10): p. 1731-1738.
131. Ahmed, A., et al., *T-LYMPHOCYTE MATURATION: CELL SURFACE MARKERS AND IMMUNE FUNCTION INDUCED BY T-LYMPHOCYTE CELL-FREE PRODUCTS AND THYMOSIN POLYPEPTIDES.* Annals of the New York Academy of Sciences, 1979. **332**(1): p. 81-94.
132. Peng, Y., et al., *Effects of thymic polypeptides on the thymopoiesis of mouse embryonic stem cells.* Cell biology international, 2008. **32**(10): p. 1265-1271.
133. Yao, Q., et al., *Thymosin-α1 modulates dendritic cell differentiation and functional maturation from human peripheral blood CD14< sup>+</sup> monocytes.* Immunology letters, 2007. **110**(2): p. 110-120.
134. Garaci, E., *Thymosin alpha1: a historical overview.* Annals of the New York Academy of Sciences, 2007. **1112**: p. 14-20.
135. Li, J., C.H. Liu, and F.S. Wang, *Thymosin alpha 1: Biological activities, applications and genetic engineering production.* Peptides, 2010. **31**(11): p. 2151-2158.
136. Zhang, Y.-Y., et al., *Treatment with lamivudine versus lamivudine and thymosin alpha-1 for e antigen-positive chronic hepatitis B patients: a meta-analysis.* Virol J, 2009. **6**: p. 63.
137. Poo, J.L., et al., *Efficacy of triple therapy with thymalfasin, peginterferon alpha-2a, and ribavirin for the treatment of hispanic chronic HCV nonresponders.* Ann Hepatol, 2008. **7**(4): p. 369-75.
138. Camerini, R., et al., *Studies of therapy with thymosin α1 in combination with pegylated interferon α2a and ribavirin in nonresponder patients with chronic hepatitis C.* Annals of the New York Academy of Sciences, 2007. **1112**(1): p. 368-374.
139. Chadwick, D., et al., *A pilot study of the safety and efficacy of thymosin α1 in augmenting immune reconstitution in HIV-infected patients with low CD4 counts taking highly active antiretroviral therapy.* Clinical & Experimental Immunology, 2003. **134**(3): p. 477-481.
140. Garaci, E., et al., *Combination treatment with zidovudine, thymosin α1 and interferon-α in human immunodeficiency virus infectionand interferon-α in human immunodeficiency virus infection.* International Journal of Clinical and Laboratory Research, 1994. **24**(1): p. 23-28.
141. Bachhav, Y., et al., *Effect of controlled laser microporation on drug transport kinetics into and across the skin.* Journal of Controlled Release, 2010. **146**(1): p. 31-36.
142. Haritos, A.A., G.J. Goodall, and B.L. Horecker, *Prothymosin alpha: isolation and properties of the major immunoreactive form of thymosin alpha 1 in*

rat thymus. Proceedings of the National Academy of Sciences, 1984. **81**(4): p. 1008-1011.
143. Brand, R.M., A. Wahl, and P.L. Iversen, *Effects of size and sequence on the iontophoretic delivery of oligonucleotides.* Journal of Pharmaceutical Sciences, 1998. **87**(1): p. 49-52.